

MICROCOPY RESOLUTION TEST CHART

E301929

AD-A165 792

DNA-TR-84-407

(12)

IN SITU STEAM FRACTURE EXPERIMENTS

**E. W. Peterson
P. L. Lagus
H. E. Wu
S-CUBED
A Division of Maxwell Labs, Inc.
P.O. Box 1620
La Jolla, CA 92038-1620**

31 December 1984

Technical Report

**CONTRACT Nos. DNA 001-80-C-0239
DNA 002-82-C-0031**

**Approved for public release;
distribution is unlimited.**

THIS WORK WAS SPONSORED BY THE DEFENSE NUCLEAR AGENCY
UNDER RDT&E RMSS CODES B323082466 X99QAXVA00039 H2590D
AND B345080462 J24AAXYX98376 H2590D.

OTIC FILE COPY

**Prepared for
Director
DEFENSE NUCLEAR AGENCY
Washington, DC 20305-1000**

[Handwritten mark]

[Handwritten mark]

Destroy this report when it is no longer needed. Do not return to sender.

PLEASE NOTIFY THE DEFENSE NUCLEAR AGENCY, ATTN: STTI, WASHINGTON, DC 20305-1000, IF YOUR ADDRESS IS INCORRECT, IF YOU WISH IT DELETED FROM THE DISTRIBUTION LIST, OR IF THE ADDRESSEE IS NO LONGER EMPLOYED BY YOUR ORGANIZATION.



UNCLASSIFIED

SECURITY CLASSIFICATION OF THIS PAGE

FD-A 105792

REPORT DOCUMENTATION PAGE			Form Approved OMB No. 0704-0188 Exp. Date: Jun 30, 1986	
1a. REPORT SECURITY CLASSIFICATION UNCLASSIFIED		1b. RESTRICTIVE MARKINGS		
2a. SECURITY CLASSIFICATION AUTHORITY		3. DISTRIBUTION / AVAILABILITY OF REPORT Approved for public release; distribution is unlimited.		
2b. DECLASSIFICATION / DOWNGRADING SCHEDULE N/A since Unclassified				
4. PERFORMING ORGANIZATION REPORT NUMBER(S) SSS-R-85-6960		5. MONITORING ORGANIZATION REPORT NUMBER(S) DNA-TR-84-407		
6a. NAME OF PERFORMING ORGANIZATION S-CUBED, A Division of Maxwell Labs, Inc.	6b. OFFICE SYMBOL (If applicable)	7a. NAME OF MONITORING ORGANIZATION Director Defense Nuclear Agency		
6c. ADDRESS (City, State, and ZIP Code) P.O. Box 1620 La Jolla, CA 92038-1620		7b. ADDRESS (City, State, and ZIP Code) Washington, DC 20305-1000		
8a. NAME OF FUNDING / SPONSORING ORGANIZATION	8b. OFFICE SYMBOL (If applicable)	9. PROCUREMENT INSTRUMENT IDENTIFICATION NUMBER DNA 001-80-C-0239 DNA 002-82-C-0031		
8c. ADDRESS (City, State, and ZIP Code)		10. SOURCE OF FUNDING NUMBERS		
		PROGRAM ELEMENT NO 62715H	PROJECT NO X990AXV J24AAXY	TASK NO A X
		WORK UNIT ACCESSION NO. DH999999		
11. TITLE (Include Security Classification) IN SITU STEAM FRACTURE EXPERIMENTS				
12. PERSONAL AUTHOR(S) Peterson, E. W., Lagus, P. L., Wu, H. E.				
13a. TYPE OF REPORT Technical Report	13b. TIME COVERED FROM 820601 TO 841231	14. DATE OF REPORT (Year, Month, Day) 841231	15. PAGE COUNT 130	
16. SUPPLEMENTARY NOTATION This work was sponsored by the Defense Nuclear Agency under RDT&E RMSS Codes B323082466 X99QAXVA00039 H2590D and B345080462 J24AAXYX98376 H2590D.				
17. COSATI CODES			18. SUBJECT TERMS (Continue on reverse if necessary and identify by block number)	
FIELD	GROUP	SUB-GROUP		
14	2		In Situ Steam Generation Steam Diffusion Downhole	
20	11		Material Properties Hydrofracture Tuff	
			Laboratory Tests Steam Fracture	
19. ABSTRACT (Continue on reverse if necessary and identify by block number)				
<p>A downhole steam-generation system has been developed in order to obtain <i>in situ</i> steam fracture propagation data for use in validating the predictive capability of the Los Alamos National Laboratory KRAK code. This system can produce up to 60 moles/second of steam at temperatures (1000°C) and pressures (10 MPa) representative of post-shot cavity conditions. Steam flow tests have been performed at S-CUBED in a 3-meter long by 20-centimeter diameter sand column. In addition, steam fracture experiments have been conducted at the Nevada Test Site in both a low-permeability (E.G., microdarcy range) tunnel bed and high-permeability (e.g., darcy range) paintbrush-type tuff. This paper describes the steam-generation system, the steam-flow and steam-fracture test designs, and all test results.</p>				
20. DISTRIBUTION / AVAILABILITY OF ABSTRACT <input type="checkbox"/> UNCLASSIFIED/UNLIMITED <input checked="" type="checkbox"/> SAME AS RPT <input type="checkbox"/> OTIC USERS		21. ABSTRACT SECURITY CLASSIFICATION UNCLASSIFIED		
22a. NAME OF RESPONSIBLE INDIVIDUAL Betty L. Fox		22b. TELEPHONE (Include Area Code) (202) 325-7042	22c. OFFICE SYMBOL DNA/STTI	

DD FORM 1473, 84 MAR

83 APR edition may be used until exhausted
All other editions are obsolete

SECURITY CLASSIFICATION OF THIS PAGE

UNCLASSIFIED

TABLE OF CONTENTS

Dist Special
A-1

<u>Section</u>	<u>Page</u>
LIST OF ILLUSTRATIONS - - - - -	2
LIST OF TABLES - - - - -	7
1 INTRODUCTION - - - - -	9
2 SYSTEM DESCRIPTION - - - - -	11
2-1 EQUIPMENT DESIGN - - - - -	11
2-2 INSTRUMENTATION AND CONTROL SYSTEMS - - - - -	16
2-3 PRE-FIELD TESTS - - - - -	18
3 TEST RESULTS - - - - -	21
3-1 SAND-COLUMN FLOW TESTS - - - - -	21
3-2 G-TUNNEL TEST - - - - -	24
3-3 P-TUNNEL TESTS - - - - -	34
3-3.1 CS 11+90 Test (SFT No. 2) - - - - -	35
3-3.2 CS 11+24 Test (SFT No. 3) - - - - -	43
3-3.3 CS 11+24 Test (SFT No. 4) - - - - -	51
4 DISCUSSION OF RESULTS - - - - -	56
5 CONCLUSIONS AND RECOMMENDATIONS - - - - -	59
LIST OF REFERENCES - - - - -	61



Appendices

A SITE AND MATERIAL PROPERTIES - - - - -	63
A-1 G-TUNNEL MATERIAL PROPERTIES - - - - -	63
A-2 P-TUNNEL MATERIAL PROPERTIES - - - - -	73
B DETAILED STEAM FRACTURE TEST DATA - - - - -	93
C <u>IN SITU</u> PERMEABILITY TEST ANALYSIS - - - - -	123

LIST OF ILLUSTRATIONS

<u>Figure</u>		<u>Page</u>
1	Adiabatic, constant pressure flame temperature ($\Delta H \equiv 0$) for $2H_2 + O_2 + nH_2O(l) \rightarrow (n+2) H_2O$ ideal gas equation of state assumed - - - - -	12
2	Schematic showing the steam-generation system - - - - -	13
3	Schematic showing installation of the steam-generation system in the steam-fracture source hole - - - - -	14
4	Schematic showing the steam supply manifold exit geometries for the low-flowrate and high-flowrate steam generation system - - - - -	15
5	Schematic showing complete steam fracture test system - - -	17
6	Schematic showing geometry of sand column test apparatus - -	22
7	Sand-column, steam-source region pressure, temperature, and flowrate - - - - -	23
8	Sand-column test pressure distribution history - - - - -	25
9	Sand-column test temperature histories within the chamber and at positions T3, T5, and T7 shown on Figure 6 - - - - -	26
10	Sand-column test temperature histories at positions T1, T2, T4, T6, and T8 shown on Figure 6 - - - - -	27
11	G-Tunnel steam-fracture test layout - - - - -	29
12	Schematic showing the U12g steam fracture experiment hole layout in the U12g RS14 drift mineback - - - - -	30
13	G-Tunnel test source-region pressure, temperature, and flowrate histories - - - - -	32
14	Pressure <u>versus</u> time history recorded in the diagnostic holes during the G-Tunnel steam fracture test - - - - -	33
15	Schematic showing the U12p steam fracture experiment (SFT No. 2) hole layout at CS 11+90 - - - - -	36

LIST OF ILLUSTRATIONS (Continued)

<u>Figure</u>	<u>Page</u>
16	Source region pressure, temperature, and steam flowrate histories during the P-Tunnel CS 11+90 steam-fracture experiment (SFT No. 2) - - - - - 39
17	Initial source region pressure history during the P-Tunnel CS 11+90 steam fracture experiment (SFT No. 2) - - - - - 40
18	Pressure vs. time history recorded in the diagnostic holes during the P-Tunnel CS 11+90 steam fracture experiment (SFT No. 2) - - - - - 41
19	Schematic showing the U12p steam fracture experiment (SFT No. 3 and No. 4) hole layout at CS 11+24 - - - - - 45
20	Source region pressure and water flowrates during the P-Tunnel CS 11+24 steam fracture experiment (SFT No. 3) - - - 48
21	Pressure versus time history recorded in the diagnostic holes during the P-Tunnel CS 11+24 steam fracture experiment (SFT No. 3) - - - - - 49
22	Source region pressure, temperature, and steam flowrate during the P-Tunnel CS 11+24 steam fracture experiment (SFT No. 4) - - - - - 53
23	Pressure versus time history recorded in the diagnostic holes during the P-Tunnel CS 11+24 steam fracture experiment (SFT No. 4) - - - - - 54
24	Diagnostic hole signal arrival times plotted as a function of distance from the source region - - - - - 57
A-1	Mean normal stress <u>versus</u> volumetric strain for sample taken at the 9.63 m to 9.97 m depth in U12g tunnel steam fracture hole No. 1 - - - - - 67
A-2	Mean normal stress <u>versus</u> volumetric strain for sample taken at the 9.81 m to 10.1 m depth in U12g tunnel steam fracture hole No. 2 - - - - - 68

LIST OF ILLUSTRATIONS (Continued)

<u>Figure</u>	<u>Page</u>
A-3	Mean normal stress <u>versus</u> volumetric strain for sample taken at the 9.54 m to 9.85 m depth in U12g tunnel steam fracture hole No. 4 - - - - - 69
A-4	Stress difference <u>versus</u> confining pressure for sample taken at the 9.63 m to 9.97 m depth in U12g tunnel steam fracture hole No. 1 - - - - - 70
A-5	Stress difference <u>versus</u> confining pressure for sample taken at the 9.81 m to 10.1 m depth in U12g tunnel steam fracture hole No. 2 - - - - - 71
A-6	Stress difference <u>versus</u> confining pressure for sample taken at the 9.54 m to 9.85 m depth in U12g tunnel steam fracture hole No. 4 - - - - - 72
A-7	Uniaxial strain test results for sample taken at 4.71 m to 4.75 m depth in hole U12p UG No. 2 at CS 11+90 - - - - - 83
A-8	Mean normal stress <u>versus</u> volumetric strain for sample taken at the 5.55 m to 5.91 m depth in hole U12p UG No. 2 at CS 11+90 - - - - - 84
A-9	Mean normal stress <u>versus</u> volumetric strain for sample taken at the 6.74 m to 7.04 m depth in hole U12P UG No. 2 at CS 11+90 - - - - - 85
A-10	Stress difference <u>versus</u> confining pressure for sample taken from hole U12p UG No. 2 located at CS 11+90 - - - - - 86
A-11	Unconfined compression test results for sample taken at the 4.51 m to 4.75 m depth in hole U12p UG No. 2 located at CS 11+90 - - - - - 87
A-12	Unconfined compression test results for sample taken at the 5.55 m to 5.91 m depth in hole U12p UG No. 2 located at CS 11+90 - - - - - 88
A-13	Unconfined compression test results for sample taken at the 6.74 m to 7.04 m depth in hole U12p UG No. 2 located at CS 11+90 - - - - - 89

LIST OF ILLUSTRATIONS (Continued)

<u>Figure</u>		<u>Page</u>
B-1	G-tunnel steam fracture experiment (SFT No. 1) diagnostic hole "A" pressure history - - - - -	94
B-2	G-tunnel steam fracture experiment (SFT No. 1) diagnostic hole "B" pressure history - - - - -	95
B-3	G-tunnel steam fracture experiment (SFT No. 1) diagnostic hole "1" pressure history - - - - -	96
B-4	G-tunnel steam fracture experiment (SFT No. 1) diagnostic hole "2" pressure history - - - - -	97
B-5	G-tunnel steam fracture experiment (SFT No. 1) diagnostic hole "3" pressure history - - - - -	98
B-6	G-tunnel steam fracture experiment (SFT No. 1) diagnostic hole "4" pressure history - - - - -	99
B-7	G-tunnel steam fracture experiment (SFT No. 1) diagnostic hole "C" pressure history - - - - -	100
B-8	P-tunnel CS 11+90 steam fracture experiment (SFT No. 2) diagnostic hole "A" pressure history - - - - -	101
B-9	P-tunnel CS 11+90 steam fracture experiment (SFT No. 2) diagnostic hole "B" pressure history - - - - -	102
B-10	P-tunnel CS 11+90 steam fracture experiment (SFT No. 2) diagnostic hole "1" pressure history - - - - -	103
B-11	P-tunnel CS 11+90 steam fracture experiment (SFT No. 2) diagnostic hole "2" pressure history - - - - -	104
B-12	P-tunnel CS 11+90 steam fracture experiment (SFT No. 2) diagnostic hole "3" pressure history - - - - -	105
B-13	P-tunnel CS 11+90 steam fracture experiment (SFT No. 2) diagnostic hole "4" pressure history - - - - -	106
B-14	P-tunnel CS 11+90 steam fracture experiment (SFT No. 2) diagnostic hole "C" pressure history - - - - -	107

LIST OF ILLUSTRATIONS (Concluded)

<u>Figure</u>	<u>Page</u>
B-15 P-tunnel CS 11+24 steam fracture experiment (SFT No. 3) diagnostic hole "A" pressure history - - - - -	108
B-16 P-tunnel CS 11+24 steam fracture experiment (SFT No. 3) diagnostic hole "B" pressure history - - - - -	109
B-17 P-tunnel CS 11+24 steam fracture experiment (SFT No. 3) diagnostic hole "1" pressure history - - - - -	110
B-18 P-tunnel CS 11+24 steam fracture experiment (SFT No. 3) diagnostic hole "2" pressure history - - - - -	111
B-19 P-tunnel CS 11+24 steam fracture experiment (SFT No. 3) diagnostic hole "3" pressure history - - - - -	112
B-20 P-tunnel CS 11+24 steam fracture experiment (SFT No. 3) diagnostic hole "4" pressure history - - - - -	113
B-21 P-tunnel CS 11+24 steam fracture experiment (SFT No. 3) diagnostic hole "C" pressure history - - - - -	114
B-22 P-tunnel CS 11+24 steam fracture experiment (SFT No. 4) diagnostic hole "A" pressure history - - - - -	115
B-23 P-tunnel CS 11+24 steam fracture experiment (SFT No. 4) diagnostic hole "B" pressure history - - - - -	116
B-24 P-tunnel CS 11+24 steam fracture experiment (SFT No. 4) diagnostic hole "1" pressure history - - - - -	117
B-25 P-tunnel CS 11+24 steam fracture experiment (SFT No. 4) diagnostic hole "2" pressure history - - - - -	118
B-26 P-tunnel CS 11+24 steam fracture experiment (SFT No. 4) diagnostic hole "3" pressure history - - - - -	119
B-27 P-tunnel CS 11+24 steam fracture experiment (SFT No. 4) diagnostic hole "4" pressure history - - - - -	120
B-28 P-tunnel CS 11+24 steam fracture experiment (SFT No. 4) diagnostic hole "C" pressure history - - - - -	121

LIST OF TABLES

<u>Table</u>	<u>Page</u>
1	37
<p>In situ relative gas permeability values determined from low pressure (e.g., .12-.15 MPa) gas tests conducted in the U12p steam fracture source and diagnostic holes located at CS 11+90 (SFT No. 2) - - - - -</p>	
2	46
<p>in situ relative gas permeability values determined from low pressure (e.g., .10-.15 MPa) gas tests conducted in the U12p steam fracture source and diagnostic holes located at CS 11+24 (SFT No. 3 and No. 4) - - - - -</p>	
A-1	65
<p>Physical properties, permanent volume compactions, and ultrasonic wave velocities of tuff from U12g holes No. 1, 2, and 4, steam fracture test - - - - -</p>	
A-2	66
<p>Hydrofracture data and inferred in situ stresses determined from Sandia hydrofracture test holes in the vicinity of the U12g RS-14 drift mineback - - - - -</p>	
A-3	74
<p>Physical properties, permanent volume compactions, unconfined compressive strengths, and ultrasonic wave velocities of tuff from U12p UG No. 2 located at CS 11+80 - - - - -</p>	
A-4	75
<p>Air and liquid permeability of oven dried and native state core taken from Hole U12p UG No. 2 located at CS 15+80 - - - - -</p>	
A-5	76
<p>Sample dimensions and weights before and after exposing U12p source hole No. 3 (CS 11+24) tuff (12.4 m to 12.8 m depth) to 1000°C for 30, 60, and 300 seconds - - - - -</p>	
A-6	77
<p>Permeabilities and moisture contents obtained from U12p source hole No. 3 (CS 11+24) tuff (12.4-12.8 meter depth) exposed to 1000°C for 30, 60, and 300 seconds - - - - -</p>	
A-7	81
<p>Results of post-steam fracture flow test conducted in the 10 centimeter diameter by 46 centimeter long P-Tunnel steam source region located at CS 11+90 - - - - -</p>	
A-8	82
<p>Tensile and unconfined compression strengths for core taken from U12p UG No. 2 located at CS 15+80 - - - - -</p>	

SECTION 1 INTRODUCTION

Cavity gas leakage along steam-driven fractures has long been recognized as one potential failure mechanism which may compromise the containment of underground nuclear tests. Associated fracture models are complex, as fluid condensation, heat transfer, fluid diffusion, in situ stress, rock strength, and rock failure phenomena all play important roles in the initiation, propagation, and termination of such fractures. Although a number of models have been developed, there is little data available describing steam-driven fractures. The objectives of this study have, therefore, been to generate data which can serve as a base for model development and validation.

Three types of tests have been performed. They involved steam flow through a dry sand column, and steam fracture at the Nevada Test Site (NTS) in both G-Tunnel and P-Tunnel tuffs. All tests were tailored to simulate containment phenomena in a manner consistent with models incorporated within the Los Alamos National Laboratory (LANL) numerical KRAK code.

The sand-column flow test was designed to simulate condensation, heat transfer, and fluid diffusion mechanisms without introducing the complexities associated with fracturing. The G-Tunnel test examined fracture initiation and propagation phenomena in a low-permeability tunnel-bed tuff using simulated post-shot cavity conditions. Steam fracture propagation and termination effects were examined in the high-permeability paintbrush-type tuff found in P-Tunnel. All tests were performed using downhole steam generation systems capable of producing steam at pressures and temperatures up to 10 MPa and 1000°C, respectively.

In the report which follows, the steam generation system is described in Section 2. Results of the sand column, G-Tunnel, and P-Tunnel tests are given in Section 3. These results are discussed in

Section 4. Conclusions and recommendations are presented in Section 5. For completeness, site and material property descriptions are presented in Appendix A, detailed steam fracture data are shown in Appendix B, and the analysis used to interpret the low pressure in situ permeability test data is given in Appendix C.

Work described in this paper involved a number of organizations and numerous people. It was sponsored by DNA Field Command, Albuquerque. S-CUBED developed, designed, fabricated, and fielded the downhole, steam-generation system. In addition, S-CUBED was responsible for obtaining all sand-column data and all data within the steam source region. The G-Tunnel and P-Tunnel diagnostic hole data were obtained by Sandia National Laboratories (SNL). Field operations, including selection and preparation of the test sites, were carried out under the direction of the DNA Field Command Test Construction Division. Site examination and material property tests were performed by Fennix and Scisson geologists and TerraTek, respectively.

SECTION 2 SYSTEM DESCRIPTION

The steam-generation system produces high-pressure, high-temperature steam from water-cooled combustion of hydrogen and oxygen as illustrated on Figure 1. This combustion and evaporation process occurs within a borehole at the position where the steam fracture is to be initiated. The steam-generation system can provide up to 60 moles/second of the high-pressure (10 MPa), superheated (1000°C) steam required to simulate post-shot cavity conditions.

The steam-generation system design is described in Section 2-1. Its instrumentation and control features are reviewed in Section 2-2. General results of numerous pre-field tests are summarized in Section 2-3.

2-1 EQUIPMENT DESIGN.

A schematic of the steam-generation system is shown on Figure 2. This system is composed of four major components consisting of the steam supply manifold and oxygen, hydrogen, and water supply systems. During testing, the steam supply manifold is installed within the test borehole as shown on Figure 3. The exit manifolds shown on Figure 4 serve to provide the required water mist and distributed gas sources necessary to force hydrogen/oxygen/water mixing, combustion, and vaporization.

The water flow system consists of a reservoir filled with distilled water, and a high-pressure nitrogen supply used to drive a very steady flow from the reservoir at some pre-determined flowrate and pressure. Water flowrates are monitored using a turbine flowmeter.

Separate hydrogen and oxygen supplies are used, as shown on Figure 2. However, these systems are maintained at a common line pressure using nitrogen to operate the control sides of dome regulators located on the oxygen and hydrogen lines. The nitrogen pressure is then

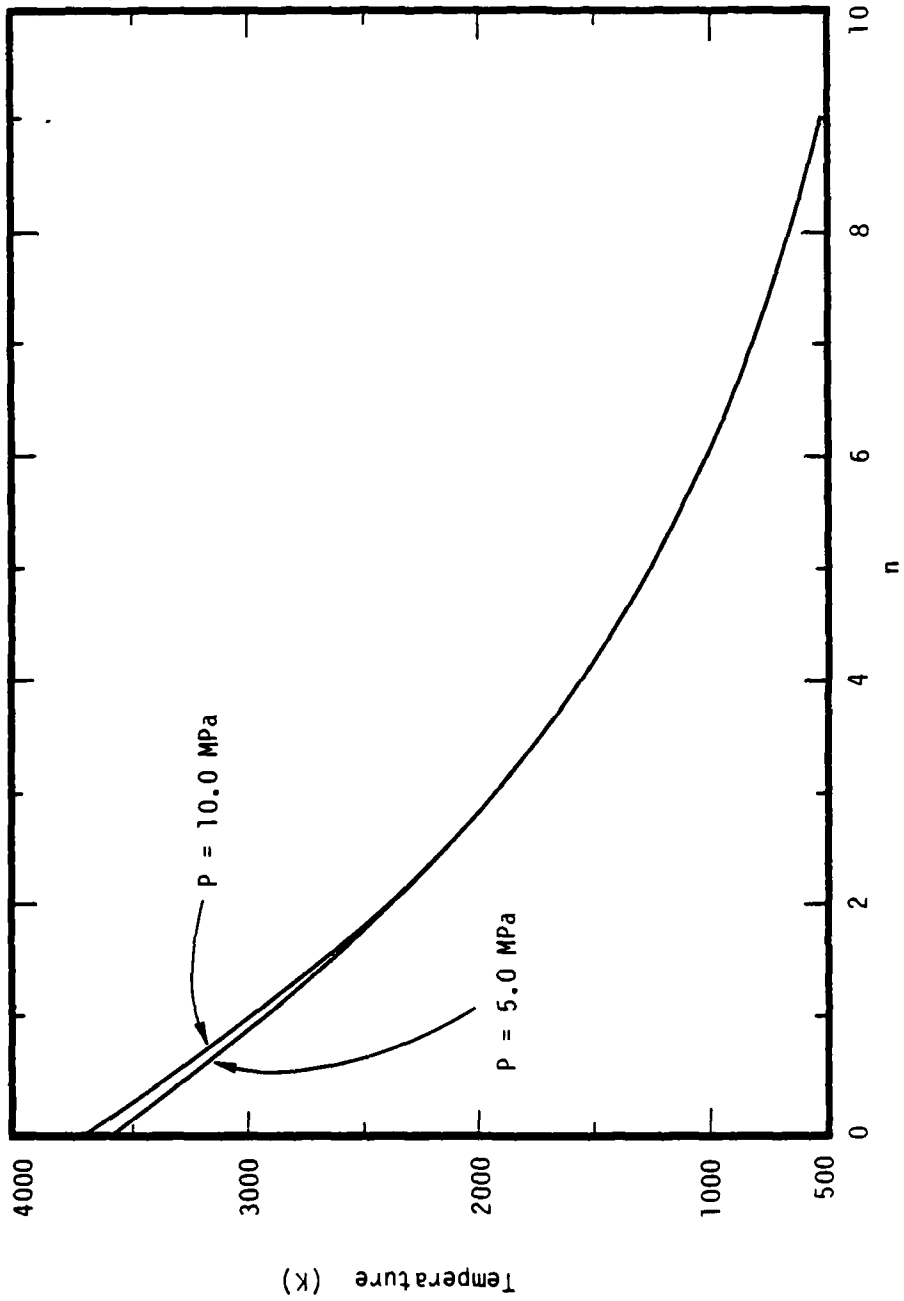


Figure 1. Adiabatic, constant pressure flame temperature ($\Delta H \equiv 0$) for $2\text{H}_2 + \text{O}_2 + n\text{H}_2\text{O}(g) \rightarrow (n+2)\text{H}_2\text{O}$ ideal gas equation of state assumed.

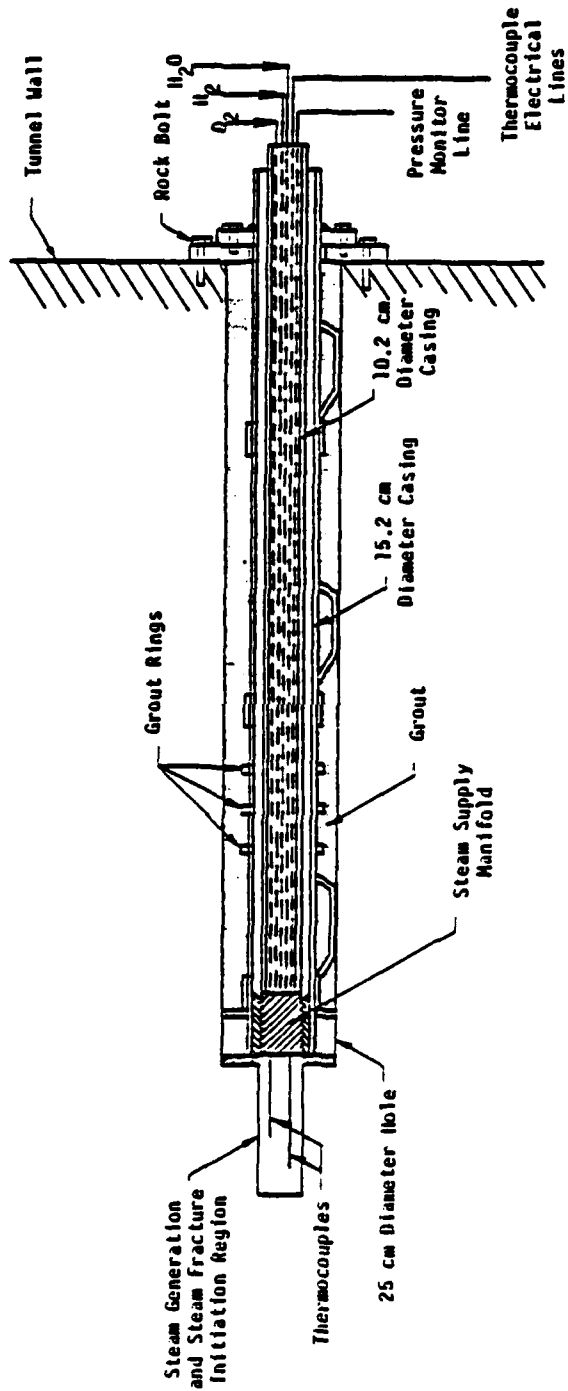
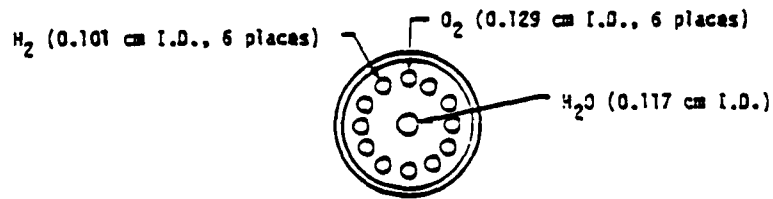
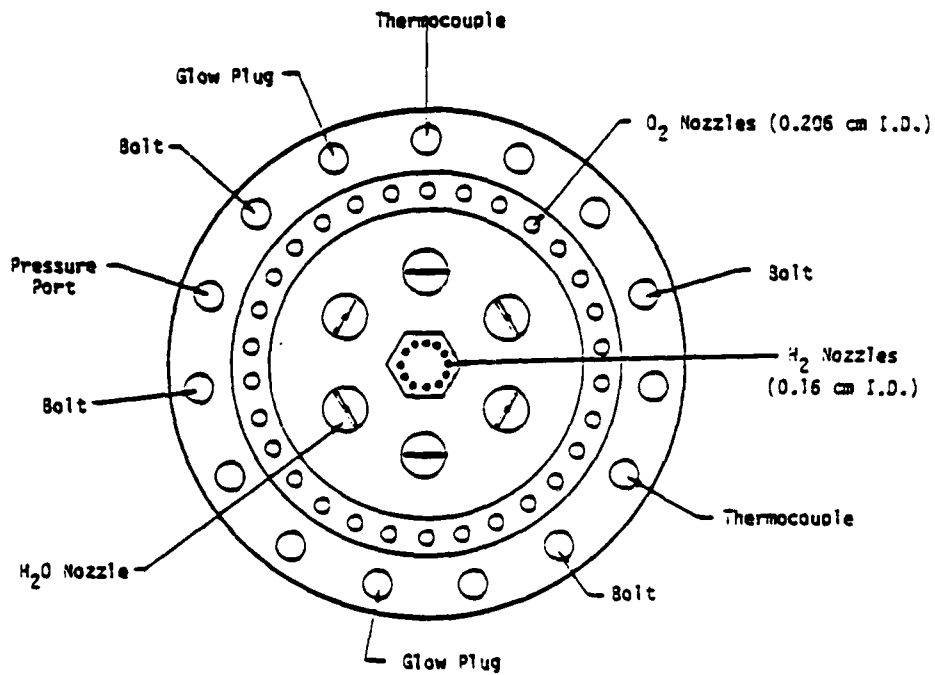


Figure 3. Schematic showing installation of the steam-generation system in the steam-fracture source hole.



a. Downstream View of Low-Flowrate Manifold.



b. Downstream View of High-Flowrate Manifold.

Figure 4. Schematic showing the steam supply manifold exit geometries for the low-flowrate and high-flowrate steam generation system.

regulated to provide the desired line pressures. Flowrates are determined based on pressure drops measured across pre-set metering valves. Check valves are included in all lines to prevent backflow.

Two steam supply exit manifolds have been used. The initial design shown on Figure 4a was used for the low-flowrate (≤ 10 moles/second) sand-column and G-Tunnel tests. A second exit manifold, shown on Figure 4b, was developed to provide the 60 moles/second flows required for the P-Tunnel tests.

The steam-generation system is installed in the borehole as illustrated on Figure 3. First, a 15 centimeter diameter section of casing is installed and grouted into the borehole, leaving only the fracture-source region open. A steam supply manifold mounted in a 10-centimeter diameter pipe is then inserted into a landing sub mounted in the 15-centimeter diameter pipe. This 10-centimeter diameter casing contains the gas, water, and pressure-sensing lines, as well as thermocouple cables.

A general schematic of the entire system as it was configured for the G-Tunnel test is shown on Figure 5. The complete system includes the monitor and control module; nitrogen, oxygen, hydrogen, and water supplies; valves, regulators, and flowmeter devices; and, the steam-fracture manifold.

2-2 INSTRUMENTATION AND CONTROL SYSTEMS.

During a test, pressures and temperatures are monitored within the steam fracture initiation region shown on Figure 3. In addition, the hydrogen and oxygen line pressures are measured upstream and downstream of the flow control valves in order to determine the respective flowrates. Water flow is monitored using a turbine flowmeter. All data plus the elapsed test time are displayed on a control panel to inform the operator of the current system state. These data are also recorded on magnetic tape and/or stripcharts.

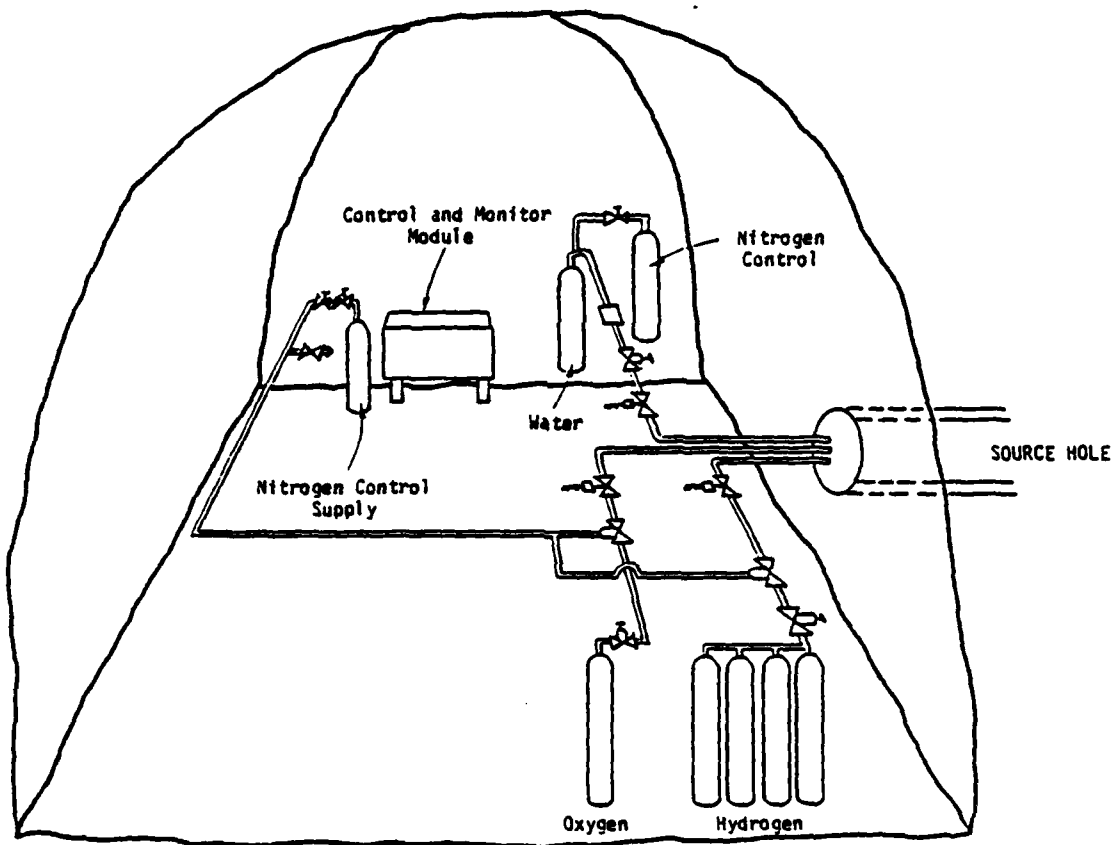


Figure 5. Schematic showing complete steam fracture test system.

Two flow options are available. One provides an approximately constant downhole temperature; the other, an approximately constant downhole pressure. In the first, a servo control automatically adjusts the water flow to maintain a constant downhole temperature. In the second, all metering valve settings and upstream control pressures are fixed. However, actual flowrates are approximately inversely proportional to the downstream pressure. As a result, a fairly-constant, steam-source region pressure is maintained. The temperature feedback control system was used for the sand-column tests with marginal success. It was found that the thermocouple and motor-driven valve responses were too slow to maintain a constant steam-source temperature. As a result, fixed flow settings were used during the G-Tunnel and P-Tunnel tests.

Test operation is controlled by the operator's "dead-man" switch. When this switch is depressed, the elapsed time counter is triggered and solenoid valves on the water and nitrogen lines energized. Nitrogen then pressurizes the dome regulators which, in turn, allow flow of oxygen and hydrogen. When de-energized, the dome regulators are unloaded by diverting the nitrogen through a vent. In the event of power failure or switch opening, all solenoid valves close and the hydrogen, oxygen, and water flows terminate.

2-3 PRE-FIELD TESTS.

The steam generation system was tested extensively at the S-CUBED operated Green Farm Test Site. Objectives of these tests were to develop the system, generate the necessary operation skills required for fielding, and to determine the hydrogen, oxygen, and water flow settings required to produce the desired field test pressure and temperature conditions. General results of these tests will be described in the following paragraphs.

Preliminary steam generation system tests showed that continuous downhole temperature control was not feasible because:

- The thermocouple/valve-control response was slow compared to the rate at which the flame temperature changed with water addition,
- The thermocouples in the combustion region were continually subject to changing temperatures as a result of an unsteady flame position, and
- Run-to-run differences in measured temperature occurred (even with identical downhole pressures)--again suggesting a variability in flame position.

Typical variations in the measured downhole temperature are represented by the G-Tunnel and P-Tunnel test results.

The temperature measurement problem was recognized during the initial steam-generation system development tests. Since solutions to this problem are time-consuming and expensive, emphasis was placed on performing the tests described in this report. It is, therefore, recommended that all associated analysis use the measured downhole pressure and calculated energy associated with the hydrogen/oxygen/water combustion/vaporization process as initial conditions.

Field simulation tests were also performed. The in situ source region was modeled by attaching a section of steel oil field tubing to the steam-generation system shown on Figure 3. This tubing possessed a diameter and length equivalent to that of the in situ source region. Diffusion or fracture flow from the source region was simulated by placing a number of small (approximately 0.2-centimeter diameter) holes around the tubing circumference. The steam-generation system performance was assumed satisfactory if the source region pressure equaled that calculated based on the hydrogen/oxygen/water flow and energy values.

Uniformly-low temperatures were measured during the field simulation tests. Measured temperatures ranged from 0°C (thermocouples burned off) to about two-thirds of the calculated value. The low temperature reading is partially the result of heat transfer to the tubing which makes up the pressure chamber. In addition, the variable temperature readings may result because of the aforementioned unsteady flow conditions.

A number of tests were conducted to verify ignition in the 10-centimeter diameter by 46-centimeter long P-tunnel (SFT No. 2) source region. During these tests, which were run using the field test flow conditions, ignition always occurred. In fact, ignition always occurred during tests conducted at the Green Farm Test Site.

Video records of the simulated P-Tunnel test confirm that immediate ignition occurs. They also show that the quantity of steam flowing from the circumferential holes varies with time. This confirms previous results which suggested non-steady flow within the steam-generation/vaporization region.

SECTION 3 TEST RESULTS

3-1 SAND-COLUMN FLOW TESTS.

A sand-column steam-flow test was performed to simulate steam condensation, heat transfer, and diffusion effects in a setting which was independent of crack initiation, propagation, and termination phenomena. Results of this test were transmitted to LANL where they have been used for model validation studies (Reference 1).

A schematic of the sand-column geometry, pressure, and temperature instrumentation is shown on Figure 6. This column was filled with Overton sand having a 48-percent porosity, 37-darcy permeability, and an approximate 0.3-percent saturation. The steam-source region consisted of a 61-centimeter long by 19.5-centimeter diameter plenum located directly between the steam supply manifold and sand surface. Gas and water mixing, combustion, and vaporization take place within this void region. During this test, the steam generator controls were set to provide 2.7 moles/second of steam at a pressure and temperature of 1.5 MPa and 650°C, respectively.

The sand-column test steam-source region pressure, temperature, and flowrate are shown on Figure 7. These data were taken from digital recordings with the data points plotted every 15 seconds. Variations in the temperature and flowrate, therefore, do not reflect the actual frequency response, but rather illustrate the inability of the temperature/water flow feedback control system to maintain a constant steam-generation temperature. The chamber pressure is seen to slowly rise to the 1.48 MPa level, with the temperature and flowrate oscillating around the 500°C and 2.5 moles/second values, respectively. The lower, measured chamber temperature, as compared to the design temperature, resulted primarily from heat loss to the structural apparatus and to the liner. Some uncertainty in the chamber temperature reading also exists because of the non-uniform conditions prevalent within the combustion/vaporization region.

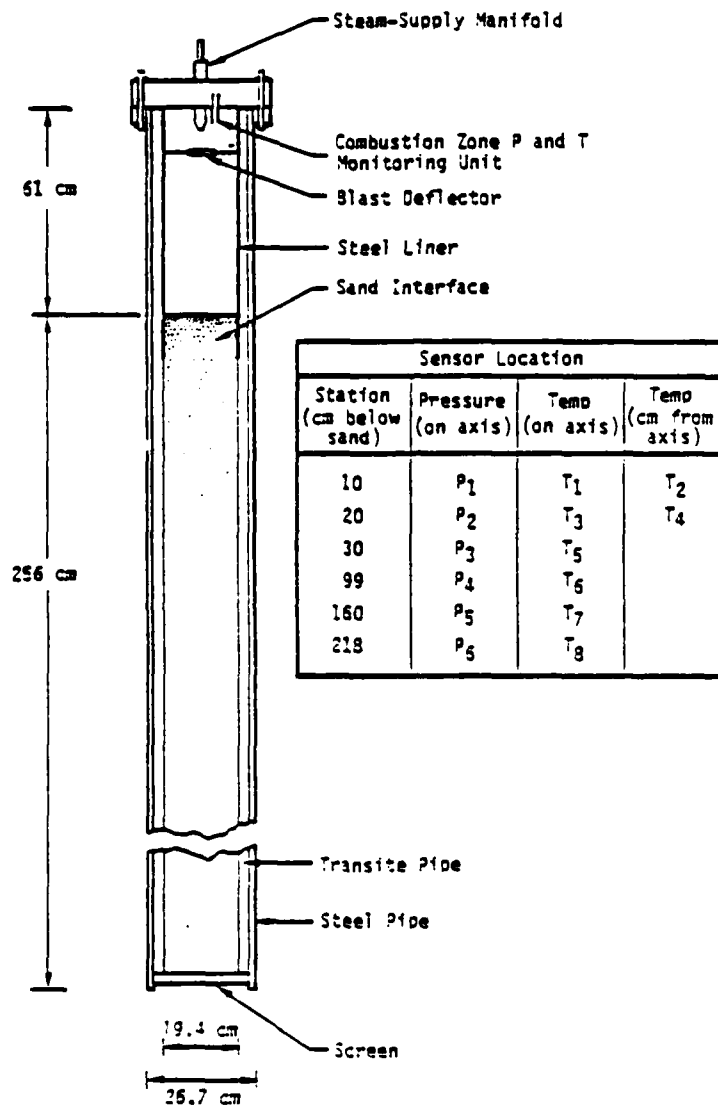


Figure 6. Schematic showing geometry of sand-column test apparatus.

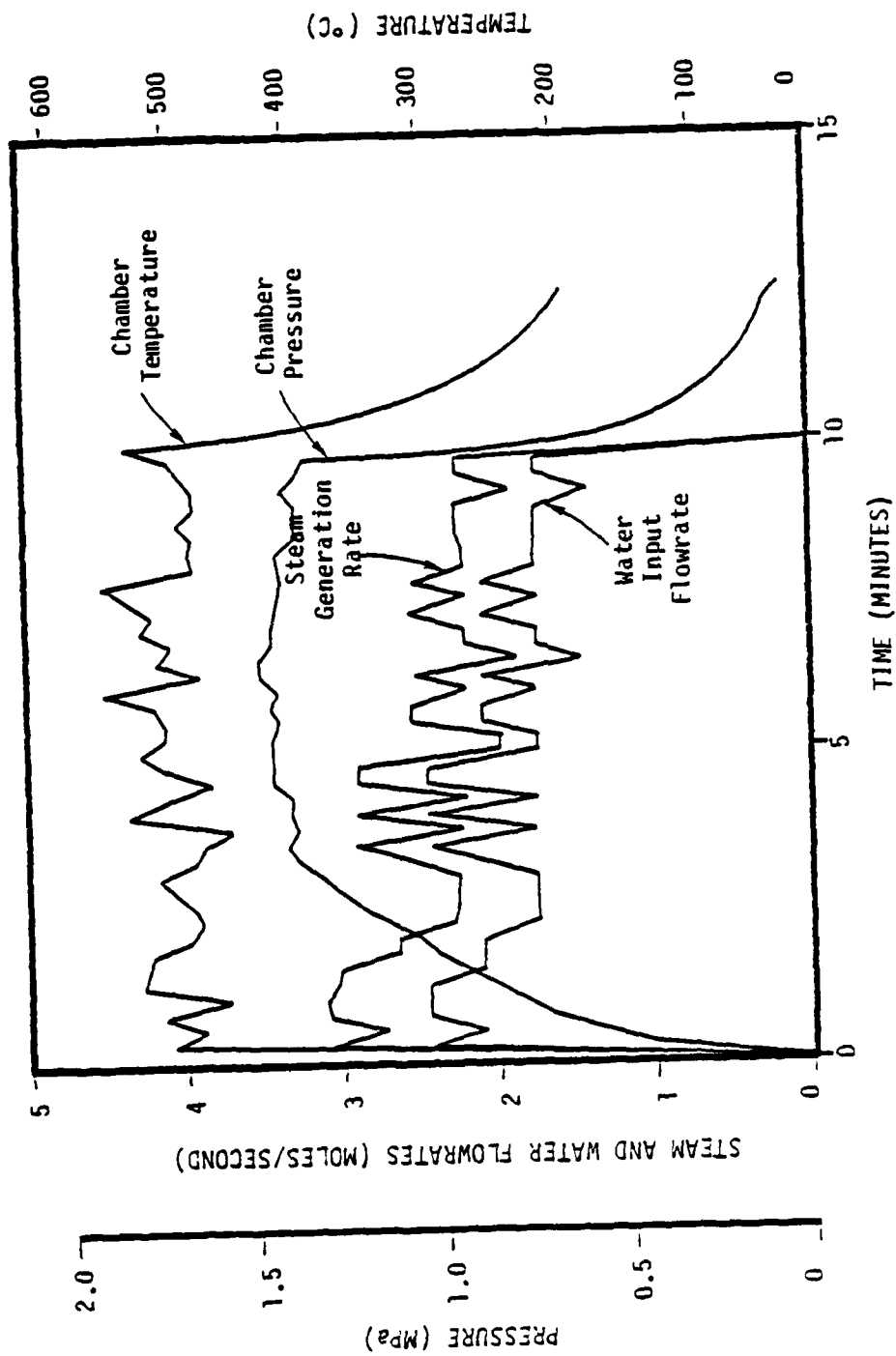


Figure 7. Sand-column, steam-source region pressure, temperature, and flowrate.

The pressure distribution within the sand column is shown on Figure 8. As the initially-unsaturated column fills with fluid and steam, the pressure is seen to gradually rise to an approximate steady-state value within the first 5.0 minutes of the test.

Temperature histories within the sand column are shown on Figures 9 and 10. It is of interest to examine one of these histories in some detail. Consider the response T5 shown on Figure 9. For the first approximately 30 seconds there is no response. A water slug whose temperature increases rapidly with time is then observed. At about 1.0 minute, water at position T5 has approached the saturation temperature at the local pressure and, as indicated by the knee and first relatively-flat portion on the data curve, the flow passing T5 is in the mixed-phase region. After about 4.5 minutes, the flow consists of super-heated steam and the temperature rapidly rises to that within the chamber region.

Flow at the top of the sand column is non-uniform. Temperatures T1 and T2 on Figure 10 show that at a depth of 10 centimeters into the sand, the center of the column is cooler than the outside. A similar non-uniformity may exist within the plenum region. This disparity between the centerline and off-center temperatures rapidly disappears, as indicated by the T3 (Figure 9) and T4 (Figure 10) data at the 20-centimeter depth.

The sand-column test results provide both pressure and temperature data for use in validation of multi-phase flow models describing condensation/vaporization, heat-transfer, and fluid/vapor diffusion effects. These data show flow of fluid, multi-phase steam, and saturated steam through an initially dry, ambient-temperature, sand column.

5-2 G-TUNNEL TEST

The first steam fracture test (i.e. SFT No. 1) was conducted at NTS in G-Tunnel on May 26, 1982. The test objective was to obtain data on

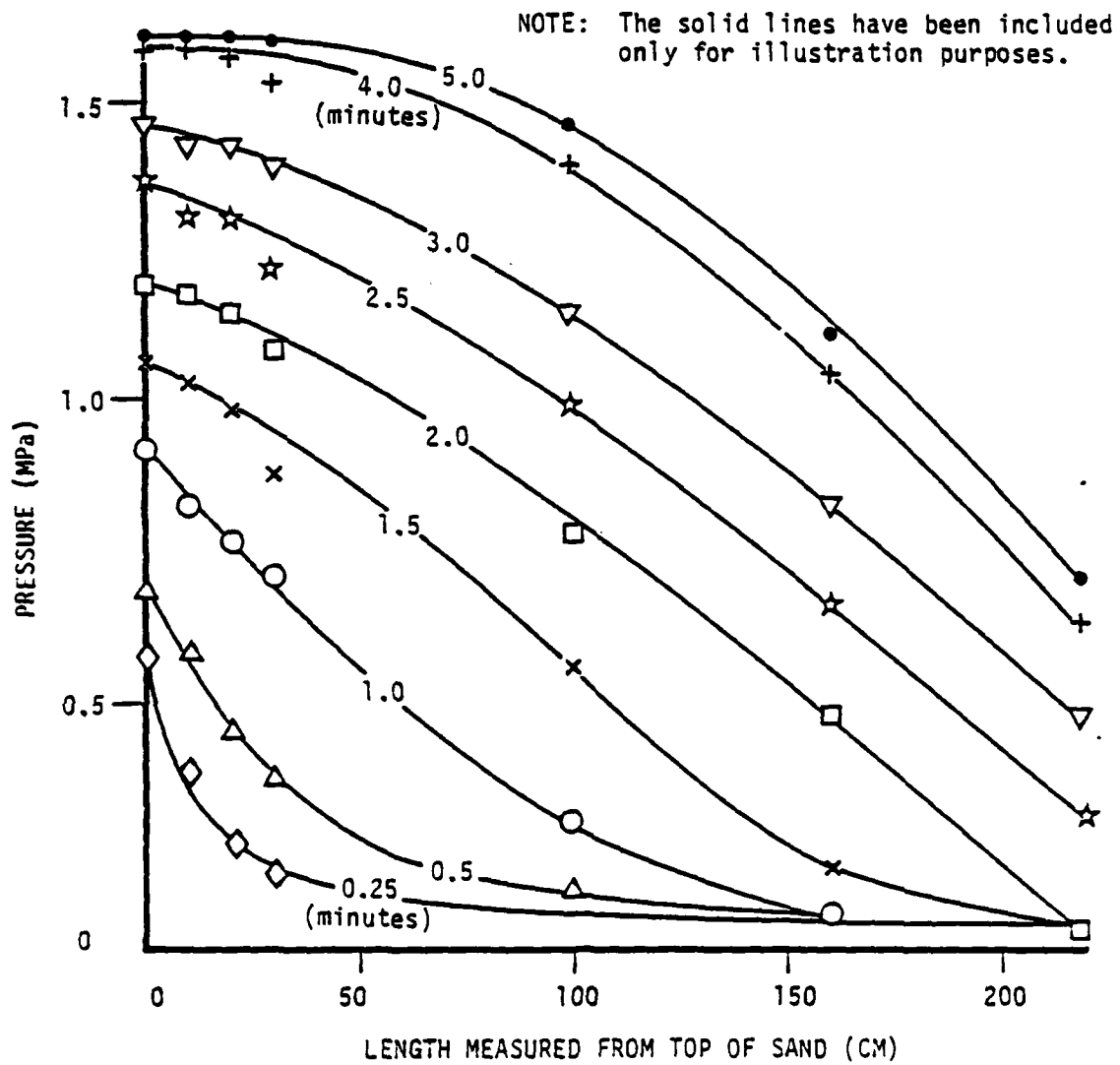


Figure 8. Sand-column test pressure distribution history.

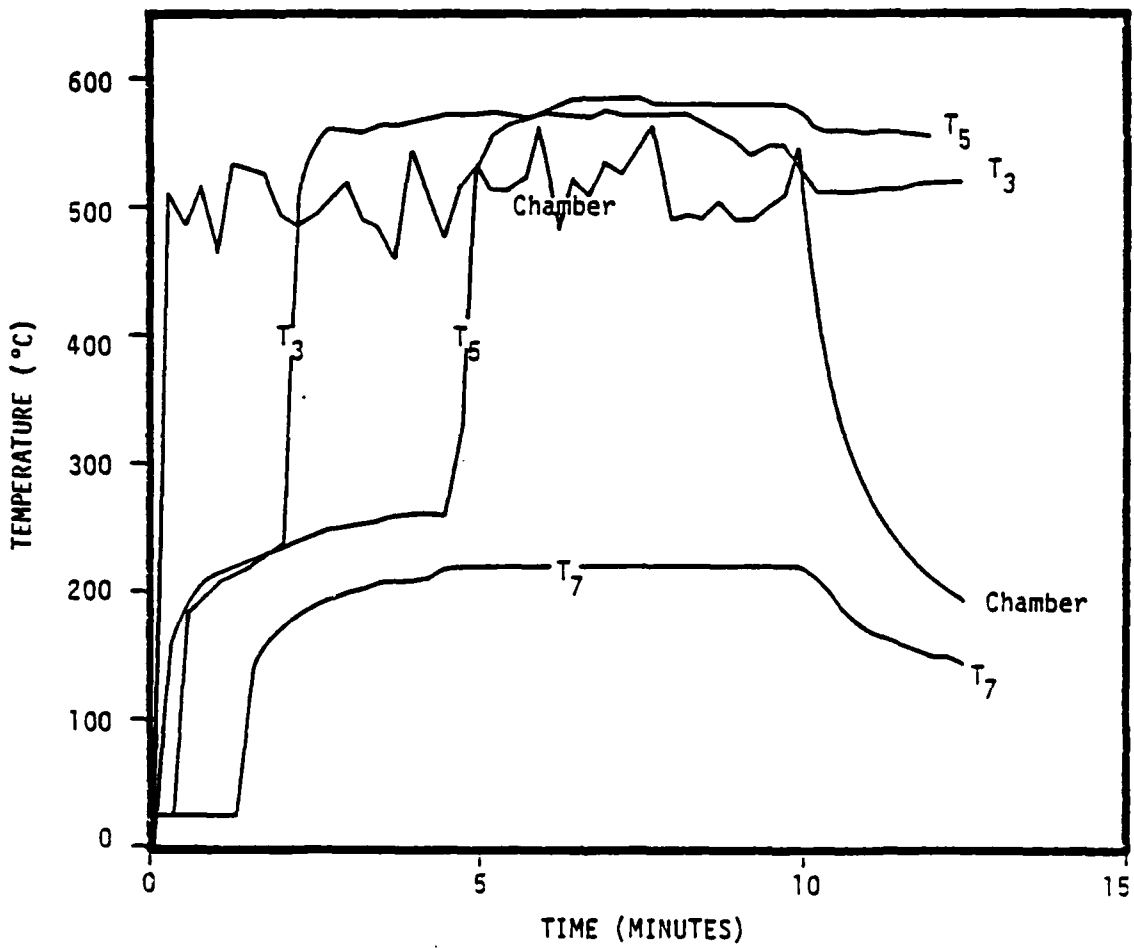


Figure 9. Sand-column test temperature histories within the chamber and at positions T3, T5, and T7 shown on Figure 6.

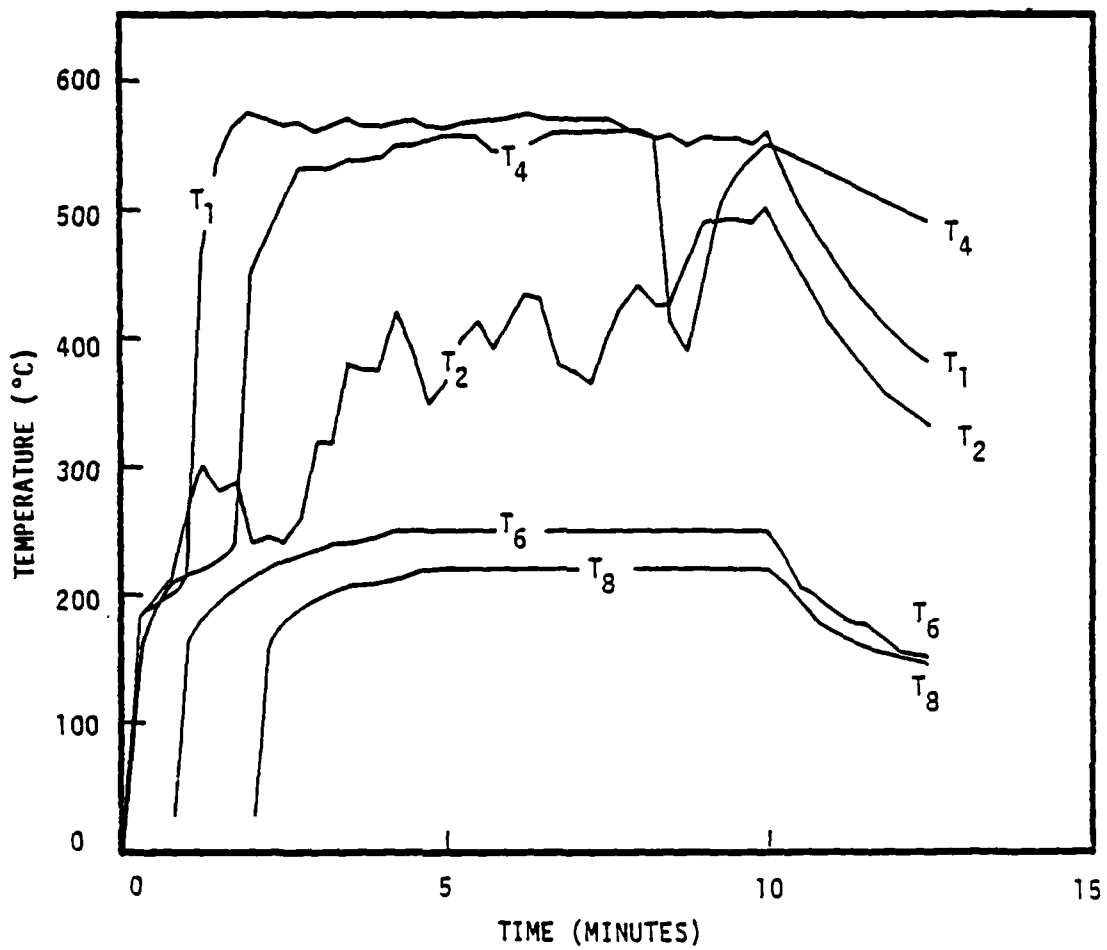


Figure 10. Sand-column test temperature histories at positions T1, T2, T4, T6, and T8 shown on Figure 6.

steam fracture initiation and propagation in a typical low-permeability, welded, tunnel-bed tuff. Results of this test were transmitted to LANL, where they have been used for model validation studies (Reference 1).

This test was conducted in the G-Tunnel RS-14 drift in the middle of a 2.5-meter thick layer of red ashfall tuff, at a depth which exhibited a 8.2 MPa overburden pressure (Reference 2). Laboratory tests performed by TerraTek on cores taken at this location had an average 40 percent porosity, 94.1 percent saturation level, and a calculated 2.3 percent air void. Permeability tests performed on these core samples, using a brine solution with the sample maintained at a 1.4 MPa overburden stress and 0.69 MPa pore fluid pressure, resulted in an average 7.8 microdarcy fluid permeability. Detailed site and material properties information is provided in Appendix A.

Prior to performing the steam fracture test, a short, low-pressure, in situ, air permeability test was performed from the steam fracture source region. During an 8-minute period, there was no observed pressure decay from a shut-in pressure of 0.2 MPa. Within the accuracy of the instrumentation, this implies a relative gas permeability of less than 100 microdarcies.

A schematic of the test layout is shown on Figure 11. Details of the source and diagnostic hole layouts are given on Figure 12. The source region was located at a depth of 10 meters from the working face. The source and diagnostic holes were located at 0.5-meter spacings, with diagnostic hole "B" located directly above the source hole.

The steam-generation system was installed within the source hole shown on Figure 12 in the manner illustrated on Figure 3. The steam-source region consisted of the open portion (approximately one-third of the volume was filled with grout) of a 25-centimeter diameter by 112-centimeter long section located at the bottom of the hole. Hydrogen/oxygen/water mixing, combustion, and vaporization (i.e., steam generation) occurred within this region.

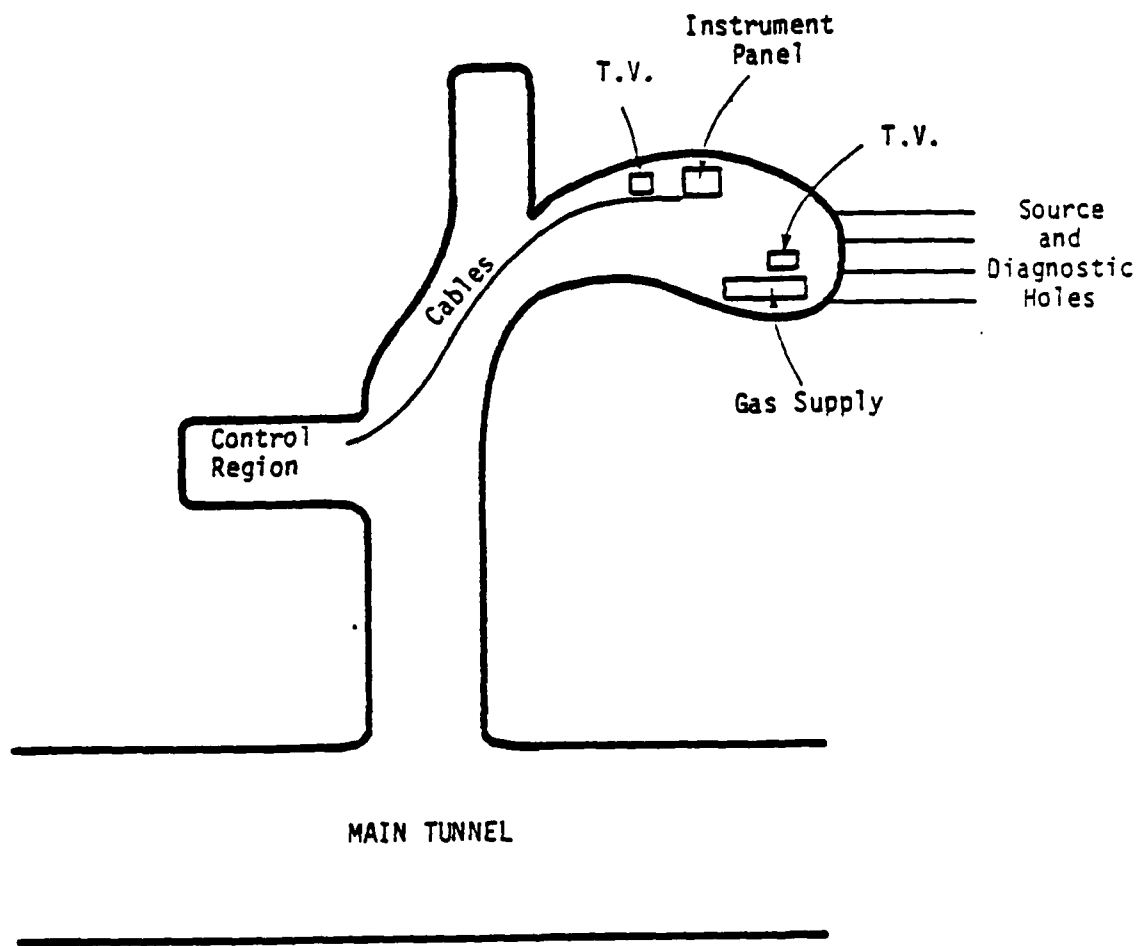


Figure 11. G-Tunnel steam-fracture test layout.

During the test, straddle packers were installed in diagnostic holes 1, 2, 3, and 4 to isolate a 3.0-meter interval centered around the source region. Holes A, B, and C were shut-in at the tunnel face. Prior to initiation of the steam-fracture test, the enclosed regions of the diagnostic holes were water-filled at low pressure to ensure immediate recognition of a pressure signal associated with any fracture penetration.

Test results are shown on Figures 13 and 14. The initial breakdown pressure of 8.1 MPa occurs at 8.4 seconds and is seen on Figure 13 to be followed by an approximate 6.9 MPa sustaining pressure. A source region temperature and flow of about 625°C and 8.8 moles/second, respectively, are maintained until test termination after 187 seconds at which time the hydrogen supply is expended.

A summary of the diagnostic hole pressure histories is shown on Figure 14. Detailed diagnostic hole pressure data are given in Appendix B. Pressure arrivals are seen to first occur at the innermost diagnostic holes A (9.5 seconds), B (8.9 seconds), and 1 (8.9 seconds). The advancing pressure front then intersects holes 2 (11.9 seconds), 3 (18.8 seconds), 4 (28.5 seconds), and C (46.4 seconds) in sequence. Diagnostic hole pressures are of only qualitative interest, unless the state of the fluid entering these holes can be accurately defined. Arrival times should, therefore, be used for model development and validation purposes. It is, however, of interest to note that once the diagnostic holes were pressurized by the fracture fluid they maintained an almost constant pressure of about 5.2 MPa. This is only slightly larger than the estimated minimum 4.9 MPa in situ stress (Appendix A and Reference 2).

Prior to initiation of the test, the steam-generation system was configured to provide 5 moles/second of 700°C steam at a 10 MPa downhole pressure. Because the sustaining pressure was lower, 1130°C steam was produced at an approximate 8 moles/second flowrate.

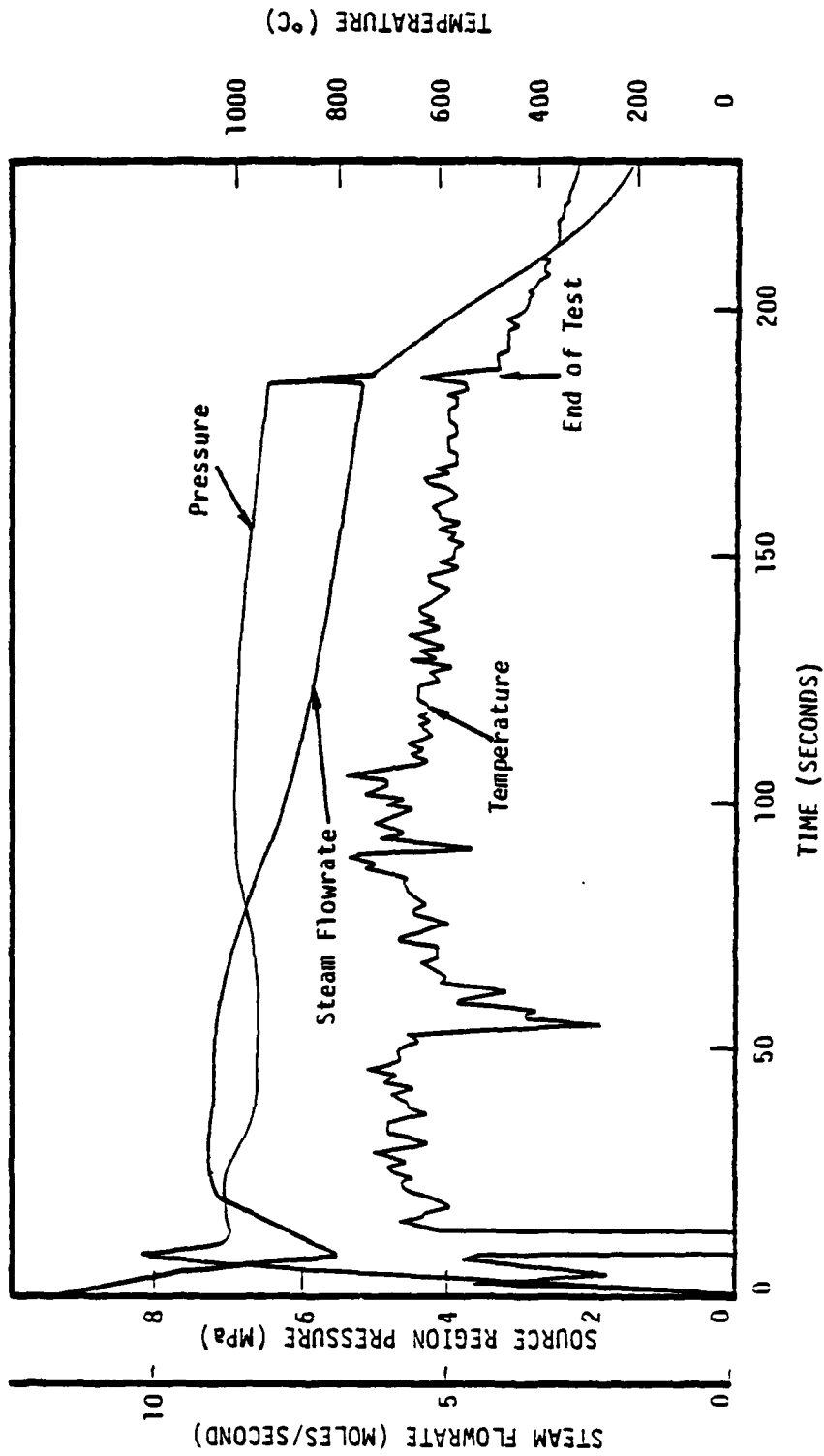


Figure 13. G-Tunnel test source-region pressure, temperature, and flowrate histories.

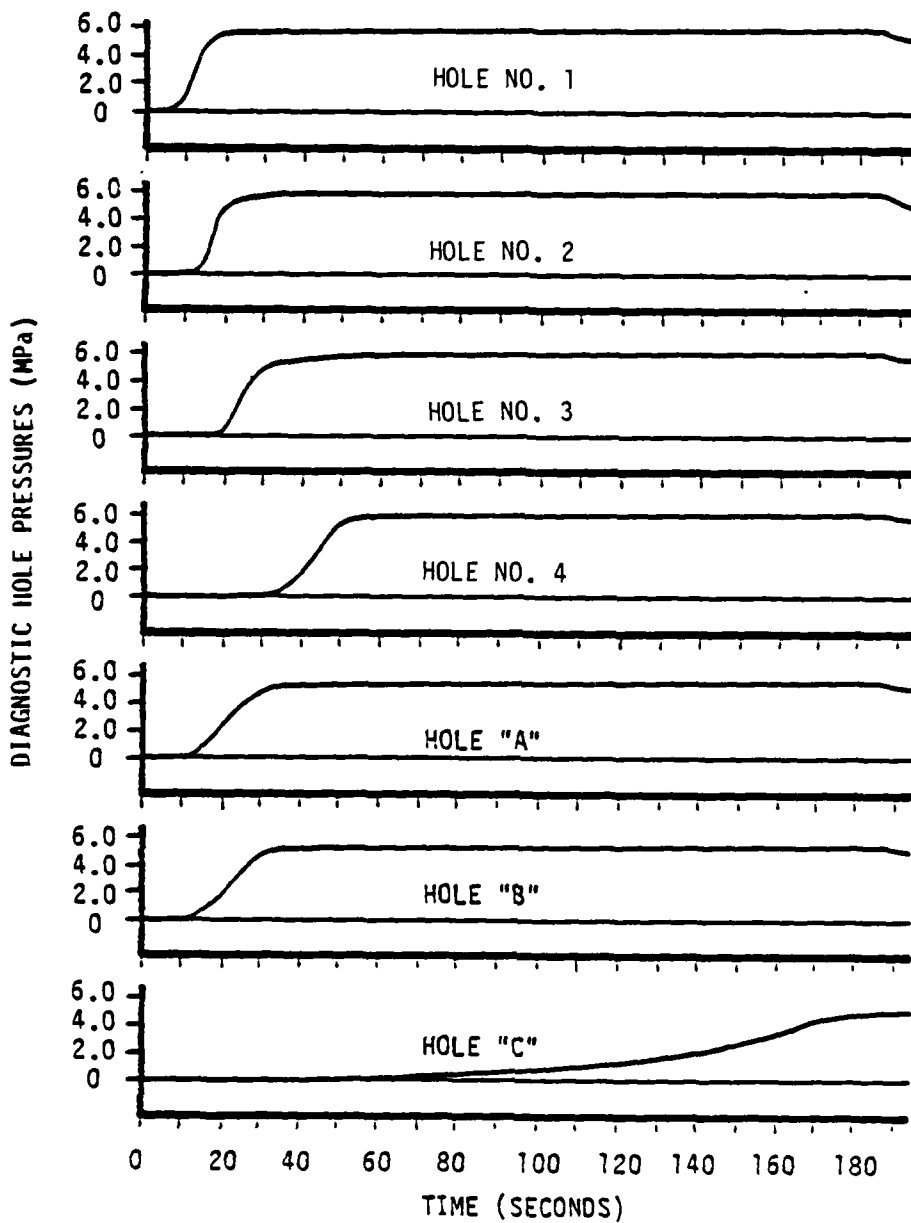


Figure 14. Pressure versus time history recorded in the diagnostic holes during the G-Tunnel steam fracture test.

The 625°C measured downhole temperature is thought to be lower than the 1130°C calculated value primarily as a result of heat loss to the borehole wall. For analysis purposes it is, therefore, recommended that the downhole pressure and hydrogen/oxygen/water combustion/vaporization energy density be used to define the source conditions and that wall heat transfer be included in the model.

During this test, the steam-generation system was operated in the constant flow mode described in Section 2-2. As seen on Figure 13, the downhole pressure and steam flowrate traces are relatively constant throughout the test. In contrast, the measured temperature fluctuates significantly--again, reflecting the turbulence (e.g., the thermocouple may, at times, be partially in a water spray area) existing within the steam-generation region.

3-3 P-TUNNEL TEST.

Three steam-fracture tests were performed at NTS in P-Tunnel. The test objectives were to obtain data on steam fracture propagation and termination phenomena in a typical high-permeability paintbrush-type tuff.

The first P-Tunnel steam fracture test (i.e. SFT No. 2) was performed at CS 11+90 on December 16, 1982. The second and third P-Tunnel tests (i.e. SFT No. 3 and No. 4) were conducted at CS 11+24 on December 22, 1983.

All P-Tunnel tests were conducted in a coarse-grained, porous, vitric ashfall tuff at a depth which exhibited a 3.9 MPa overburden pressure. A summary of the site and material properties information is given in the following paragraphs. Detailed information is provided in Appendix A.

Laboratory tests performed by TerraTek on P-Tunnel core samples taken at this location had an average 44.2 percent porosity, 83.2 percent saturation level, and a calculated 7.6 percent air void. Airflow tests

performed on dried samples gave an average 541 millidarcy gas permeability, while tests performed on samples heated to 1000°C had an average 165 millidarcy value. Tests performed on these samples in their native state gave relative air permeabilities ranging from an initial value of 56 millidarcies to a final value of 147 millidarcies after approximately 25 minutes of testing. Water flow tests performed on native state samples gave an initial permeability value of 360 millidarcies, and final values of 216 millidarcies after 25 minutes of testing.

Core samples taken from the source hole had an average tensile strength of 1.1 MPa, as measured by TerraTek. An overcore test performed by Fenix and Scisson in 1982, at the 1.05 meter to 1.21 meter depth in a hole drilled at CS 15+33, indicated a minimum principle stress of about 0.75 MPa. Grout fracture tests performed at CS 15+80, at a depth ranging between 4.0 and 7.3 meters in a vertical hole, implied the breakdown pressure was less than 3.1 MPa.

3-3.1 CS 11+90 Test (SFT No. 2).

A schematic of the source and diagnostic hole layouts is given on Figure 15. The steam-source region was located 9.75 meters (or approximately 2.7 tunnel diameters) outside the tunnel wall. Stress concentrations which may exist close to the wall should, therefore, have little impact on either the fracture breakdown or sustaining pressure. All holes are separated by a 38-centimeter spacing, with diagnostic hole B located directly above the source hole.

Low pressure gas flow tests were performed in the source and all diagnostic holes prior to conducting the steam-fracture test. The resulting relative gas permability values, determined as described in Appendix C, are summarized in Table 1. Permeabilities are seen to range between 450 and 60 millidarcies, with the average being 267 millidarcies. As shown in Table 1, the relative gas permeability decreased as the tunnel

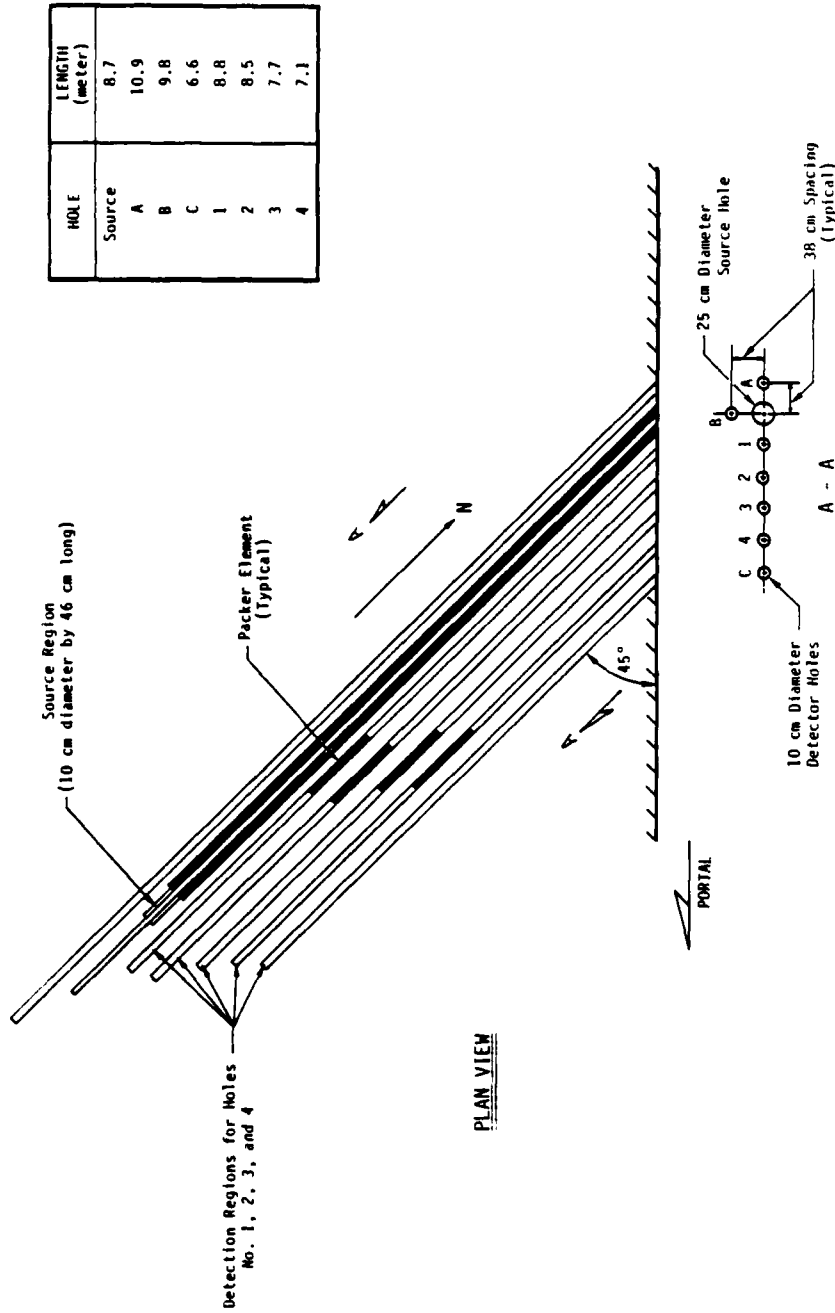


Figure 15. Schematic showing the U12p steam fracture experiment (SFT No. 2) hole layout at CS 11+90. (Taken from DNA Drawing M-2736-06)

Table 1. In situ relative gas permeability values determined from low pressure (e.g. .12-.15 MPa) gas tests conducted in the U12p steam fracture source and diagnostic holes located at CS 11+90 (SFT No. 2).

Hole	Test * Interval (meter)	Permeability (darcy)
Source	.46	.44
A	4.6	.30
B	3.4	.14
C	3.3	.06
1	3.1	.06
2	3.6	.45
3	3.0	.29
4	3.1	.16

* The test interval is measured from the bottom of the hole as shown on sketch.

wall was approached. The measured source area in situ permeability values were a factor of two to six times higher than the laboratory-determined native state relative air permeabilities.

The steam-generation system was installed within the source hole shown on Figure 15 in the manner illustrated on Figure 3. The steam-source region consisted of a 10-centimeter diameter by 46-centimeter long open section located at the end of this hole. Hydrogen/oxygen/water mixing, combustion, and vaporization (i.e., steam generation) occurred within this region.

During the test, packers were installed in diagnostic holes 1, 2, 3, and 4 to isolate the bottom three meters. Holes A, B, and C were shut-in at the surface. Prior to initiation of the steam-fracture test, these isolated regions of the diagnostic holes were water-filled at low pressure to ensure immediate recognition of the pressure signal associated with fracture penetration. It should be noted that even though the diagnostic hole surfaces had been glazed with a sodium silicate wash, pressure decay occurred within a few minutes after shut-in at an initial 0.03 MPa pressure.

Test results are shown on Figures 16 through 18. Figure 16 shows that following test initiation, the source region pressure increased to an unexpectedly high value of about 5.5 MPa within 1.7 seconds and, thereafter, remained relatively constant until 40.5 seconds--at which time there occurred a pressure spike exceeding 6.9 MPa. This pressure excursion was coincident with observed blowouts from both the source hole and diagnostic hole 1. During the blowout, the source region pressure dropped to less than 0.7 MPa--after which it slowly increased to the 6.2 MPa level. Following the initial blowout there occurred intermittent leakage with corresponding burning in the tunnel. The test was, therefore, terminated after 59 seconds.

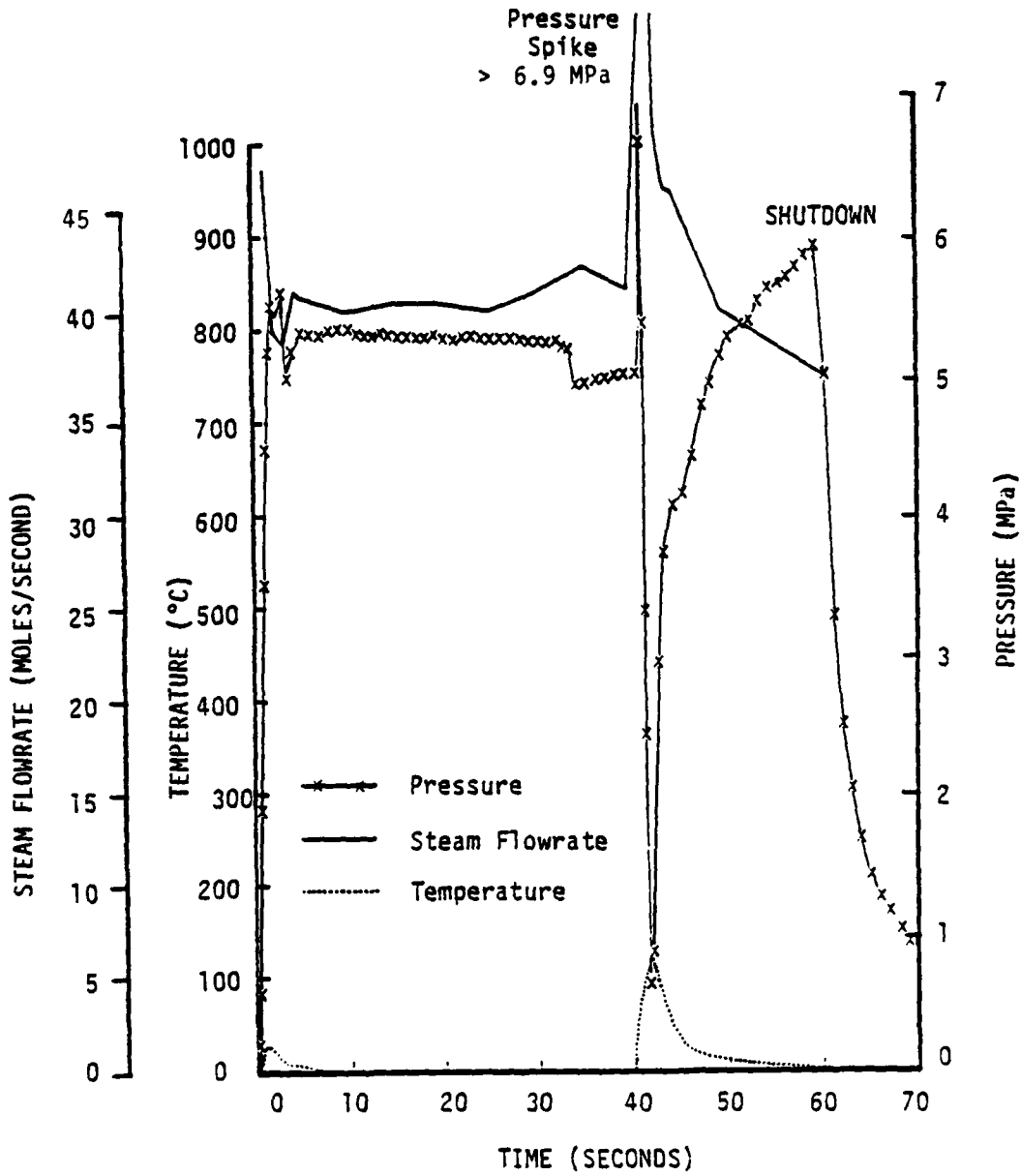


Figure 16. Source region pressure, temperature, and steam flowrate histories during the P-Tunnel CS 11+90 steam-fracture experiment (SFT No. 2).

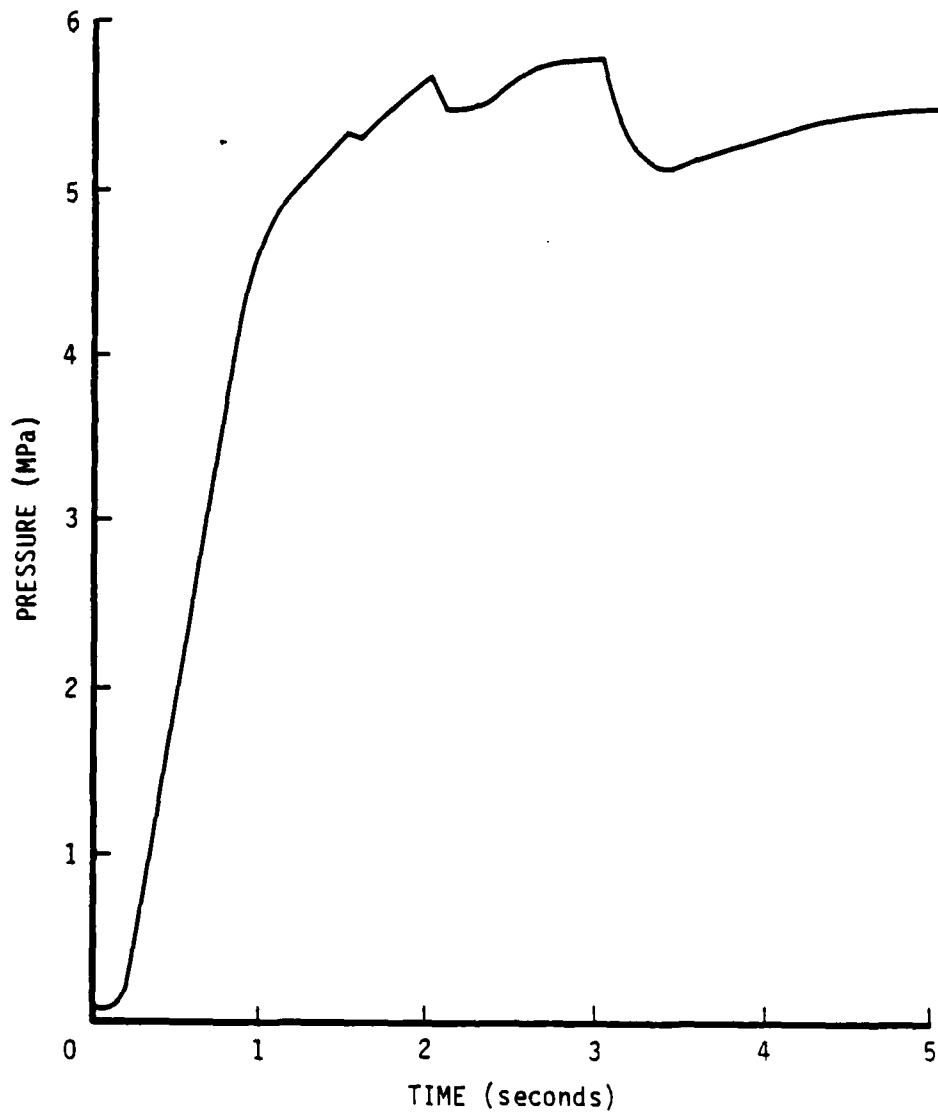


Figure 17. Initial source region pressure history during the P-Tunnel CS 11+90 steam fracture experiment (SFT No. 2).

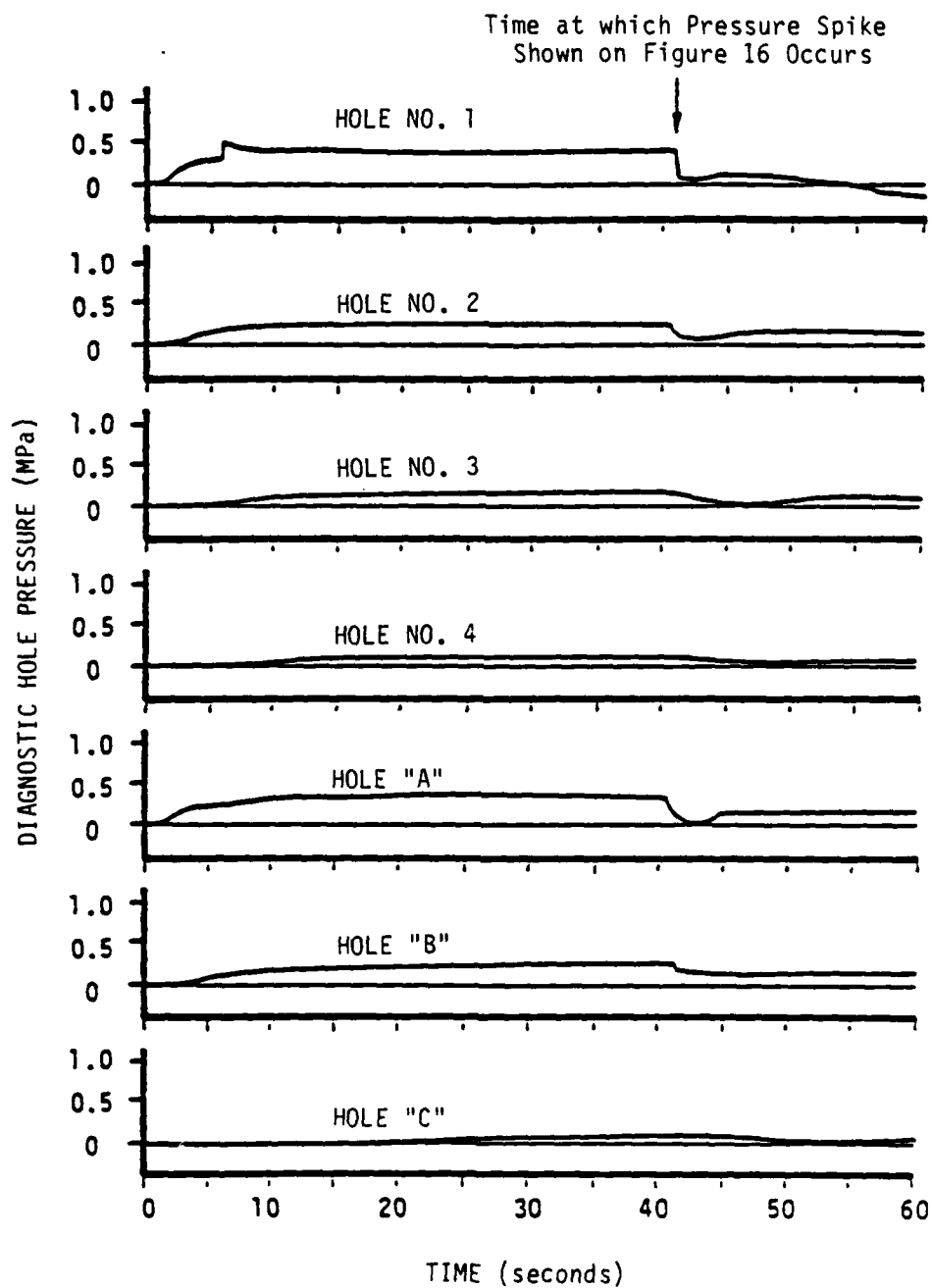


Figure 18. Pressure versus time history recorded in the diagnostic holes during the P-Tunnel CS 11+90 steam fracture experiment (SFT No. 2).

The source region pressure history over the initial 5 seconds is shown on Figure 17. By the time signal arrival occurred in adjacent diagnostic holes A and 1, the source region pressure had increased to about 4.6 MPa. The first pressure peak of 5.6 MPa was approached at about the time of signal arrival in hole 2. After a slight decay, a maximum source pressure of 5.8 MPa was attained at 3 seconds. It is not clear that either peak represents a meaningful fracture breakdown pressure. These early-time pressure variations may be associated with the steam generation system starting dynamics.

A summary of the diagnostic hole pressure histories is shown on Figure 18. Detailed diagnostic hole pressure data are given in Appendix B. Pressure arrivals are seen to first occur at the innermost diagnostic holes A (1.1 seconds), B (2.4 seconds), and 1 (0.9 seconds). The advancing pressure front then intersects holes 2 (1.9 seconds), 3 (3.6 seconds), 4 (7.5 seconds), and C (10.5 seconds), in sequence. The source region pressure spike at 40.5 seconds can be seen in hole 1. Following this spike the source and diagnostic holes A, B, 1, 2, 3, and 4 simultaneously (i.e. within 0.2 seconds) begin to lose pressure. Pressure decay began in hole C about 0.7 seconds later.

Prior to initiation of the test, the steam-generation system was configured to provide 60 moles/second of 700°C steam at a 3.1 MPa down-hole pressure. Because the sustaining pressure was higher, a flow of 42 moles/second of 1300°C steam should have been generated.

Temperature measurements indicate that sustained combustion did not occur in the source region. As shown on Figure 16, only two small temperature spikes were observed. The first occurred when the test started, while the second took place at 40.5 seconds. This second excursion is coincident with the observed pressure spike. Similar data were recorded on both thermocouples located in the source region. Subsequent visual examination of the thermocouples also indicated that they had not been subjected to high temperatures. Except for the short time

periods shown on Figure 16, combustion and associated vaporization apparently, did not occur in the region where the thermocouples were positioned.

Examination of the thermocouple data suggest a cold flow mixture of hydrogen, oxygen, and water (at least in the source region) was responsible for maintaining a steady-state, downhole pressure which significantly exceeded that of the overburden. However, when the tunnel was re-entered approximately 10 minutes after the test, loud boiling sounds could be heard which seemed to originate within the formation in the vicinity of the test and diagnostic holes. These sounds were identical to those heard following SFT No. 4, in which steam is known to have been produced. This latter observation suggests steam generation occurred, but not in the vicinity of the thermocouples.

Tests were subsequently conducted at the S-CUBED operated Green Farm Test Site to determine if the small (10-centimeter diameter by 46-centimeter long) source region could have inhibited ignition and subsequent hydrogen/ oxygen/water combustion and vaporization. As discussed in Section 2-3, satisfactory ignition and steam generation were obtained during all tests including those which simulated the SFT No. 2 flow, pressure, and source volume conditions.

3-3.2 CS 11+24 Test (SFT No. 3).

A steam-fracture test was performed at NTS in P-Tunnel at CS 11+24 on December 22, 1983. This test was intended as a replicate of the December 16, 1982 test in order to resolve uncertainties concerning steam generation and fracture versus diffusion flow. The objective of the SFT No. 3 test was to obtain data on steam-fracture propagation and termination phenomena in a typical, high-permeability, paintbrush-type tuff.

A schematic of the source and diagnostic hole layouts is given on Figure 19. The steam-source region was located 12.8 meters (or approximately 3.2 tunnel diameters) outside the tunnel wall. Stress concentrations which may exist close to the wall should, therefore, have little impact on either the fracture breakdown or sustaining pressure. All holes are separated by a 38-centimeter spacing with diagnostic holes B and F2 located directly above the source hole.

The source hole at CS 11+24 was surrounded by 13 diagnostic holes. Seven of these holes were used to monitor pressure, while six were designed as fracture-monitor holes. The hole spacings were developed based on results of the CS 11+90 test (SFT No. 2). During that test, a pressure signal traveled 190 centimeters to the outer diagnostic hole in 10.5 seconds. The hole layout for the CS 11+24 test was, therefore, extended an additional 190 centimeters to ensure that the generated diffusion or fracture front did not penetrate beyond the diagnostic system.

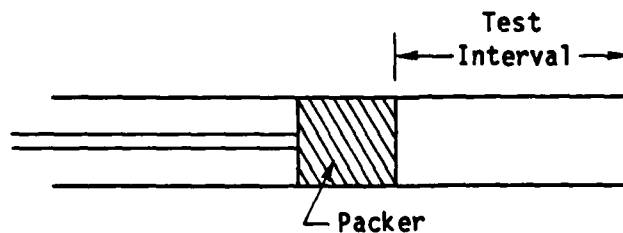
Since diffusion flow and fracture propagation produce virtually identical diagnostic hole pressure data, six diagnostic holes were equipped with fracture identification systems. These systems consisted of optical fibers mounted, using stand-offs, to PVC tubes. The tube/optical fiber was then grouted in a diagnostic hole. The intent was that if a fracture penetrated a diagnostic hole the fiber would break, or at least stretch, and the resulting arrival signal would be recorded. This first attempt at isolating and measuring fracture (i.e., rather than fracture and/or diffusion) arrival did not work. However, the concept warrants additional consideration.

Low-pressure gas flow tests were performed in the source and diagnostic holes prior to conducting the steam-fracture test. The resulting relative gas permeability values, determined as described in Appendix C, are summarized in Table 2. Measured relative gas permeability values for Holes C, 1 through 4, and F₁, F₃, and F₄ ranged between 13 and 41 millidarcies, with the average being 25 millidarcies.

Table 2. In situ relative gas permeability values determined from low pressure (e.g., .10 - .15 MPa) gas tests conducted in the U12p steam fracture source and diagnostic holes located at CS 11+24 (SFT No. 3 and No. 4).

Hole	Test * Interval (meter)	Permeability (darcy)	Comment
Source	2.2	.042	
A	6.1	.44	Consistent with fracture
B	6.1	.33	Consistent with fracture
C	6.1	.013	
1	6.1	.013	
2	6.1	.021	
3	6.1	.023	
4	6.1	.025	
F1	6.1	.033	
F2	6.1	.16	Consistent with fracture
F3	6.1	.032	
F4	6.1	.041	
F5	-	-	Did not test
F6	-	-	Did not test

* The test interval is measured from the bottom of the hole as shown on sketch below



The source region had a 42-millidarcy value. Fenix and Scisson geologists (Reference 4) reported a visual fracture between Holes A and B. These holes, plus F2, had relative gas permeabilities of 440, 330, and 160 millidarcies, respectively. With the exception of Holes A, B, and F2, these measured *in situ* permeability values are similar to the laboratory-determined native state relative air permeability (see Appendix A).

The steam-generation system was installed within the source hole shown on Figure 19 in the manner illustrated on Figure 3. The steam-source region consisted of a 25-centimeter diameter by 61-centimeter long open section located at the end of the source hole. Hydrogen/oxygen/water mixing, combustion, and vaporization (i.e., steam generation) occurred within this region.

During the test, straddle packers were installed in diagnostic holes 1, 2, 3, and 4 to isolate the 3-meter interval centered around the source region. Holes A, B, and C were shut-in at the tunnel face. Prior to the initiation of the steam-fracture tests, these isolated regions of the diagnostic holes were water-filled at low pressure to ensure an immediate recognition of any pressure signal associated with either fracture or diffusion flow. The diagnostic holes were glazed with a sodium silicate solution to retard water flow from the hole into the formation. Once glazed, these holes could maintain pressure for a few minutes after they were shut-in at 0.03 MPa pressure.

Test results are shown on Figures 20 and 21. Following test initiation, the source region pressure increased to 3.9 MPa within 13 seconds. The pressure remained at this level for approximately 4 seconds, and then gradually decayed to 3.5 MPa at 56 seconds--after which the test was terminated. Following the 5 second starting transient, both the water and oxygen flowrates remained relatively constant.

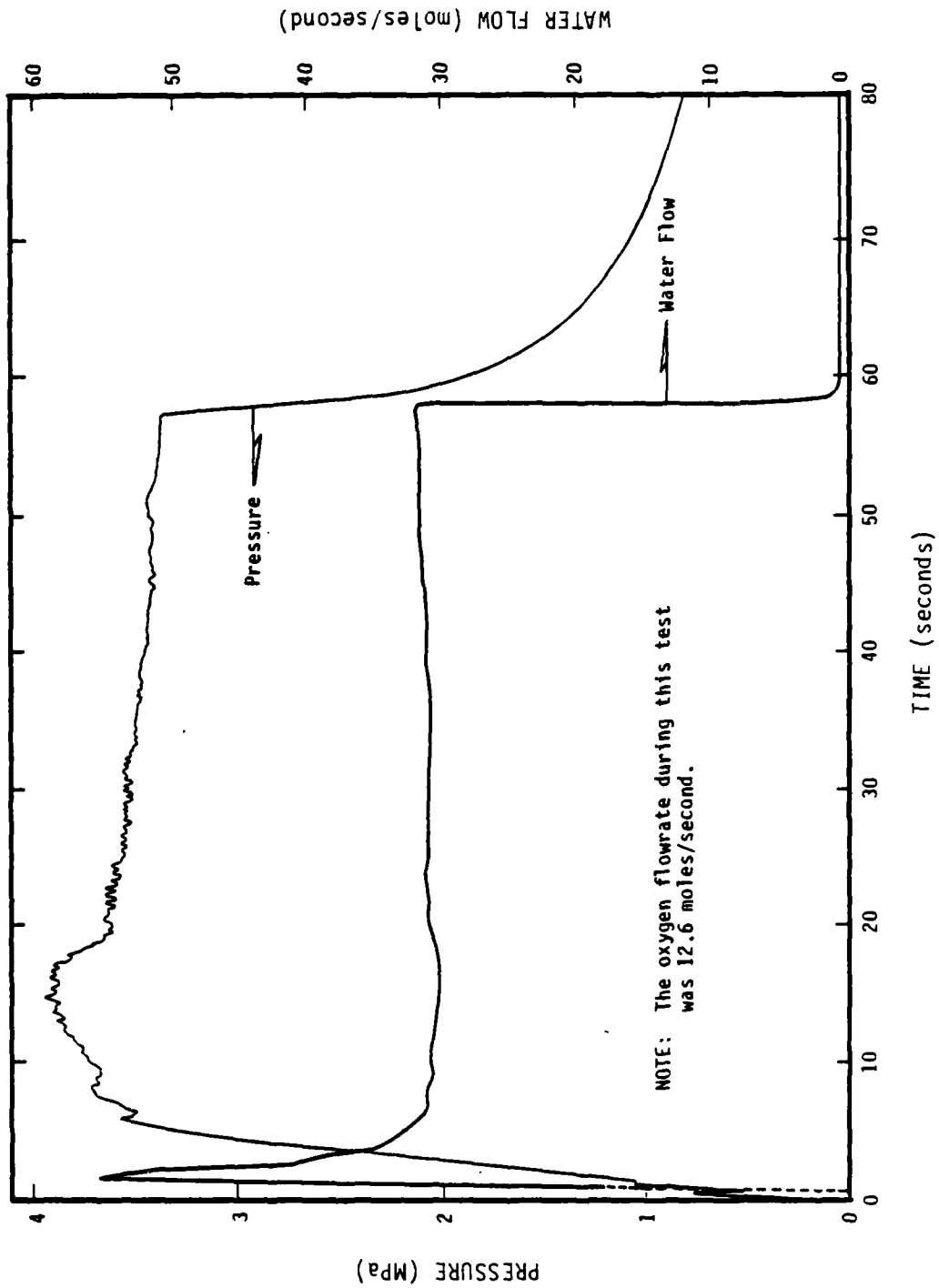


Figure 20. Source region pressure and water flowrates during the P-Tunnel CS 11+24 steam fracture experiment (SFT No. 3).

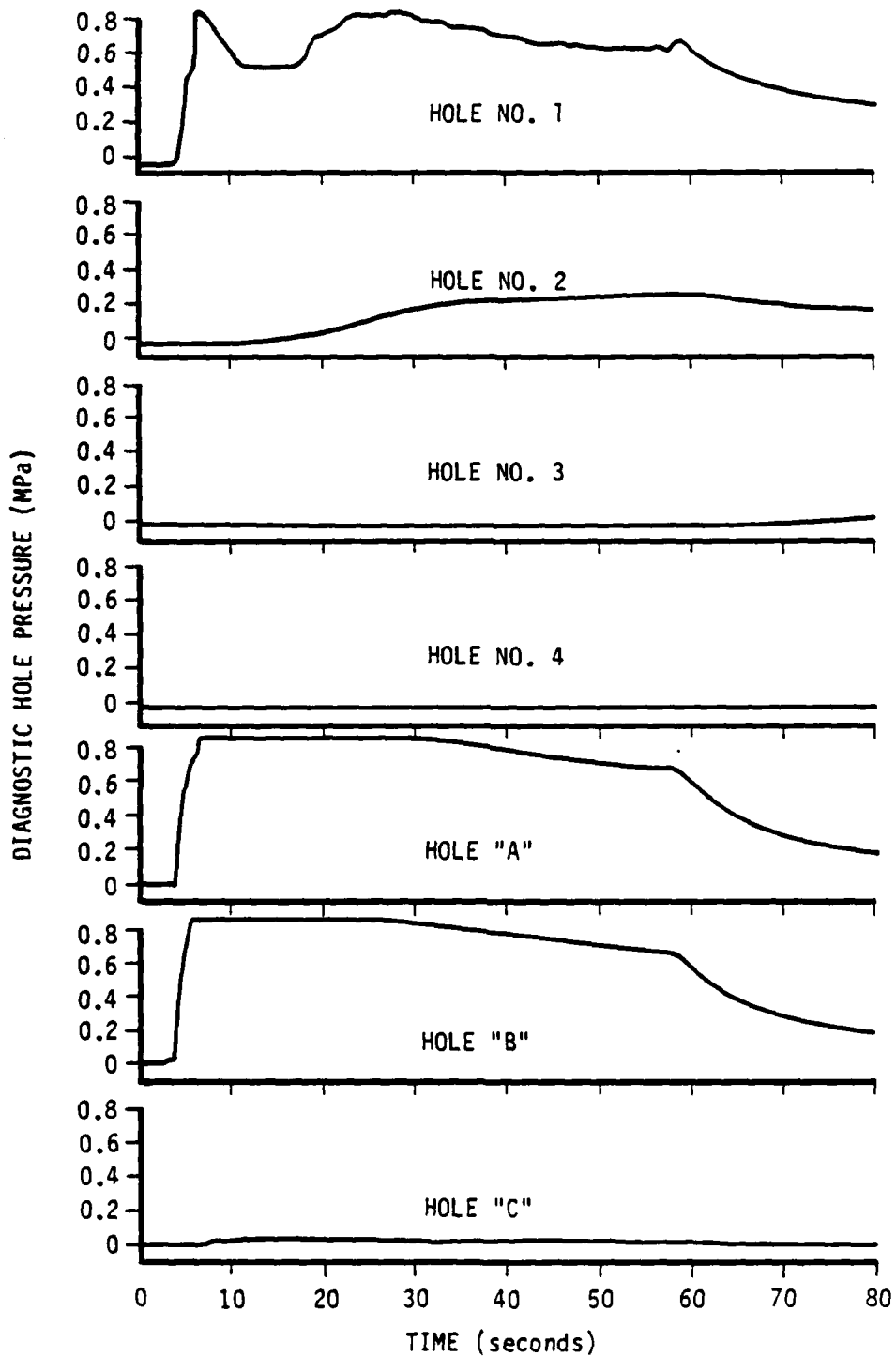


Figure 21. Pressure versus time history recorded in the diagnostic holes during the P-Tunnel CS 11+24 steam fracture experiment (SFT No. 3).

During this test, a hydrogen line fitting separated. This may have occurred during the first 2 seconds, when the small irregularity is seen on the source-region pressure curve shown on Figure 20. Since there was no hydrogen flow to the source region, combustion/vaporization did not occur. The pressure histories shown on Figures 20 and 21, therefore, result from injection of a cold water/oxygen mixture.

It should be noted that the test had run between 10 and 30 seconds before it was determined that an ignition failure, and associated hydrogen leak, had occurred. Since the fracture/diffusion signal had already penetrated to diagnostic hole No. 2, the test was continued in order to obtain fracture arrival time data out to larger radii. The test was terminated at 56 seconds because of the hydrogen leak.

The source-region pressure history is shown on Figure 20. Pressure increased from 2.5 MPa to 3.0 MPa during the interval in which pressure front arrival occurred in adjacent diagnostic holes A, B, and 1. Pressure front arrival also occurred in hole No. 2 before the source region pressure peaked.

A summary of the diagnostic hole pressure histories is shown on Figure 21. Detailed diagnostic hole pressure data are given in Appendix B. Pressure arrivals are seen to occur at the innermost diagnostic holes A (3.9 seconds), B (3.2 seconds), and 1 (4.10 seconds). The advancing pressure front then intersects hole No. 2 (11.5 seconds), and finally reaches hole No. 3 (62.7 seconds) at a time after the source region flow had been terminated. There was no signal arrival at hole No. 4. Beginning at 7.1 seconds, diagnostic hole C exhibited an unusual response which was uncharacteristic of other diagnostic hole data.

Pressure decay began in holes A (2.0 seconds), B (2.0 seconds), and 1 (2.2 seconds) after shutdown. This decay was seen promptly in hole No. 2 (4.4 seconds), but was quite slow in affecting hole No. 3 (145 seconds). The decay signal could not be distinguished in hole C.

Prior to initiation of the test, the steam-generation system was configured to provide 60 moles/second of 700°C steam at a 3.1 MPa downhole pressure. These conditions are identical to the flow conditions for the P-Tunnel CS 11+90 test (SFT No. 2). An actual flow of about 44 moles/second (i.e., water and oxygen) was obtained with a 3.5 MPa downhole pressure.

3-3.3 CS 11+24 Test (SFT No. 4).

A second steam-fracture test was performed in P-Tunnel at CS 11+15 on December 22, 1982. This test used the source and diagnostic holes described in the previous section. Prior to this test, the hydrogen line fitting was replaced.

The primary test objective was to, again, evaluate steam-fracture propagation/termination phenomena. However, the probability of realizing this objective was limited by the possibility that fracturing had occurred during SFT No. 3. A second objective was to gain field experience with the steam-generation system.

The as-built P-Tunnel source and diagnostic hole layouts used for this test are shown on Figure 19. Two changes were made. Because a relatively-small pressure signal had been obtained in diagnostic hole No. 3, and none in hole No. 4 during SFT No. 3, the straddle packers were removed and single packers installed at a depth of approximately 3 meters. This change was made in case the fracture had bypassed the straddle region in the outer two diagnostic holes.

Prior to the steam-flow test, a low-pressure airflow test was performed in the source hole. Results of this test indicated the source region had a 0.52 darcy relative gas permeability. This is approximately one order of magnitude larger than that obtained prior to SFT No. 3. During this low-pressure test, air was observed to flow into diagnostic

holes A, B, and 1. This increased permeability value was not surprising, since the SFT No. 3 results suggested a fracture may have been produced which connected the source region with holes A, B, 1, and 2.

Because of the possible presence of a fracture, diagnostic holes A, B, and 1 were not filled with water. If filled, the water may have flowed into the source region, thereby preventing combustion. Since these diagnostic holes were not water-filled, sharp pressure arrivals would not be expected.

Test results are shown on Figures 22 and 23. Following test initiation, the source pressure increased to 4.6 MPa within 4 seconds. The pressure then slowly decayed to 3.3 MPa by the time the test was completed at 80 seconds. The recorded source-region temperature peaked at 1000°C, and remained higher than 800°C for the duration of the test. A second temperature probe, which was read only on a meter contained on the control panel, provided readings which were higher than 1000°C throughout the entire test. A relatively-constant 48 moles/second steam flow-rate was produced.

A summary of the diagnostic hole pressure histories is shown on Figure 23. Detailed diagnostic hole pressure data are given in Appendix B.

During this test, the diagnostic hole timing signal did not trigger the diagnostic hole recording system upon steam generator initiation. However, the time between the signal arrival and decay initiation at diagnostic holes A, B, and 1 was identical to the 80-second test duration. This suggests that there exists a fracture connecting these holes to the source region. Note that if one assumes that the diagnostic hole pressure decay begins 2.0 seconds after completion of the test (as it did in SFT No. 3), then it must also be assumed that the first arrival in these holes occurred 2.0 seconds following test initiation. During this test, a pressure arrival was measured in hole No. 2 after 21.5 seconds. The pressure signal did not penetrate to holes 3, 4, or C.

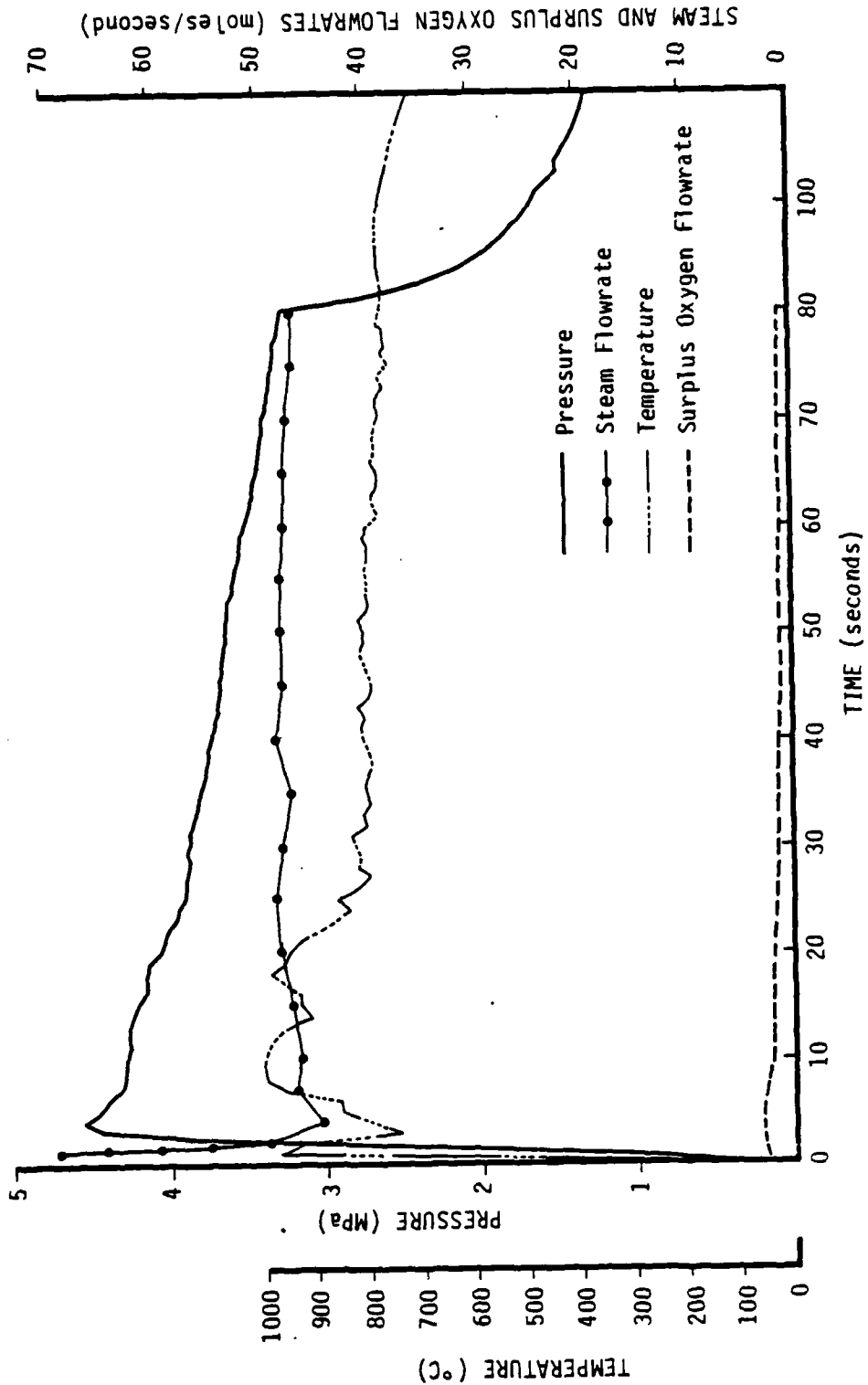


Figure 22. Source region pressure, temperature, and steam flowrate during the P-Tunnel CS 11+24 steam fracture experiment (SFT No. 4).

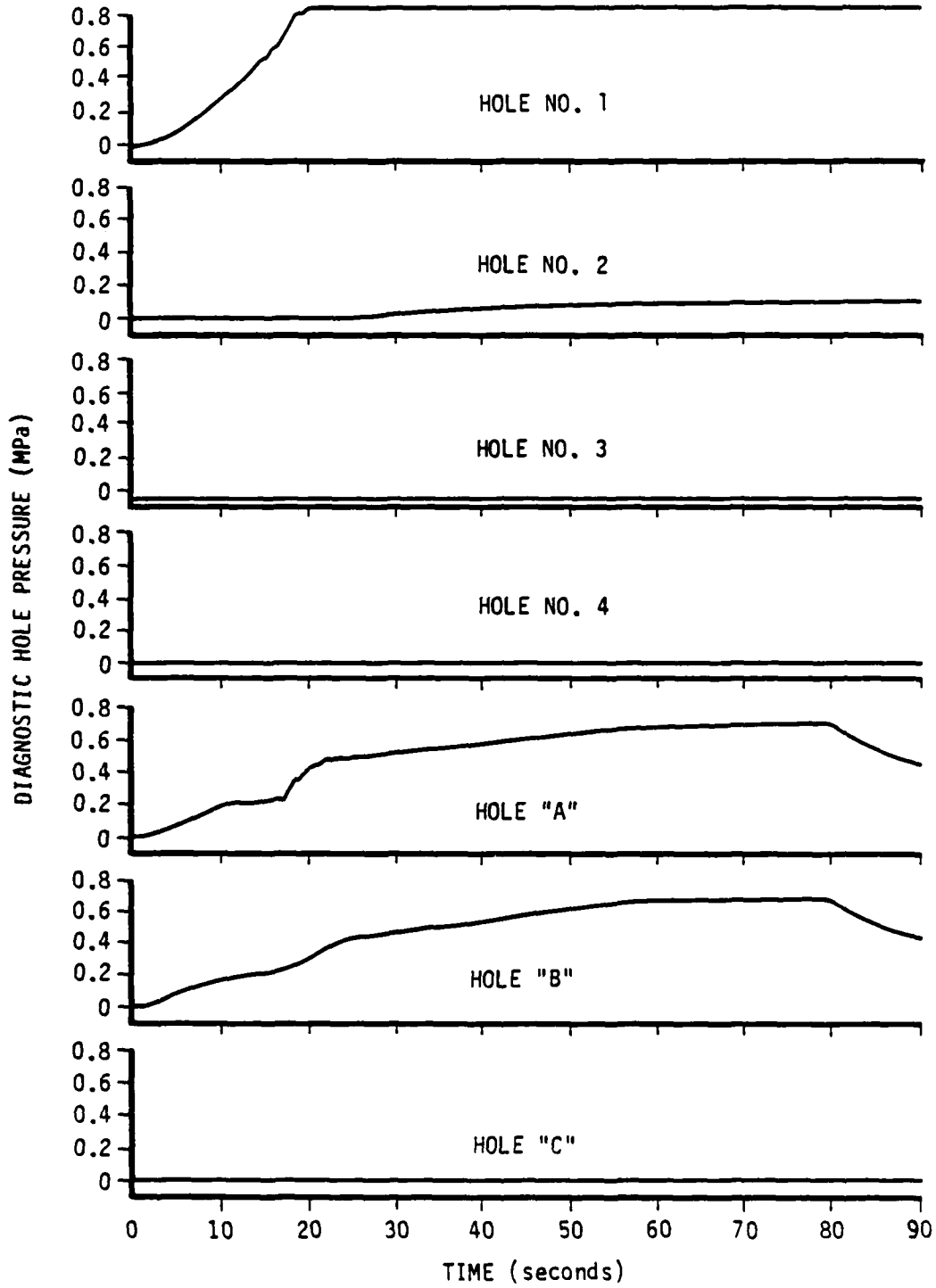


Figure 23. Pressure versus time history recorded in the diagnostic holes during the P-Tunnel CS 11+24 steam fracture experiment (SFT No. 4).

This test provided three important results. First, it demonstrated that the highly-porous P-Tunnel formation could sustain a downhole steam pressure greater than the minimum in situ stress. Second, the test region emitted post-test boiling sounds identical to those heard following SFT No. 2--thereby suggesting that steam generation did occur during the test at CS 11+90. Finally, the test again demonstrated successful steam generator ignition and operation under field conditions.

SECTION 4 DISCUSSION OF RESULTS

The G-Tunnel test (SFT No. 1) was conducted in a low-permeability (approximately 10^{-6} darcy) welded tuff in which fluid diffusion from the fracture would not be expected to influence the fracture propagation rate. The resulting data were classic in form. As shown on Figure 13, the initial breakdown pressure of 8.1 MPa occurred at 8.4 seconds, and was followed by a 6.9 MPa sustaining pressure. Furthermore, the propagating fracture sequentially intersected the diagnostic holes, as shown on Figure 14.

A plot of fracture penetration distance versus time is shown on Figure 24. Signal arrivals in this plot are measured from the 8.1-second breakdown time for SFT No. 1. Note that the fracture tip moved at a rate which is nearly proportional to the one-third power of time. This is the rate at which a fluid-driven fracture would propagate assuming a constant source flowrate and zero formation permeability. At the time of the test, this apparently-low propagation velocity was confusing.

Subsequent calculations (Reference 1) have shown that the G-Tunnel test fracture propagation velocity is heat-transfer dominated. The crack surface area was found to increase at a rate which allowed sufficient heat transfer to produce nearly-complete steam condensation. As a result, the steam fracture propagation rate is similar to that of a standard hydrofracture.

The SFT No. 1 results show the strong heat transfer influence on steam fracture propagation. Results of calculations which neglect heat transfer give propagation rates which are much faster than obtained during this test.

The P-Tunnel tests (SFT No. 2, 3, and 4) were conducted in a high-permeability ($> 10^{-2}$ darcy) low-strength, paintbrush tuff in which fluid diffusion from the fracture was expected to influence the fracture

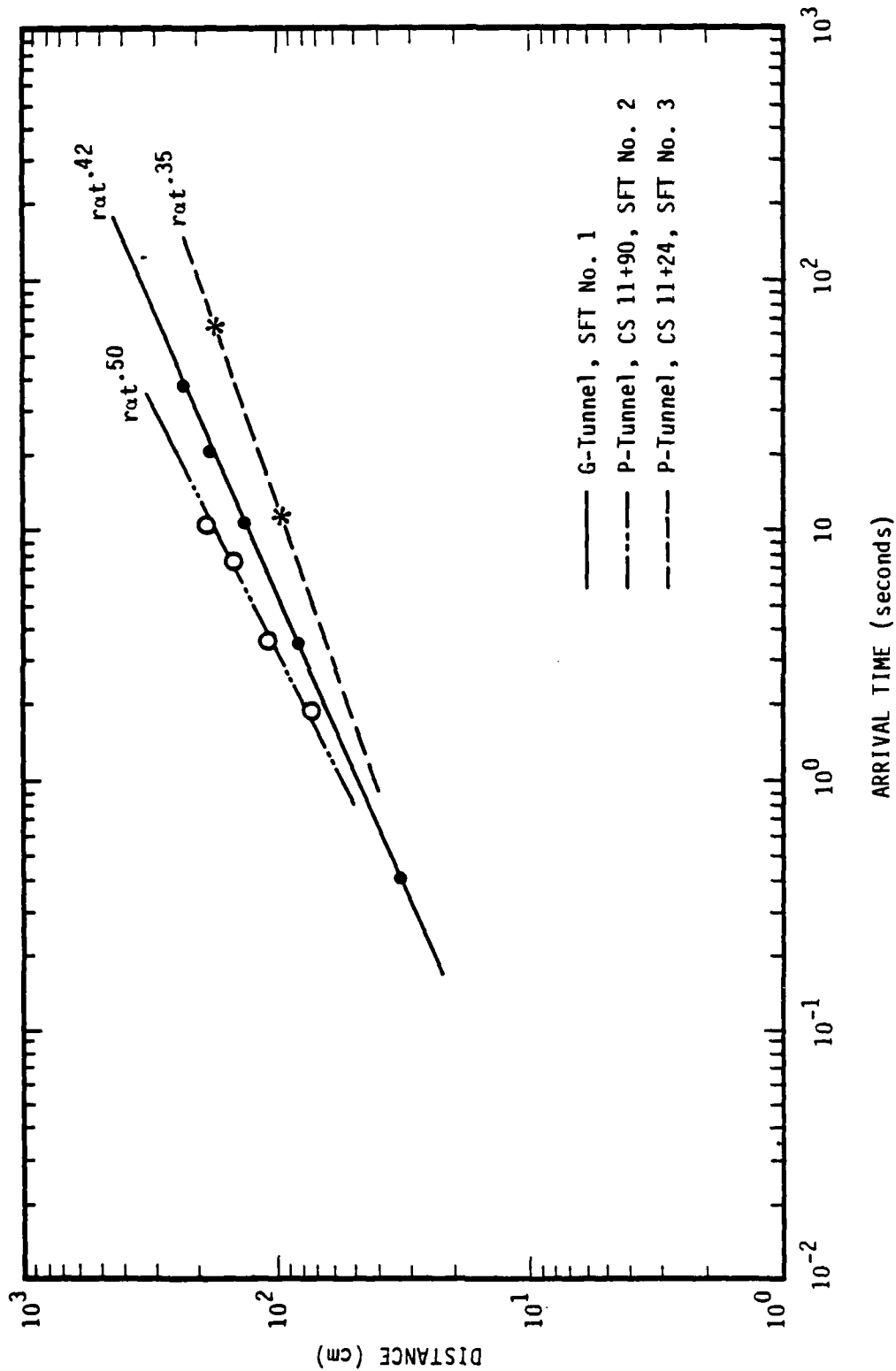


Figure 24. Diagnostic hole signal arrival times plotted as a function of distance from the source region.

propagation rate. The resulting data were not classic in form. The most surprising result was a sustaining pressure which was high compared to either the overburden pressure or the minimum in situ stress. In addition, as shown on Figures 16 through 23, it was difficult to identify a breakdown pressure.

Fracture penetration distance versus time results for P-Tunnel are also shown on Figure 24. In the absence of an identifiable fracture breakdown, signal arrival times were simply measured from the beginning of the test. The P-Tunnel velocities implied by these data are, therefore, not as accurate as the G-Tunnel results. Even so, the measured propagation velocities for the G-Tunnel and P-Tunnel formations, whose permeabilities differ by at least four orders of magnitude, were surprisingly similar.

Modeling was performed to understand the P-Tunnel data. Results of those studies are described in detail in Reference 5. Briefly, it was found that:

- Poroelastic pressures, induced by fluid penetration around the borehole, tend to increase local compressive stresses by an amount which could be comparable to the rise in pore pressure. This increase in the total confining stress tends to inhibit fracture growth--thereby increasing borehole pressure.
- Poroelastic stresses tend to decrease the effective stresses (total compressive stress less pore pressure) around the borehole--thus leading to earlier failure (which could not be identified during the starting transient) since the stress within the rock matrix becomes less compressive.

P-Tunnel and G-Tunnel fracture propagation rates are similar and are both controlled by diffusion processes. In the P-Tunnel test, fluid diffusion from the fracture into the surrounding material slowed fracture growth. In G-Tunnel, the slow growth rate was caused by heat transfer from the fluid within the fracture to the surrounding formation.

SECTION 5
CONCLUSIONS AND RECOMMENDATIONS

The downhole steam-generation system can be used to simulate high-temperature, high-pressure, post-shot cavity conditions. This system has been used to perform steam-flow tests in a sand column; a low-permeability, welded, tunnel-bed tuff; and, a high-permeability paintbrush-type tuff. This system could also be used to study heat transfer, surface blow-off, or material erosion rates under typical post-shot cavity conditions.

The sand-column test generated data which describe phase changes and flow of water, mixed-phase steam and water, and superheated steam through a porous medium. These data can be used for verification and development of models describing condensation/heat-transfer/fluid diffusion phenomena.

Classic fracture data were obtained from the G-Tunnel test. Results show the fracture breakdown pressure, sustaining pressure, and fracture propagation velocity. These data provide an excellent base for development and/or verification of steam-fracture models for low-permeability materials where heat transfer is significant, but in which fluid diffusion from any resulting fracture is small.

The P-Tunnel test results are somewhat ambiguous, as one cannot be certain that steam generation occurred within the source region during SFT No. 2. However, these tests did provide data which may be of great significance to containment. In particular, the data showed that the high-permeability, low-strength, paintbrush-type tuffs can support sustaining pressures on the order of (or larger than) the overburden pressure. The existing P-Tunnel data can be used for development and verification of fracture models for high-permeability materials where fluid diffusion and, possibly, heat transfer is large. It is suggested

that the SFT No. 2 test results can be used for these studies under the assumption that steam generation did occur. If the studies disprove this assumption, then an additional steam fracture test in the paintbrush tuffs may be required.

LIST OF REFERENCES

1. Travis, B. J., "Comparison of the KRAK Model with Experimental Data," Proceedings, Second Symposium on Containment of Underground Nuclear Explosions, Volume 2, Kirtland AFB and Albuquerque, New Mexico, August 1983.
 2. Smith, C. W., Vollendorf, W. C., and Warren, W. E., "In Situ Stress from Hydraulic Fracture Measurements in G-Tunnel, Nevada Test Site," SAND 80-1138, April 1981.
 3. O'Brien, M. B., "Results of Steam Hydraulic Fracture Drilling," Memo from Fenix and Scisson to J. W. LaComb of DNA, April 28, 1982.
 4. Brandt, J. M., "Location of Fractures in U12p Tunnel SFT No. 2," Memo from Fenix and Scisson to E. W. Peterson of S-CUBED, December 15, 1983.
 5. Duff, R. E., et al., "Late Time Containment Research," S-CUBED Report (SSS-R-85-6898), September 1984.
-
- A-1 Smith, R.H., Letter Report from TerraTek to J. La Comb of DNA, July 7, 1982.
 - A-2 Brace, W.F., Walsh, J.B. and Frangos, W.T., "Permeability of Granite Under High Pressure," J. Geophys. Res. 73, 2225-2236 (1968).
 - A-3 Smith, C.W., Vollendorf, W.C., and Warren, W.E., "In situ stress from hydraulic fracture measurements in G-Tunnel, Nevada Test Site", SAND 80-1138, April 1981.
 - A-4 Wooley, C.H., Letter Report from TerraTek to J. La Comb of DNA, March 27, 1984.
 - A-5 Smith, R.H., Letter Report from TerraTek to J. La Comb of DNA, September 27, 1982.
 - A-6 Schulenburg, K.L., Memo from Fenix and Scisson, Inc. to J. La Comb of DNA, September 27, 1984.
 - A-7 Baldwin, M.J., and Brandt, J.M., memo from Fenix and Scisson, Inc. to B.L. Ristvet of DNA, September 24, 1982.
 - A-8 Waltman, Schulenburg, Reeves, "Report on an In Situ Stress Measurement in U-12P Tunnel." Fenix and Scisson, Inc. Internal Report, October 6, 1982.
 - A-9 Obert, L., "In Situ Stresses in Rock, Ranier Mesa, Nevada Test Site", Applied Physics Laboratory U.S., Bureau of Mines, September 1964.

APPENDIX A
SITE AND MATERIAL PROPERTIES

In situ and laboratory test data relevant to the steam fracture experiments are presented in this Appendix. Results of laboratory physical properties tests, in situ permeability tests, and in situ stress measurements are included. The G-Tunnel and P-Tunnel data are presented in Sections A-1 and A-2, respectively. Note that the data and associated discussion presented in Appendix A were predominantly taken from the listed references.

A-1 G-TUNNEL MATERIAL PROPERTIES.

Tests were performed by TerraTek (Reference A.1) on core obtained from the U12g steam fracture hole Nos. 1, 2, and 4. In addition to a liquid permeability measurement, for each sample the standard suite of mechanical, ultrasonic velocity, and physical properties tests were conducted.

Table A-1 lists the physical properties, ultrasonic velocities, measured permanent compactions and permeabilities. Permeabilities, which ranged between 6.8 to 9.2 microdarcies, were measured at a nominal stress state of 1.36 MPa overburden stress and 0.68 MPa pore fluid pressure using a 1 percent CaCl_2 brine as the permeating fluid. A transient pulse technique similar to that used by Brace (Reference A-2) was used for each test.

Figures A-1 through A-3 show the volume strain versus mean normal stress, and Figures A-4 through A-6 show the confining stress versus stress difference. The permanent compactions for the three samples ranged from 1.1 percent to 2.8 percent. The maximum stress differences ranged from 30 to 50 MPa.

Estimates of in situ stresses have been made by Sandia (Reference A-3) at numerous locations within G-Tunnel. The most relevant data for the RS-14 drift mineback region are thought to result from the HF 20, HF 39 and HF 40 tests. These data suggest in situ stresses for σ_1 , σ_2 , and σ_3 of 8.79 MPa, 6.63 MPa, and 4.90 MPa, respectively; σ_1 is vertical and is within 7 percent of the estimated 8.2 MPa overburden pressure, σ_2 is horizontal in the plane of the fracture N42°E, and σ_3 is directed horizontal and normal to the fracture plane N48°W. Table A-2 shows the fracture breakdown, driving and shut-in pressures observed during tests conducted in the HF 20, HF 39, and HF 40 holes.

The 25 cm diameter by 112 cm long steam fracture source region was examined using a borescope subsequent to the G-Tunnel steam fracture test. The borehole surface appeared undamaged. There was no evidence of any fractures or spall. However, it was evident that the grout mass, which prior to the test had filled one-third of the test region, had been subjected to high temperatures as it had been rubblized.

Table A-1 Physical properties, permanent volume compactions, and ultrasonic wave velocities of tuff from U12g holes No. 1, 2, and 4, steam fracture test. (Taken from Reference A-1)

Drill Hole Depth (m)	Density			Water by Wet Weight (Percent)	Porosity (Percent)	Saturation (Percent)	Calc. Air Voids (Percent)	Meas. Permanent Comp (Percent)	Velocity		Perme- ability (darcy) $\times 10^{-6}$
	As-Received (g/cc)	Dry (g/cc)	Grain (g/cc)						Long (km/s)	Shear (km/s)	
SF No. 1 9.97	1.84	1.47	2.43	20.1	39.5	93.6	2.5	2.8	2.90	1.37	7.4
SF No. 2 10.1	1.86	1.48	2.46	20.3	39.8	95.1	2.0	1.1	2.76	1.32	6.8
SF No. 3 9.85	1.83	1.45	2.44	20.8	40.6	93.7	2.5	2.5	2.83	1.31	9.2

Table A-2 Hydrofracture data and inferred *in situ* stresses determined from Sandia hydrofracture test holes in the vicinity of the U12g RS-14 drift mineback. (Taken from Reference A-3)

Hole No. (Orientation) Zone (m)	Overburden (m)	Breakdown P_C (MPa)	Frac/Driving P_f (MPa)	Inst. Shut-In P_{si} (MPa)
HF 20 (H) N71°E 4.5 - 11.5 22.5 - 29.5 42.5 - 49.5 62.5 - 69.5	437	5.44 7.48 7.89 10.3	1.90 4.97 6.80 6.46	1.36 4.42 5.44 5.10
HF 39 (H) S19°E 17.5 - 22.5 42.5 - 47.5 72.5 - 77.5	442	12.2 11.4 10.9	5.68 5.52 6.97	4.63 4.75 5.10
HF 40 (H) N19°W 40 - 45 40 - 45	437	11.4 11.9	5.22 5.18	4.89 4.83

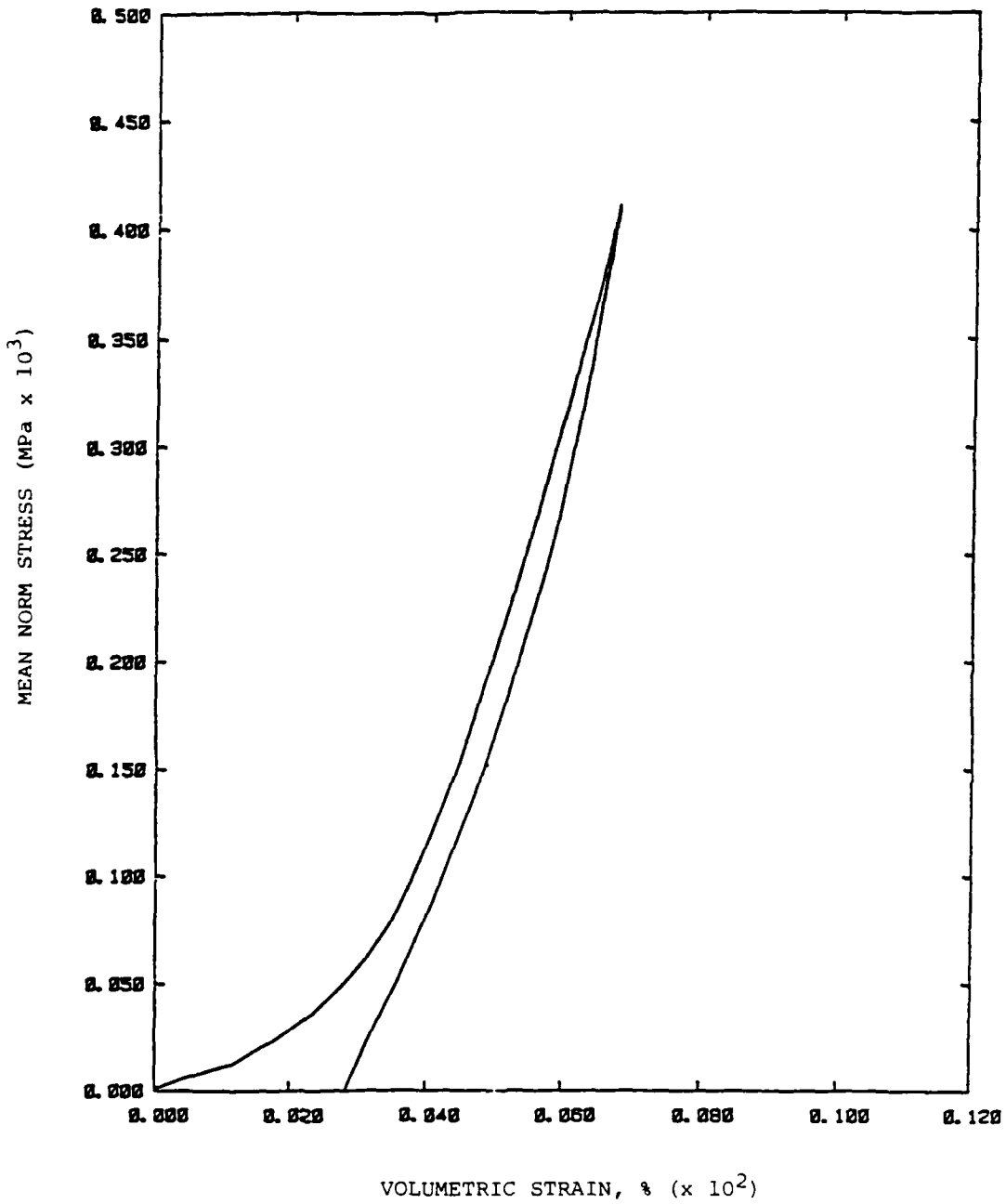


Figure A-1 Mean normal stress versus volumetric strain for sample taken at the 9.63 m to 9.97 m depth in U12g tunnel steam fracture hole No. 1. (Taken from Reference A-1)

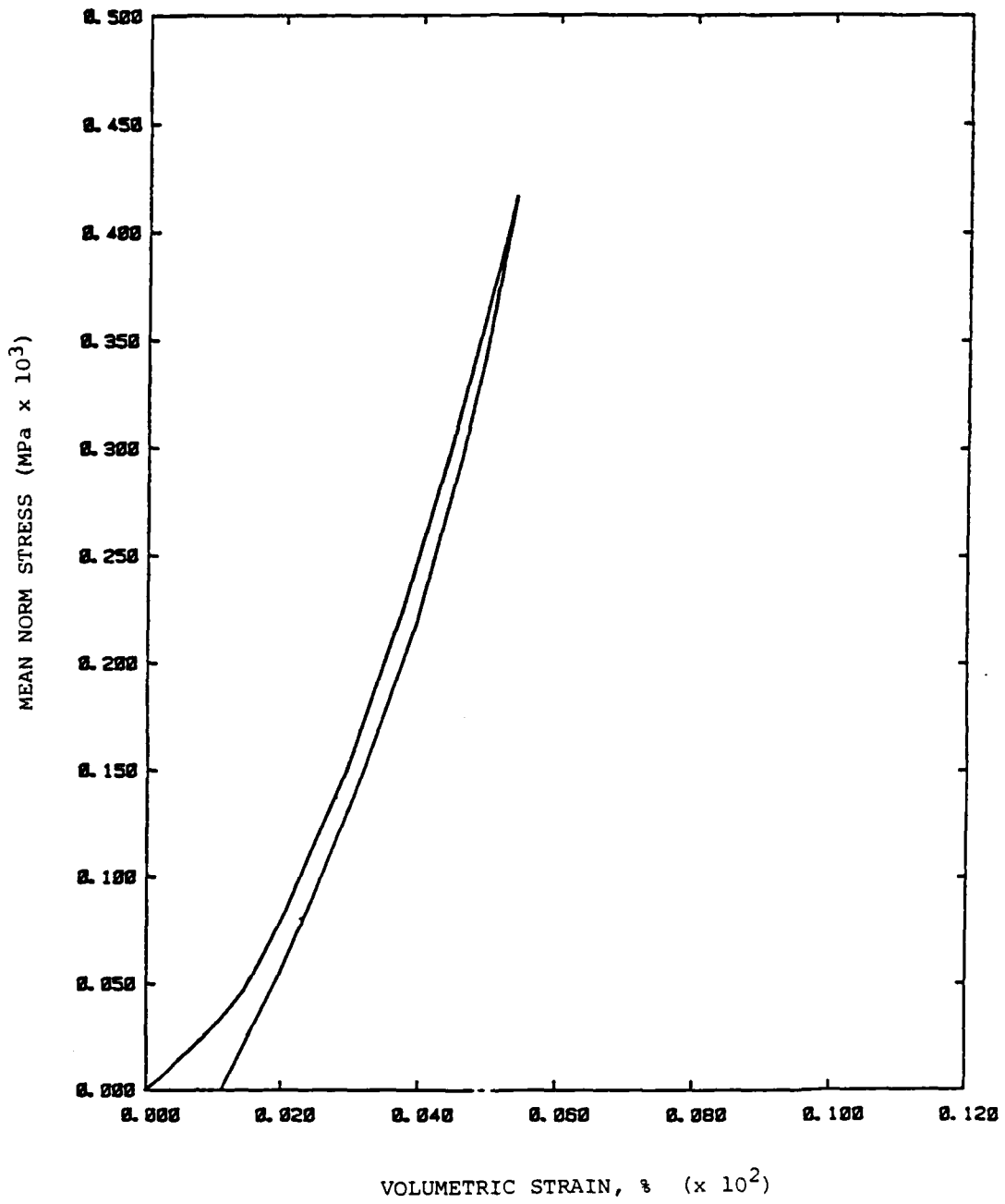


Figure A-2 Mean normal stress versus volumetric strain for sample taken at the 9.81 m to 10.1 m depth in U12g tunnel steam fracture hole No. 2. (Taken from Reference A-1)

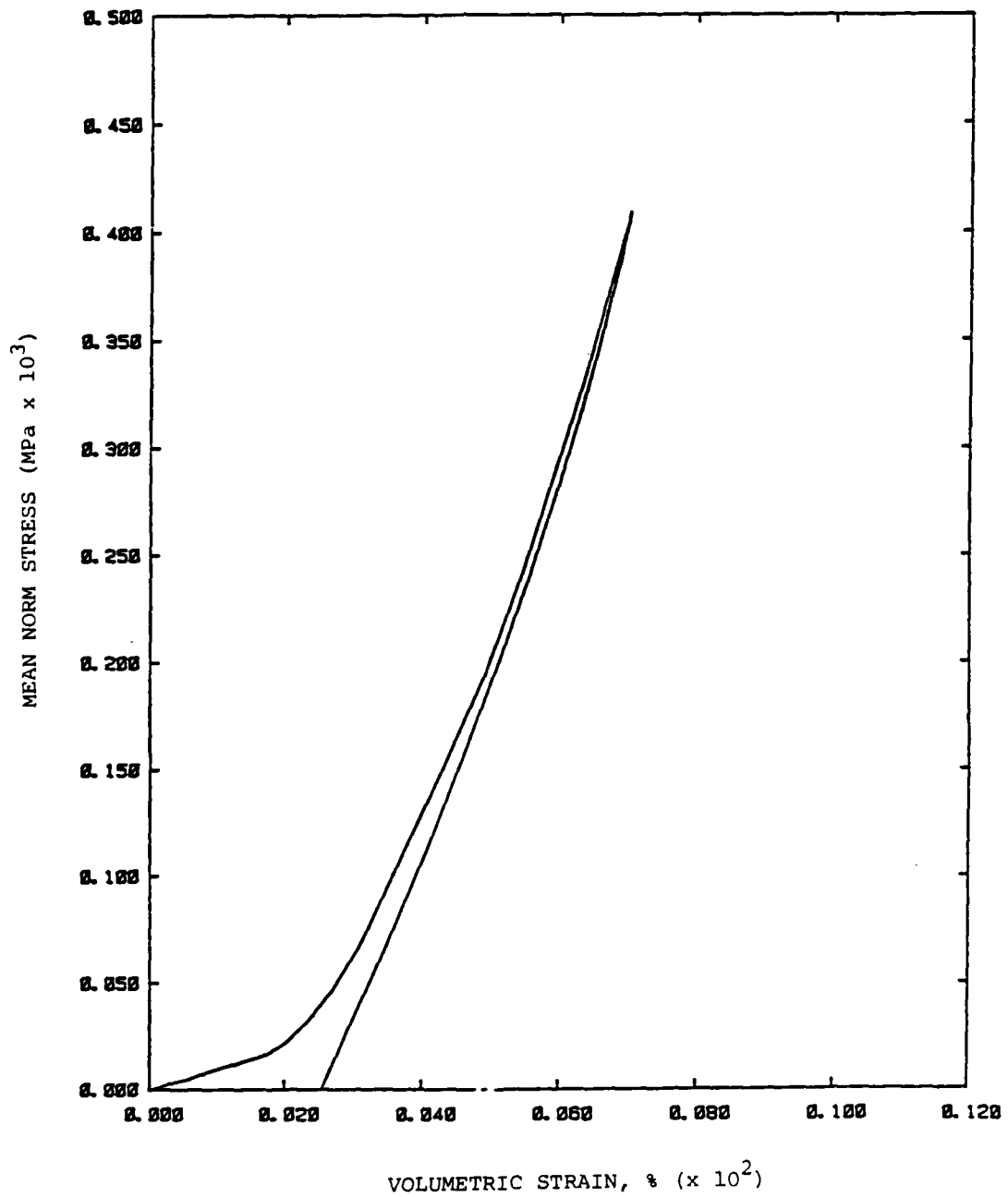


Figure A-3 Mean normal stress versus volumetric strain for sample taken at the 9.54 m to 9.85 m depth in U12g tunnel steam fracture hole No. 4. (Taken from Reference A-1)

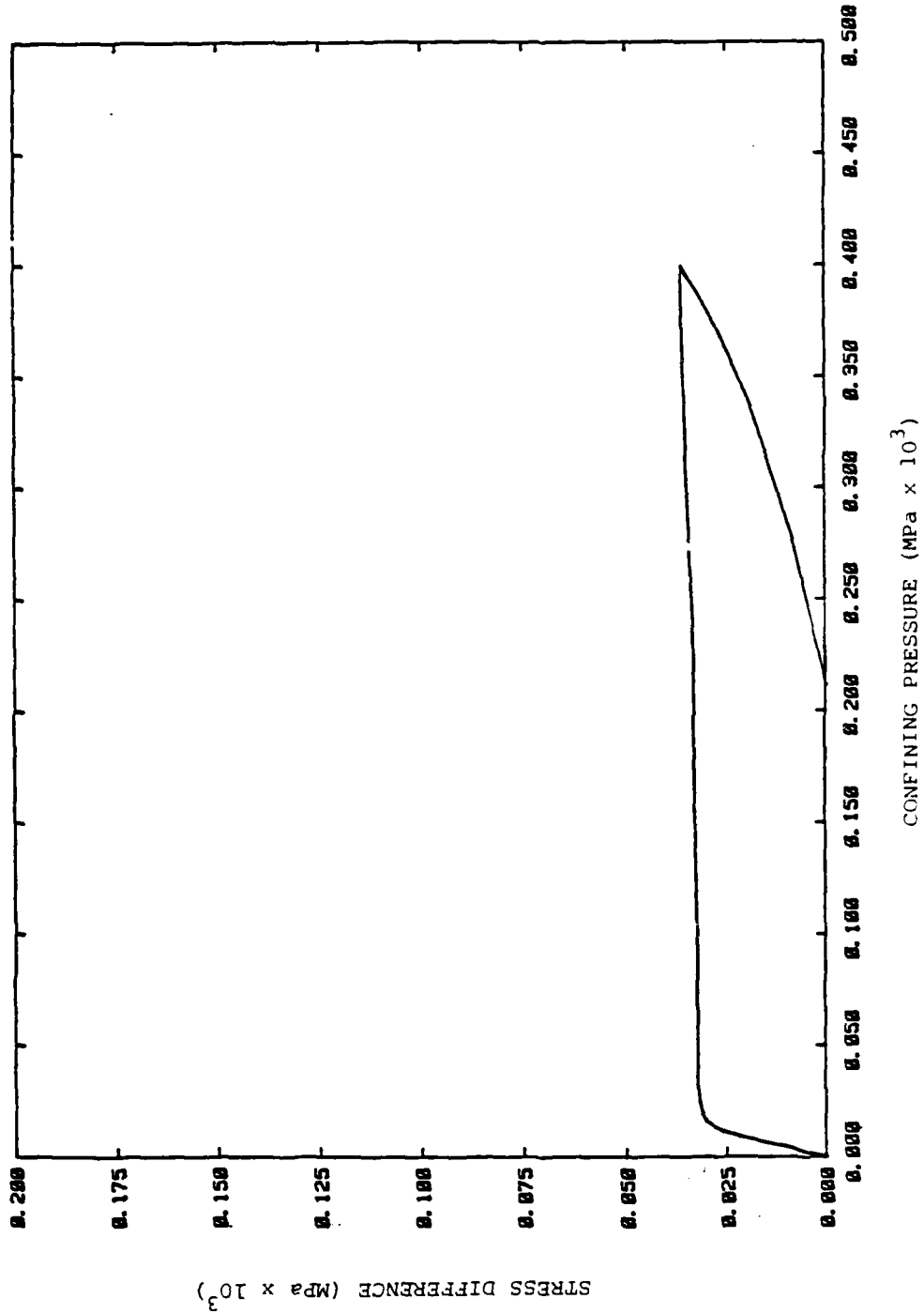


Figure A-4 Stress difference versus confining pressure for sample taken at the 9.63 m to 9.97 m depth in U12g tunnel steam fracture hole No. 1. (Taken from Reference A-1)

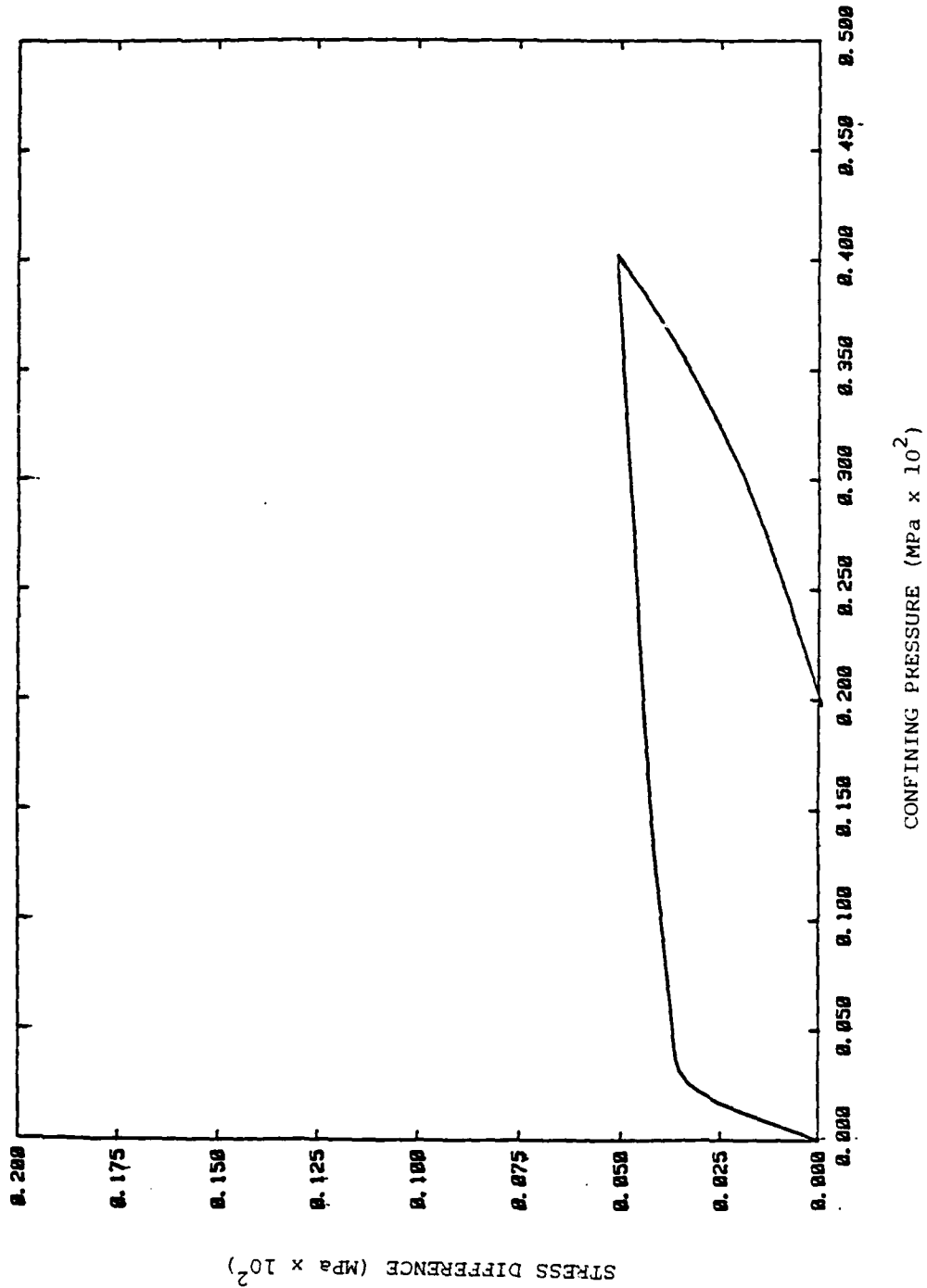


Figure A-5 Stress difference versus confining pressure for sample taken at the 9.81 m to 10.1 m depth in U12g tunnel steam fracture hole No. 2. (Taken from Reference A-1)

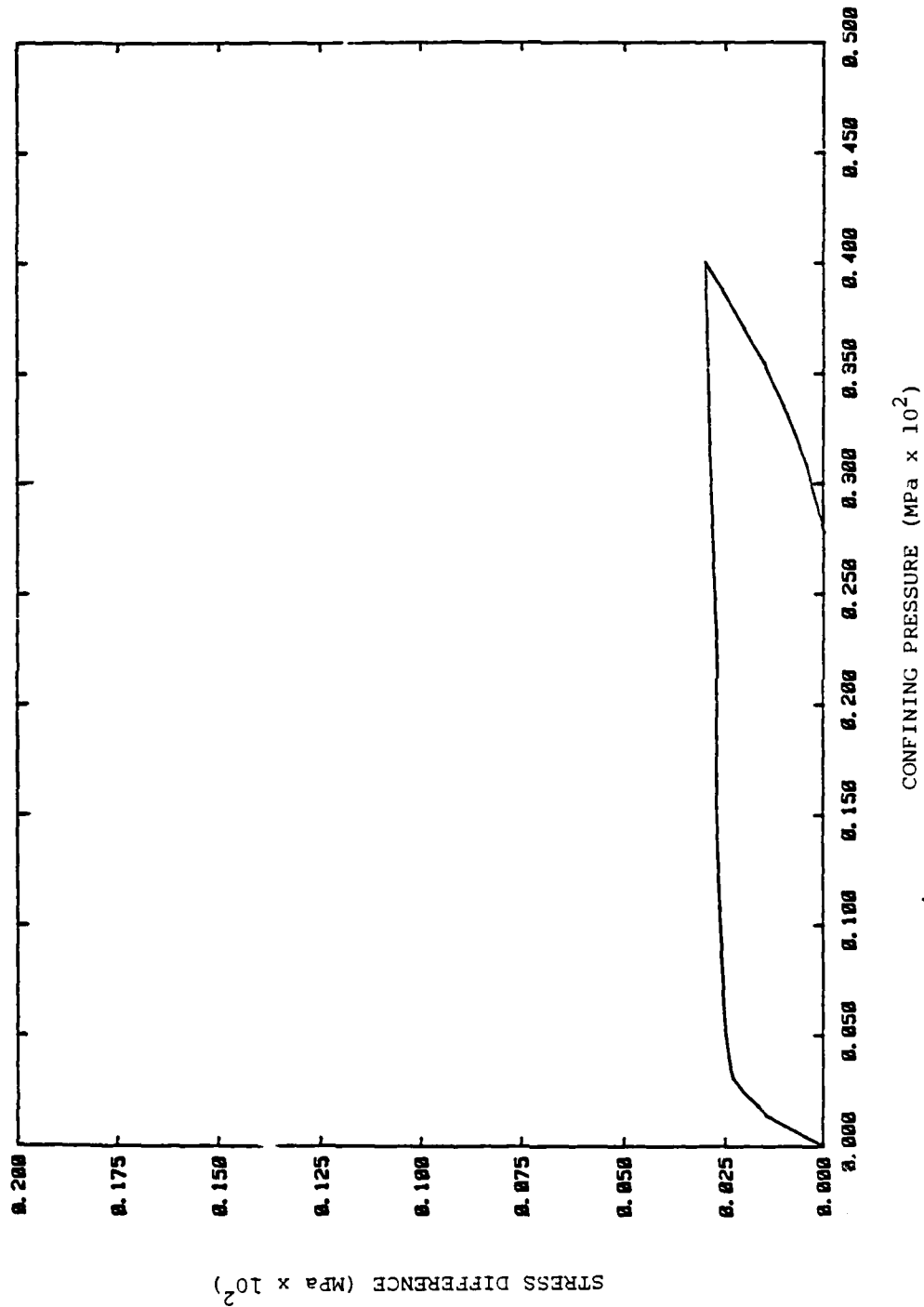


Figure A-6 Stress difference versus confining pressure for sample taken at the 9.54 m to 9.85 m depth in U12g tunnel steam fracture hole No. 4. (Taken from Reference A-1)

A-2 P-TUNNEL MATERIAL PROPERTIES.

Tests were performed by TerraTek (Reference A-4 and A-5) on core obtained from the U12p UG No. 2 and SH No. 3 holes located at CS 15+80 and CS 11+24, respectively. Mechanical properties, physical properties, permeability, and ultrasonic velocity tests have been completed on the U12p UG No. 2 core. Measurements of moisture content and gas permeability were conducted on the U12p SH No. 3 core.

Table A-3 lists the physical properties, measured permanent compaction and ultrasonic velocity data as a function of hole depth. Table A-4 lists the permeabilities of oven dried samples to nitrogen, and of native state core to both nitrogen and water. Results of the heat addition tests are presented in Tables A-5 and A-6.

The permeability data listed in Table A-3 were acquired from steady-state measurements on 2.5 cm long by 2.5 cm diameter samples. A sample from each depth was vacuum-oven dried at approximately 60°C for 24 hours. This sample was then tested to determine its permeability to dry nitrogen. Native state cores of the same dimensions were also tested for nitrogen permeability. The range of values listed under "Native State Air Permeability" in Table A-4 results from the permeating air drying the sample during the test. The effect of this drying is to cause a steady increase in the nitrogen permeability. This was observed over the entire 25-minute test duration. Presumably, it would continue until the sample was completely dried. The maximum permeability value that would be eventually attained is best estimated by the permeability of the oven dried samples. In the case of the liquid permeabilities, the opposite trend is observed. The initial measurement is the highest. The decrease in permeability is likely due to mobile fines restricting the pore throats. The total time span over which the permeabilities were measured was approximately 25 minutes.

Table A-3 Physical properties, permanent volume compactions, unconfined compressive strengths, and ultrasonic wave velocities of tuff from UI2p UG No. 2 located at CS 11+80. (Taken from Reference A-1)

Drill Hole Depth (m)	Density			Water by Wet Weight (Percent)	Porosity (Percent)	Saturation (Percent)	Calc. Air Voids (Percent)	Meas. Permanent Comp (Percent)	Velocity	
	As-Received (g/cc)	Dry (g/cc)	Grain (g/cc)						Long (km/s)	Shear (km/s)
4.51 - 4.75	1.56	1.16	2.35	25.33	50.6	79.1	10.6	8.3	2.45	1.30
5.55 - 5.91	1.73	1.39	2.31	19.70	39.8	85.4	5.8	9.3	1.56	0.96
6.74 - 7.04	1.71	1.35	2.34	20.70	42.3	85.1	6.3	8.7	2.06	1.05

Table A.4 Air and liquid permeability of oven dried and native state core taken from Hole U12p UG No. 2 located at CS 15+80 (Taken from Reference A.4).

Sample Depth (m)	Dried Sample	Native State Sample	
	Air Permeability (md)	Air Permeability (md)*	Water Permeability (md)*
4.51 - 4.75	445	28-84	224-180
5.55 - 5.91	720	88-252	570-250
6.74 - 7.04	459	53-104	285-218

* Approximately 25 minutes elapsed between the high and the low permeability readings.

Table A-5 Sample dimensions and weights before and after exposing U12p source hole No. 3 (CS 11+24) tuff (12.4 m to 12.8 m depth) to 1000°C for 30, 60, and 300 seconds. (Taken from Reference A-5)

Sample I.D.	Total Time in Oven (Seconds)	Initial Length (cm)	Initial Diameter (cm)	Initial Weight (gms)	Post-Test Length (cm)	Post-Test Diameter (cm)	Post-Test Weight (gms)	Decrease in Weight (Percent)	Approximate Bulk Volume Decrease (Percent)
1	30	7.49	5.11	236.4	7.49	5.11	218.3	7.7	0
2	30	7.62	5.08	236.5	7.62	5.08	218.7	7.5	0
3	60	7.72	5.08	243.0	7.72	5.08	214.1	11.9	0
4	60	7.67	5.08	240.1	7.67	5.08	213.2	11.3	0
5	300	7.62	5.08	239.7	7.57	5.05	178.9	25.4	1.6
6	300	7.62	5.08	251.1	7.57	5.05	193.9	22.8	1.7

Table A-6 Permeabilities and moisture contents obtained from U12p source hole No. 3 (CS 11+24) tuff (12.4-12.8 meter depth) exposed to 1000°C for 30, 60, and 300 seconds. (Taken from Reference A-5)

Sample I.D.	Total Time in Oven (seconds)	Post-Test Permeability (md)	Post-Test Moisture Content (Percent)	Native State Moisture Content (Percent)*
1	30	--	19.8	25.2
2	30	165	--	28.1
3	60	--	15.8	
4	60	163	--	27.4
5	300	--	3.7	
6	300	1063	--	28.0

* Determined on material adjacent to the tested samples.

Heat addition tests were conducted on core taken from the U12p SH No. 3 hole source region. In these tests, native state samples were exposed to 1000°C for either 30, 60, or 300 seconds. Measurements were then conducted on these samples to determine moisture content and gas permeability. The permeability tests were performed using nitrogen; confining pressure and pore pressure were 1.7 MPa and .027 MPa, respectively.

Results of the heat addition tests are presented in Tables A-5 and A-6. Table A-5 contains sample dimensions and weights, both before and after the heating tests. Percent weight and volume reductions obtained from these data are included. Presented in Table A-6 are permeability and moisture content data for the heated samples; native state moisture contents obtained from material adjacent to the test samples are also included. As shown in this table, Samples 2 and 3 are associated with the same moisture content. This is because material used for the moisture content determination was taken adjacent to the locations of both samples on the 10-inch diameter core. The same situation also applies to Samples 4 and 5.

An expected result of these heating tests was the increase in weight loss with increasing exposure time to 1000°C. Weight reductions ranged from 6.5 percent to 25.4 percent for samples exposed for 30 and 300 seconds, respectively. Heating the samples for 30 or 60 seconds produced no measurable changes in their pre-test (native state) dimensions. Samples heated for 300 seconds did show slight decreases in both length and diameter. Calculated bulk volume reductions for both samples were approximately 1.6 percent.

Permeabilities measured for samples heated for 30 to 60 seconds were 165 and 163 md, respectively. The measured permeability of native state material was approximately 50 md. These data show that, while permeabilities were nearly identical in samples exposed for 30 or 60 seconds, there was a noticeable change in the permeability of these samples relative to native state material. The most significant effects

of heating on permeability were observed in the sample heated for 300 seconds. This sample had a measured permeability of 1086 md. Multiple fissures induced in the sample during heating probably contributed significantly to the relatively large permeability. Surface fissures were prominent up to a depth of approximately 0.1 inch below the sample surface. Surface fissures were not apparent in either of the other samples.

Samples heated for 30, 60, and 300 seconds had subsequent moisture contents of 19.8, 15.8, and 3.7 percent by weight, respectively. As seen in Table A-6, the native state moisture contents associated with these samples are 25.2, 28.1, and 27.4 percent by weight. These values, however, probably do not reflect the actual moisture contents of the test samples prior to heating because, as previously explained, the native state moisture content measurements were made on adjacent material. An effect of this is seen in Sample 3 where the moisture loss (34.5 g) calculated using the native state and post-test moisture contents is greater than the total weight loss of the sample due to heating (28.9 g).

Recall that low pressure in situ gas permeability tests were performed in both the source and diagnostic hole layouts as CS 11+90 and CS 11+24 prior to conducting the steam fracture tests. Relative gas permeabilities of 260 md and 25 md (results from fractured holes A, B, and F2 were not included) were measured at the two locations, respectively. These should be compared to the initial 60 md native state value obtained from the core samples from the UG No. 2 and SH No. 3 holes.

The 10 cm diameter by 46 cm long steam source region located at CS 11+90 was examined using a downhole T.V. subsequent to the steam fracture test. The initially circular hole was elongated (approximately 2 cm) in the horizontal direction, and its surface had been severely pitted. In addition, there existed a vertical fracture whose approximate 1 cm wide base ran the entire length of the top of the hole. It is possible that the hole damage and fracture occurred as a result of the pressure excursion described in the main body of this report.

A number of high and low pressure flow tests were conducted in the post-steam fracture test source region. Test results are shown in Table A-7. The resulting permeability values (determined as described in Appendix C) are surprisingly close to the pre-steam fracture flow test results. It should be noted that there was no evidence of fracture breakdown even during the 5.1 MPa water flow test.

The tensile strengths (as determined by Brazil test) and the unconfined compression strengths are listed in Table A-8 for core taken from the UG No.2 borehole. Figures A-7 through A-13 are plots of the data from the mechanical tests. Uniaxial strain data are shown on Figures A-7 through A-10 where mean normal stress versus volumetric strain, and stress difference versus confining pressure are plotted. Unconfined compression data are shown on Figures A-11 through A-13 as stress versus axial and lateral strain.

Analysis of the mechanical test data shows that the material undergoes large amounts of permanent compaction. All three samples exceeded the measurement range of the transducers. Further testing with extended range transducers was not possible due to a lack of sufficient sample material.

A grout fracture experiment (Reference A-6) was conducted in P-Tunnel in core hole U12p UG No. 2 located at CS 15+80. This hole was drilled vertically up and entirely through Sub-unit P-27 of the Paintbrush Tuff (Reference A-7). At this location in P-Tunnel, the unit is composed of vitric (non-zeolitized) ashfall tuff with a few thin silicified beds. The zone from approximately 4.3 m to 7.3 m (TD) in the hole is fairly uniform in composition and texture. No natural fractures were visible in the core.

During the grout fracture test, breakdown occurred at an undefined pressure value which is known to be less than 3.1 MPa. After the test, the hole was reamed to a 15 cm diameter and deepened to 7.5 meters. A

Table A-7 Results of post-steam fracture flow test conducted in the 10 centimeter diameter by 46 centimeter long P-Tunnel steam source region located at CS 11+90.

Fluid	Drive Pressure (MPa)	Permeability (Darcy)
Air	.15	.70
Air	1.4	.32
Water	.47	.36
Water	5.1	.21

Table A.8 Tensile and unconfined compression strengths for core taken from U12P.UG No. 2 located at CS 15+80. (Taken from Reference A.4).

Sample Depth (m)	Tensile* Strength (psi)	Unconfined Compressive Strength (MPa)
4.5 - 4.75	229.0	11.7
5.55 - 5.91	86.2	6.51
6.74 - 7.04	175.0	14.2

* Determined using the Brazil test method.

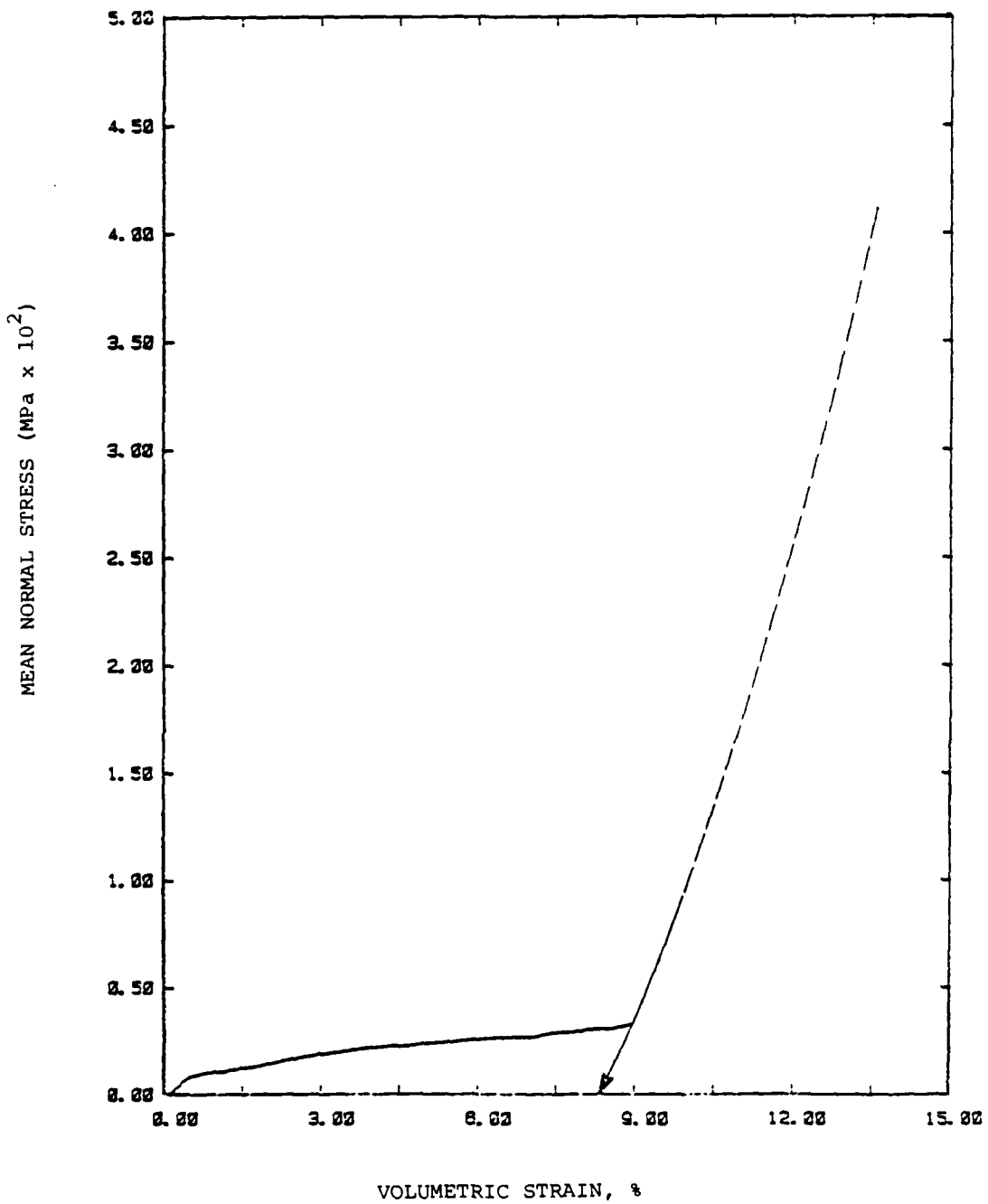


Figure A-7 Uniaxial strain test results for sample taken at 4.71 m to 4.75 m depth in hole '12p UG No. 2 at CS 11+90. (Taken from Reference A-4)

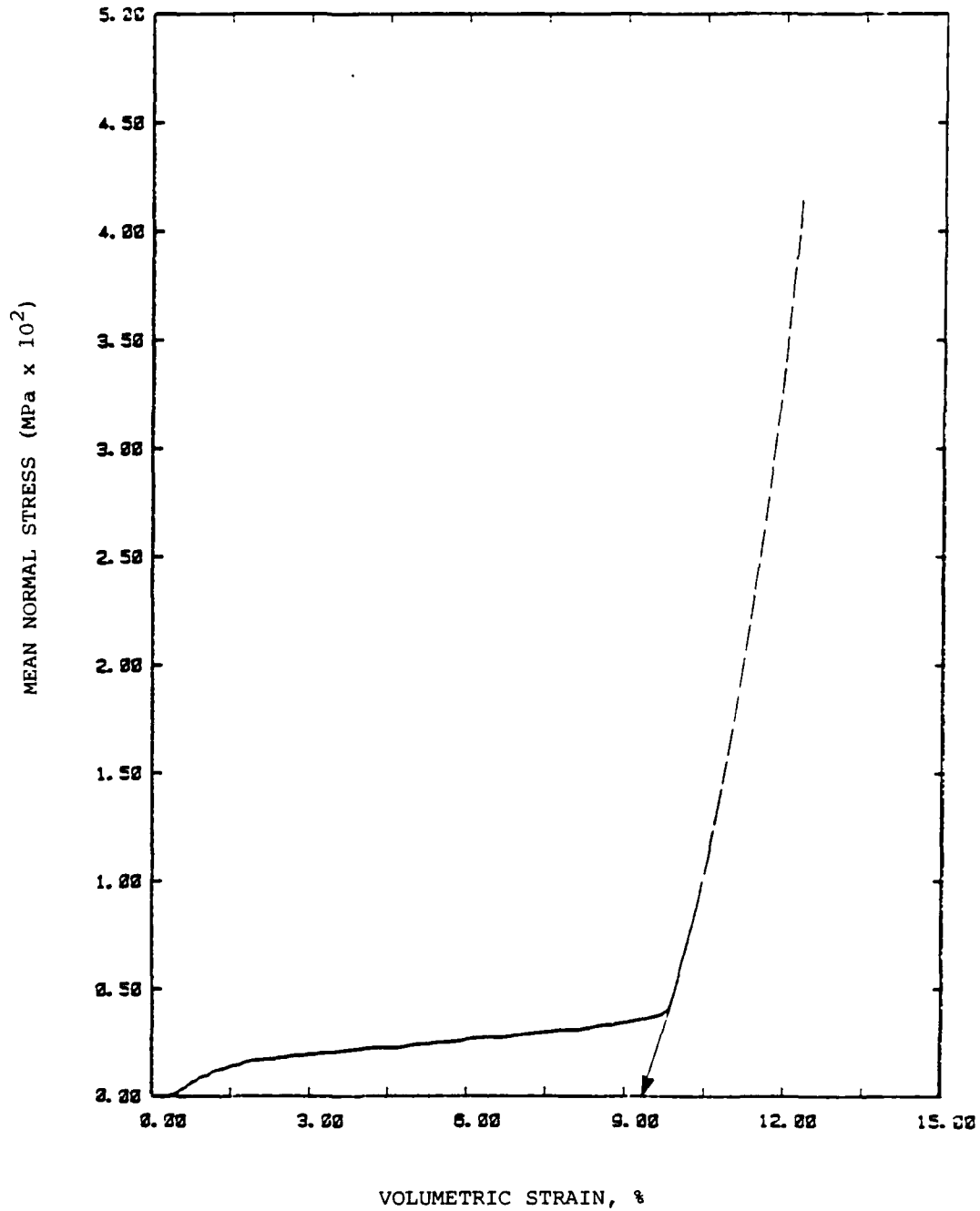


Figure A-8 Mean normal stress versus volumetric strain for sample taken at the 5.55 m to 5.91 m depth in hole U12p UG No. 2 at CS 11+90. (Taken from Reference A-4)

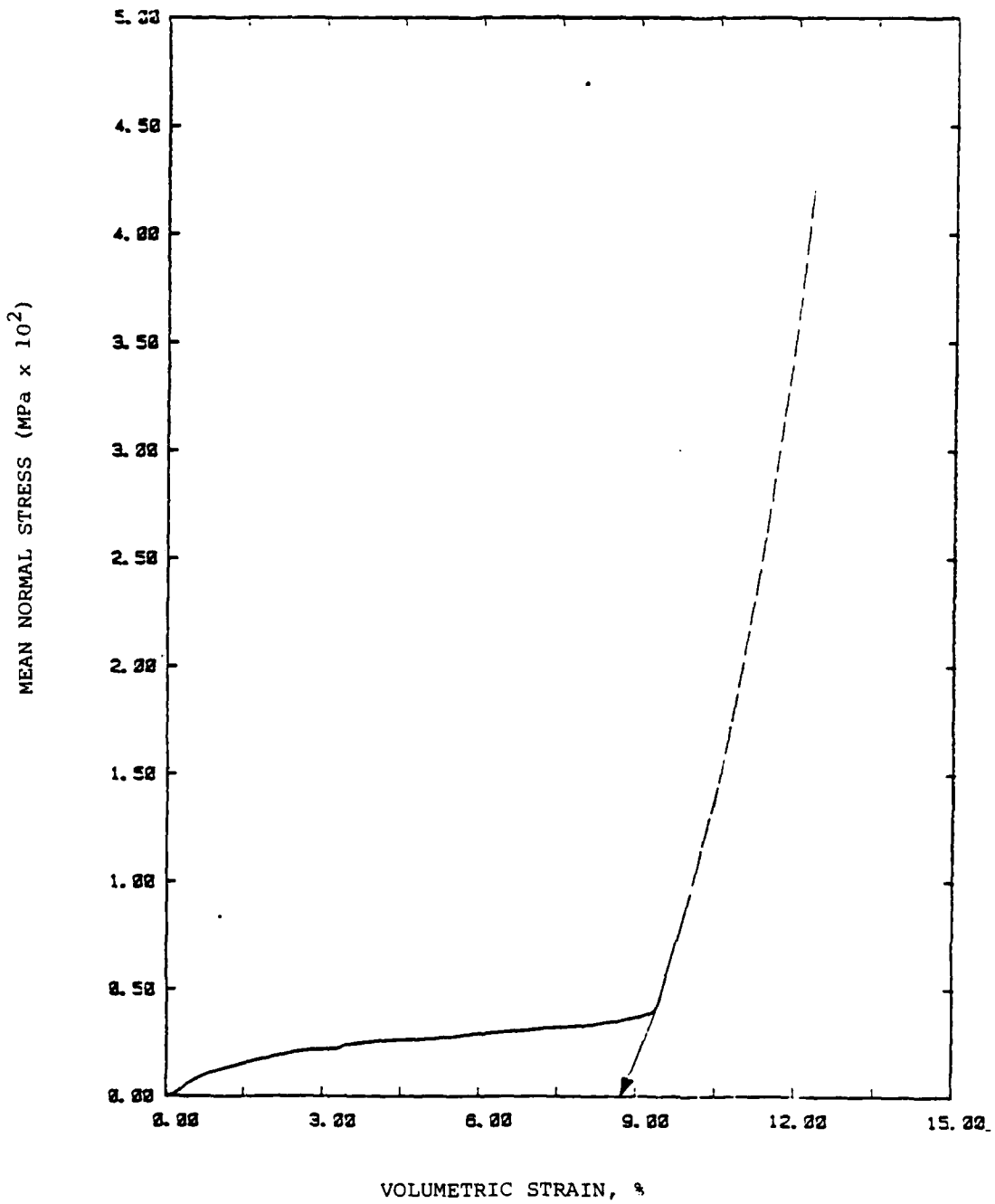


Figure A-9 Mean normal stress versus volumetric strain for sample taken at the 6.74 m to 7.04 m depth in hole U12p UG No. 2 at CS 11+90. (Taken from Reference A-4)

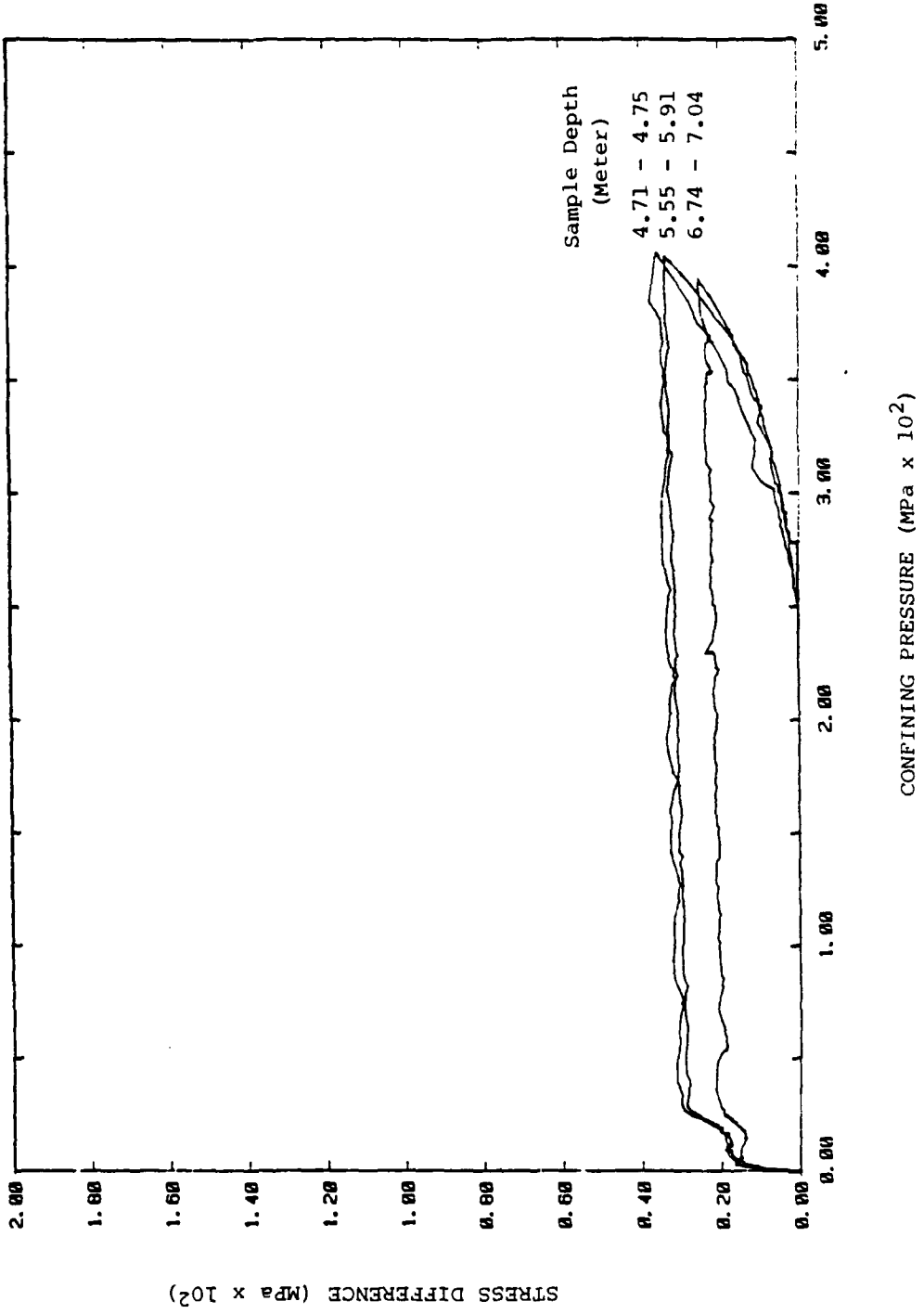


Figure A-10 Stress difference versus confining pressure for sample taken from hole U12p UG No. 2 located at CS 11+90. (Taken from Reference A-4)

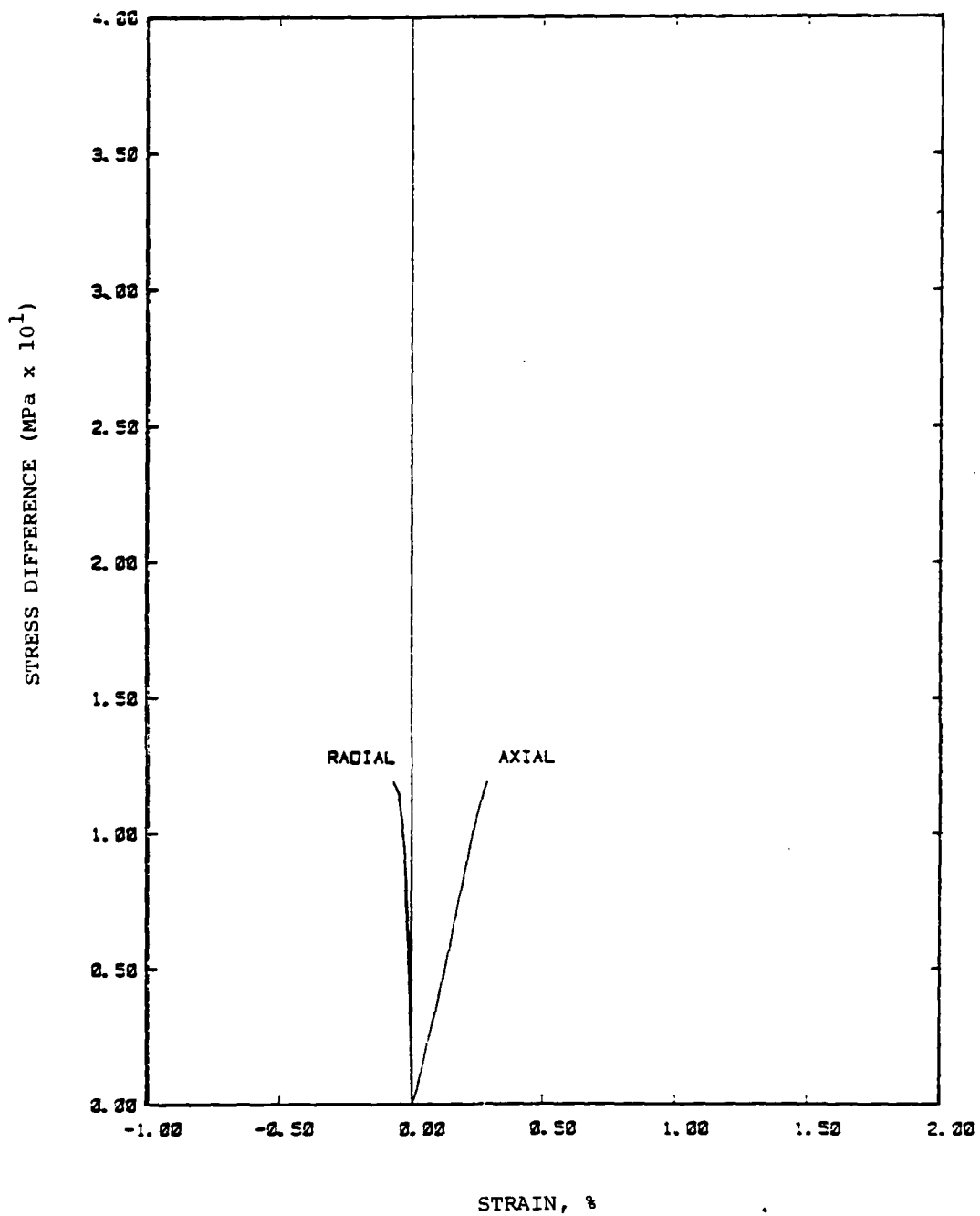


Figure A-11 Unconfined compression test results for sample taken at the 4.51 m to 4.75 m depth in hole U12p UG No. 2 located at CS 11+90. (Taken from Reference A-4)

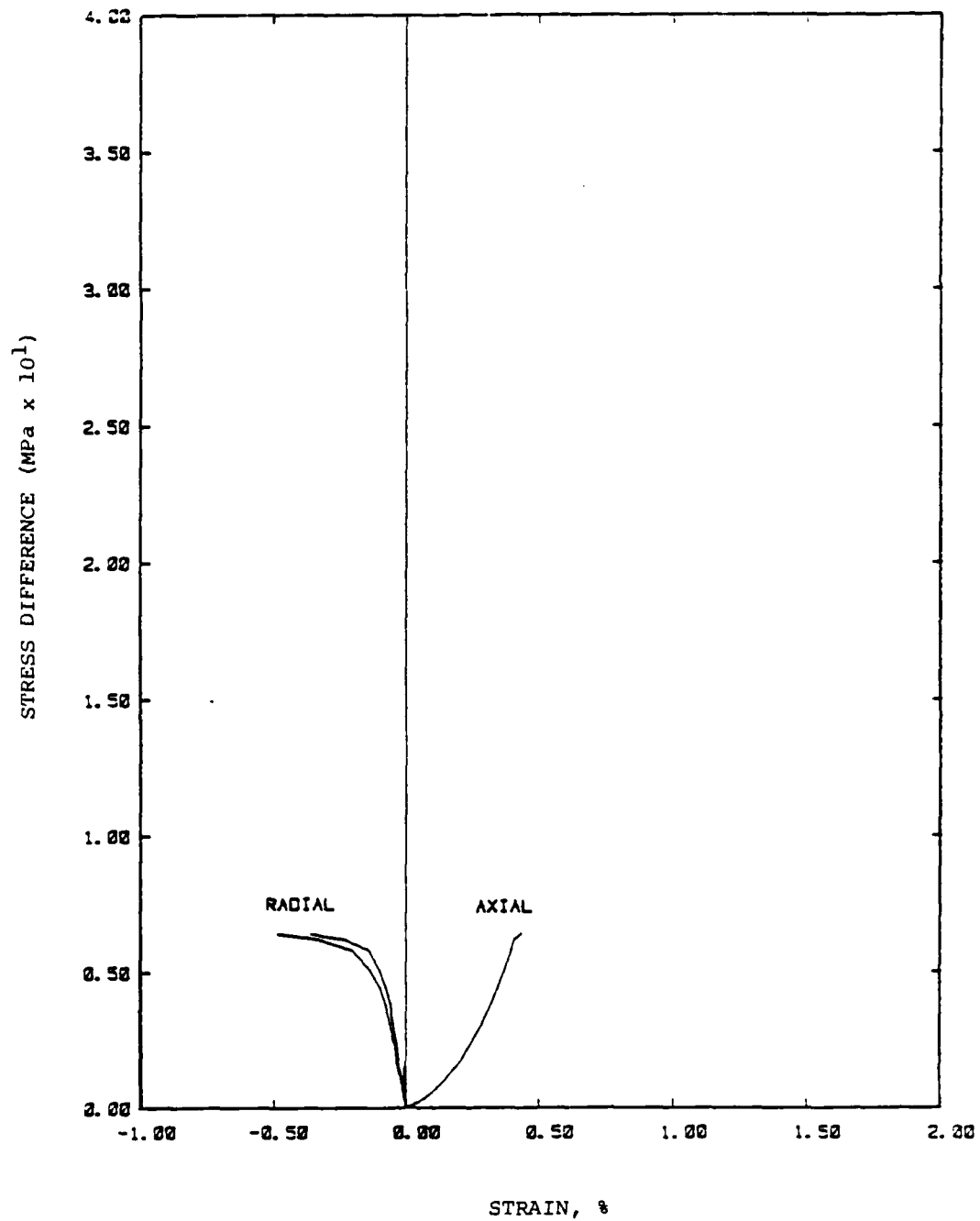


Figure A-12 Unconfined compression test results for sample taken at the 5.55 m to 5.91 m depth in hole U12p UG No. 2 located at CS 11+90. (Taken from Reference A-4)

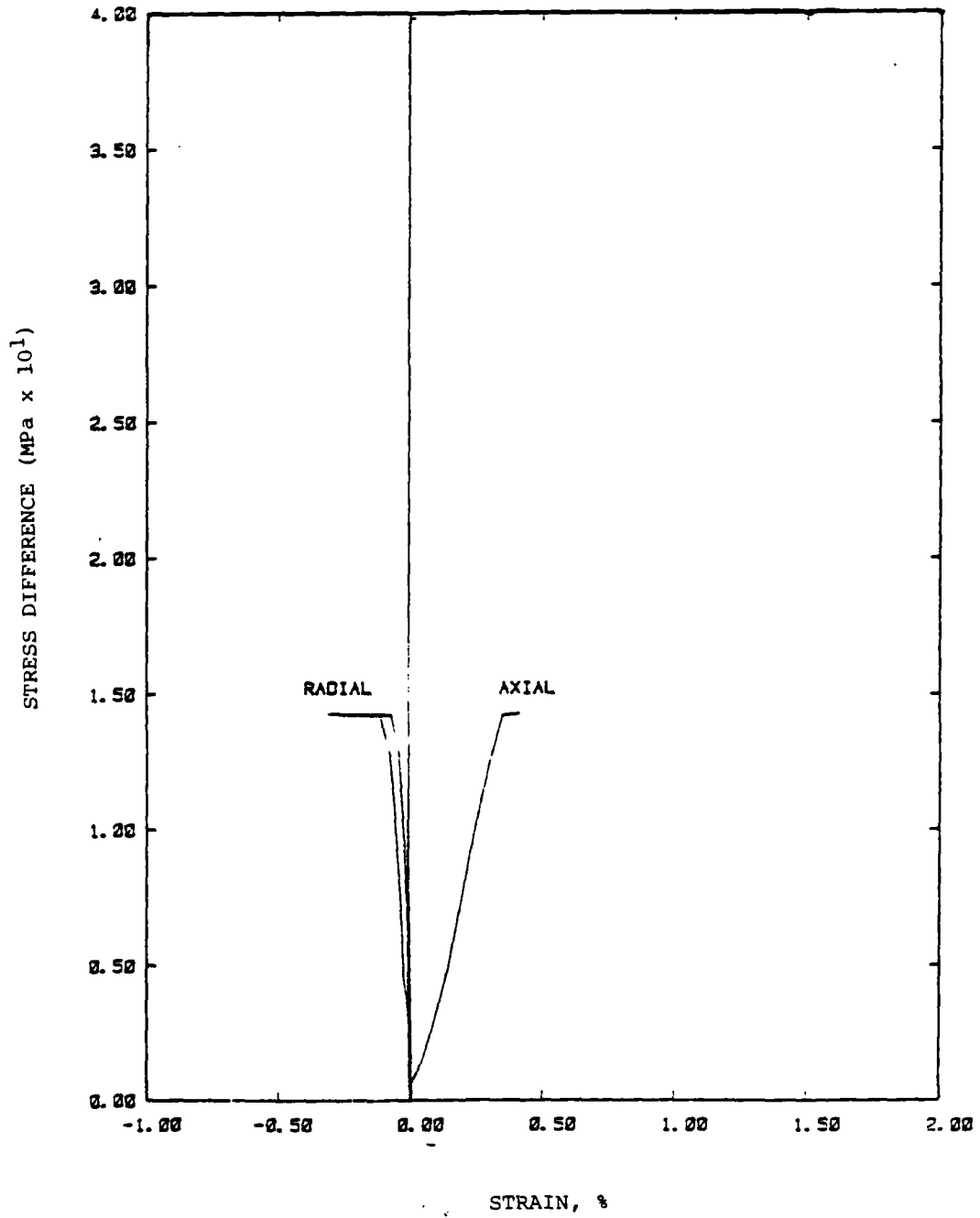


Figure A-13 Unconfined compression test results for sample taken at the 6.74 m to 7.04 m depth in hole U12p UG No. 2 located at CS 11+90. (Taken from Reference A-4)

black and white T.V. camera was run in the hole and the resulting video tape showed a vertical fracture running parallel to the axis of the hole, from approximately the 3.5 m to 6.6 m depths. The fracture was oriented approximately normal to the drift (N40°E to N50°E). However, the orientation of the fracture beyond 5.4 m, up to 6.6 m was very difficult to determine. The drill hole was then reamed to a 25 cm diameter, and another black and white T.V. camera run made. The fracture was still visible, extending approximately from 3.6 m to 5.3 m. The orientation of the fracture was determined to be approximately N75°E. In the final measurement made by Fennix and Scisson geologists using a borescope, the fracture orientation at 3.6 m and at 4.8 m was N58°E and N73°E, respectively, for an average of N65°E as shown on Figure A-3. This orientation appears fairly constant from the 3.5 m to 5.3 m depths. The fracture is 0.16 to 0.32 cm wide, and is made up of one to three planes.

In situ stresses were measured in P-Tunnel (Reference A-8) using an overcoring operation which followed the USBM procedure. The test was conducted at the 1.05 m to 1.21 m depth in a hole drilled vertically up at CS 15+33. The measured major secondary principal stress of 1.50 MPa had a bearing of N90°E, while the minor secondary principal stress of 0.75 MPa had a bearing of N0°E.

In situ stress measurements were also made in drill holes in P-Tunnel during operations NOUGAT and STORAX. The data from these measurements were presented by Obert (Reference A-9). During those tests, a borehole deformation-overcore technique was used to determine the stress value in two horizontal NX core holes labeled P-1-1 and P-1-2 located at CS 20+00.

In drill hole P-1-1 the vertical component of stress, approximately 20° off horizontal, was found to be nearly equal to that calculated for gravity stress. The horizontal stress, however, was much greater than the vertical stress--possibly indicating the presence of a horizontal tectonic force.

In horizontal drill hole P-1-2, drilled perpendicular to P-1-1, the vertical component of stress was very close to perfectly vertical, and was much stronger than the stress in the horizontal direction. The vertical stress component was also much stronger than the calculated gravity stress. This phenomenon may be related to the greater fracture frequency in core from drill hole P-1-2.

The report notes that compressive tests on 1D NX test samples indicated that core from drill hole P-1-2 averaged 70 percent greater in strength than core from drill hole P-1-1. It may be possible that P-1-2 was drilled along a particularly strongly silicified bed (Reference A-7). The NOUGAT and STORAX study is thought to offer little insight to the fracture orientation study performed at CS 15+80 or the stress measurements made at CS 15+33.

APPENDIX B
DETAILED STEAM FRACTURE TEST DATA

Detailed diagnostic hole pressure data are shown in this Appendix for the G-Tunnel (SFT No. 1) and P-Tunnel (SFT No.'s 2, 3, and 4) steam fracture tests. These data were digitized and expanded from smaller analog plots.

Since the data are difficult to read, the pressure arrival and decay times are shown on each figure. The G-Tunnel diagnostic hole pressure histories are considered good data, since the water-filled diagnostic holes did not leak. In contrast, the P-Tunnel diagnostic holes leaked to varying degrees. Consequently, the pressure rise times and associated peak values should be used with extreme caution. However, the arrival and decay times are considered to be accurate.

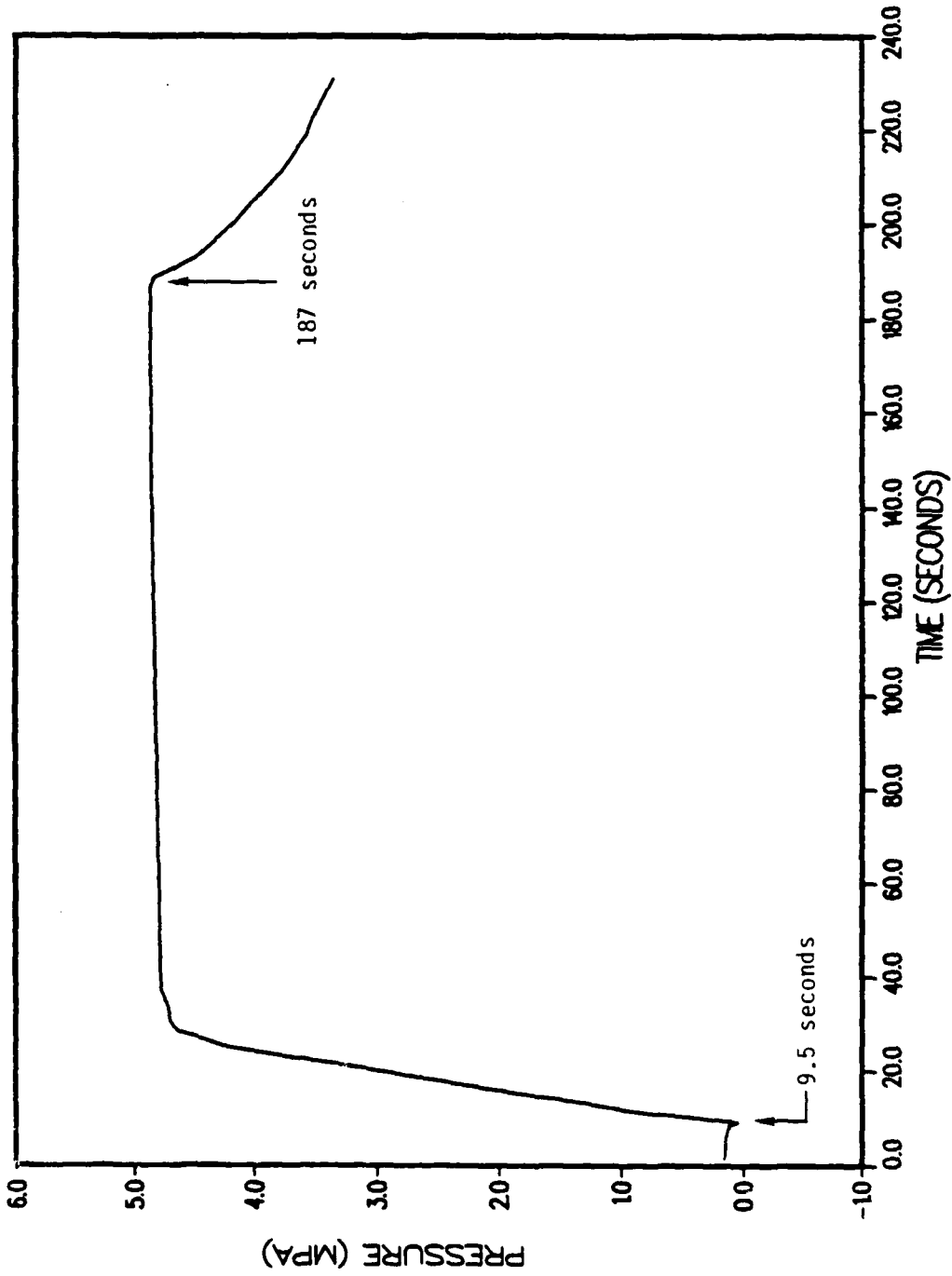


Figure B-1 G-tunnel steam fracture experiment (SFT No. 1) diagnostic hole "A" pressure history.

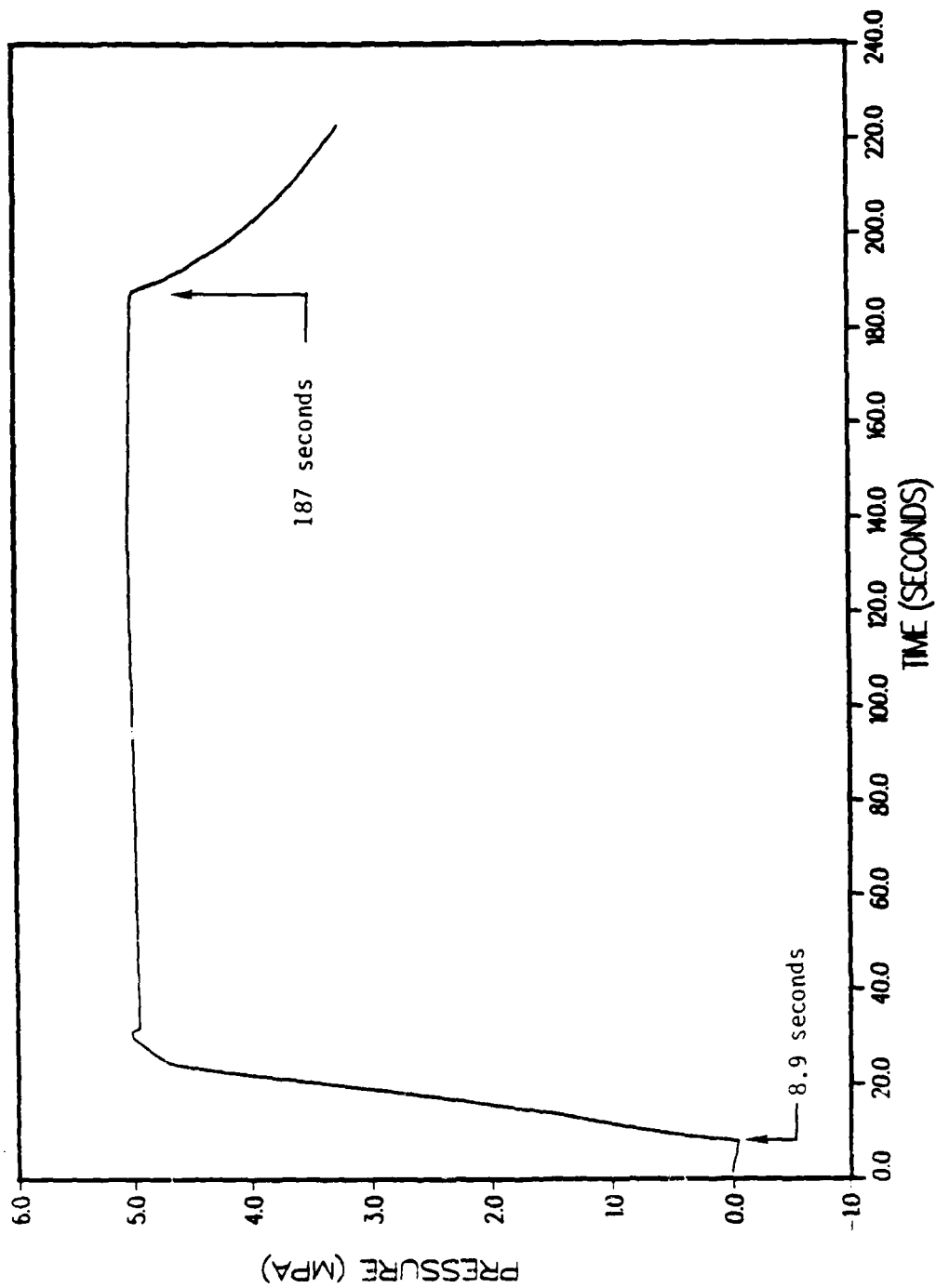


Figure B-2 G-tunnel steam fracture experiment (SFT No. 1) diagnostic hole "B" pressure history.

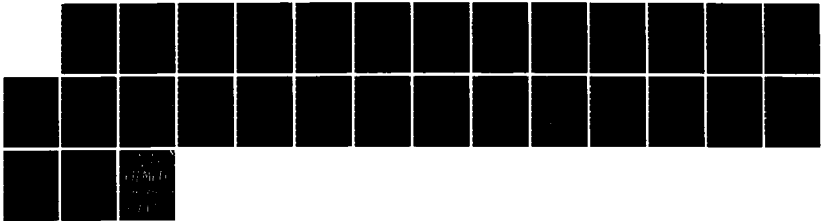
NO-A165 792

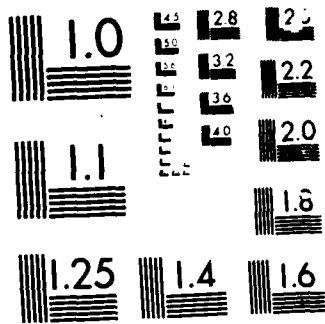
IN SITU STEAM FRACTURE EXPERIMENTS(U) S-CUBED L JOLLA 2/2
CA E W PETERSON ET AL. 31 DEC 84 SSS-R-85-6960
DNA-TR-84-407 DNA001-80-C-0239

UNCLASSIFIED

F/G 20/11

NL





MICROCOPY RESOLUTION TEST CHART

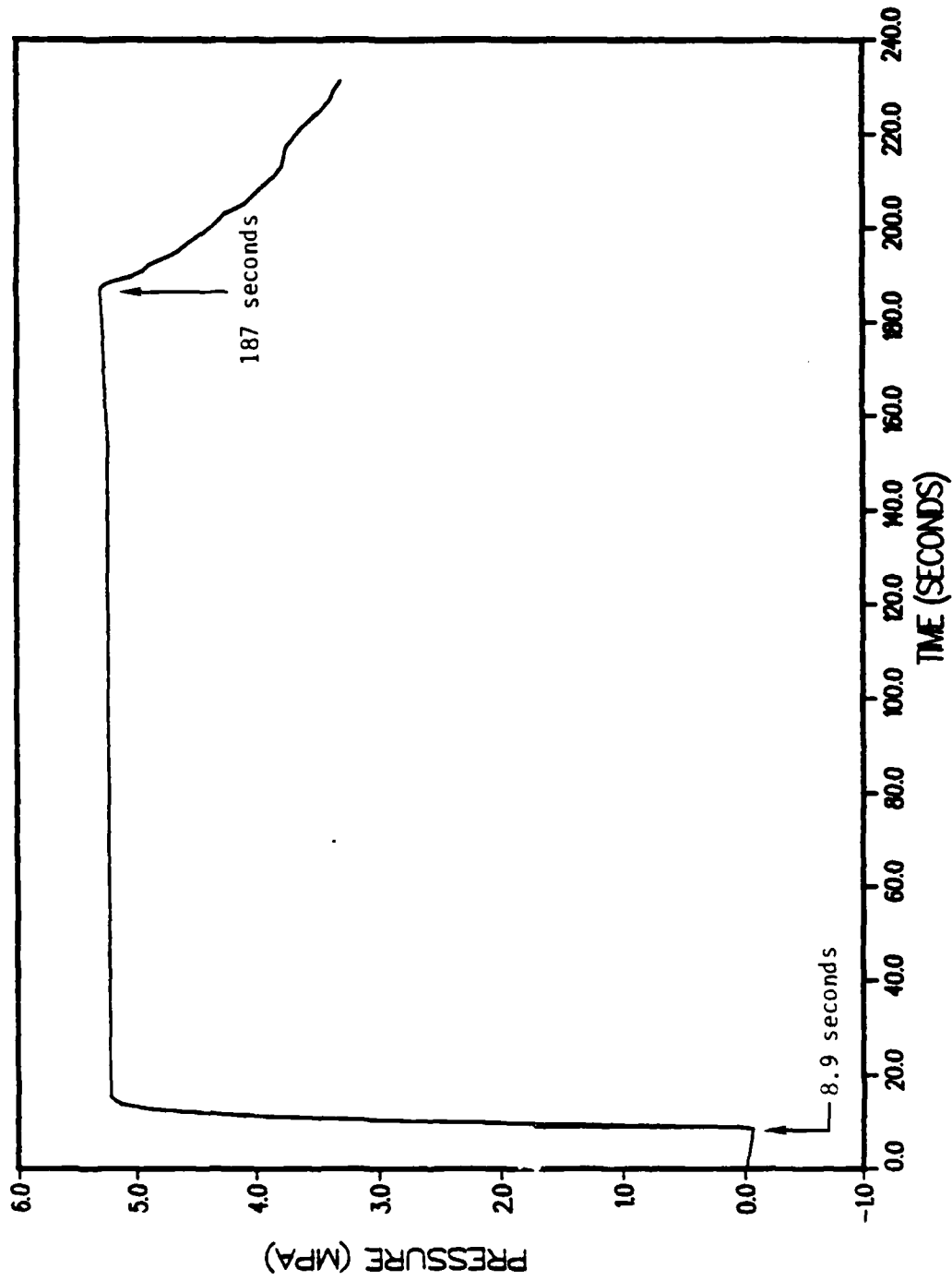


Figure B-3 G-tunnel steam fracture experiment (SFT No. 1)
diagnostic hole "1" pressure history.

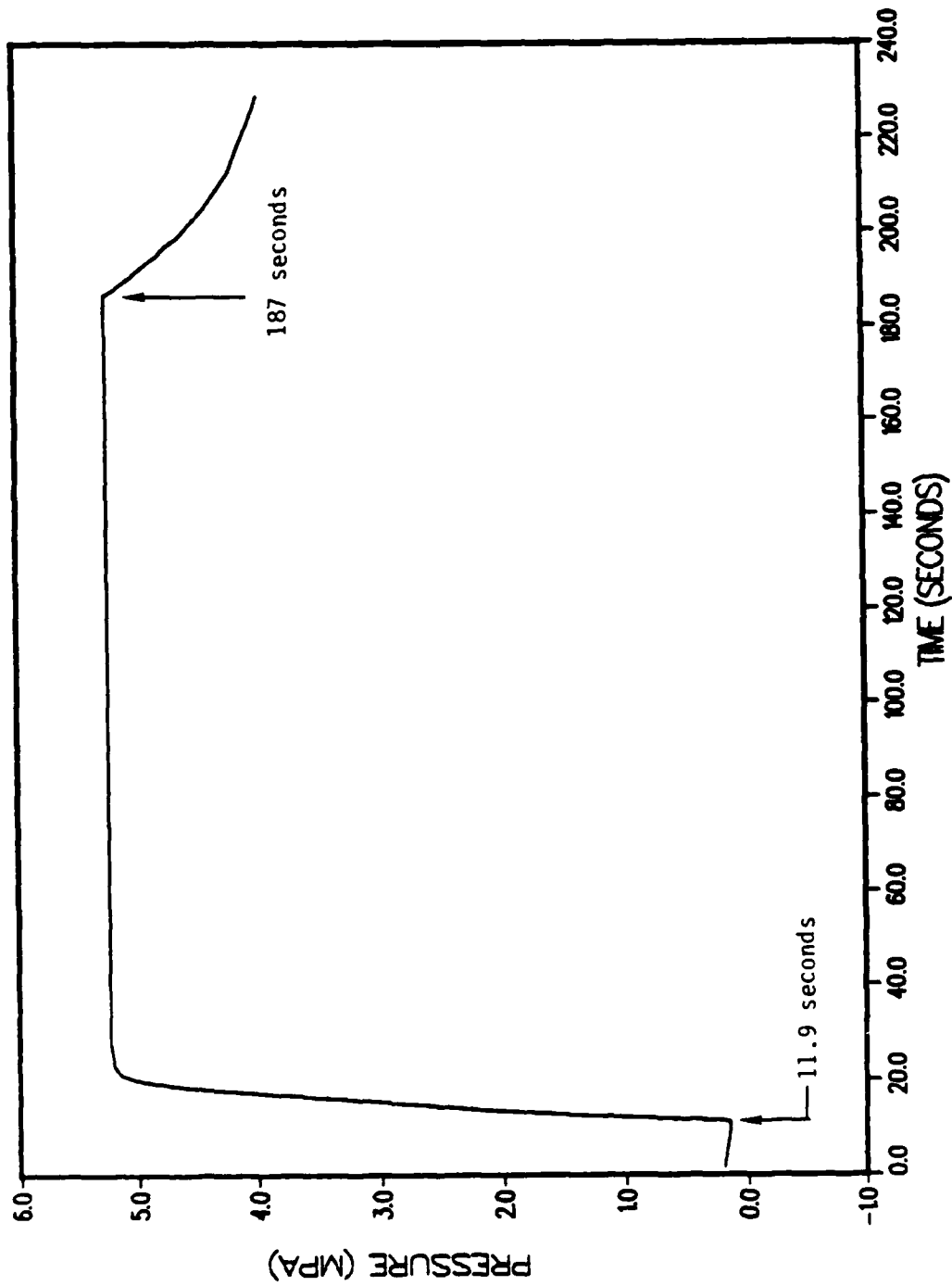


Figure B-4 G-tunnel steam fracture experiment (SFT No. 1) diagnostic hole "2" pressure history.

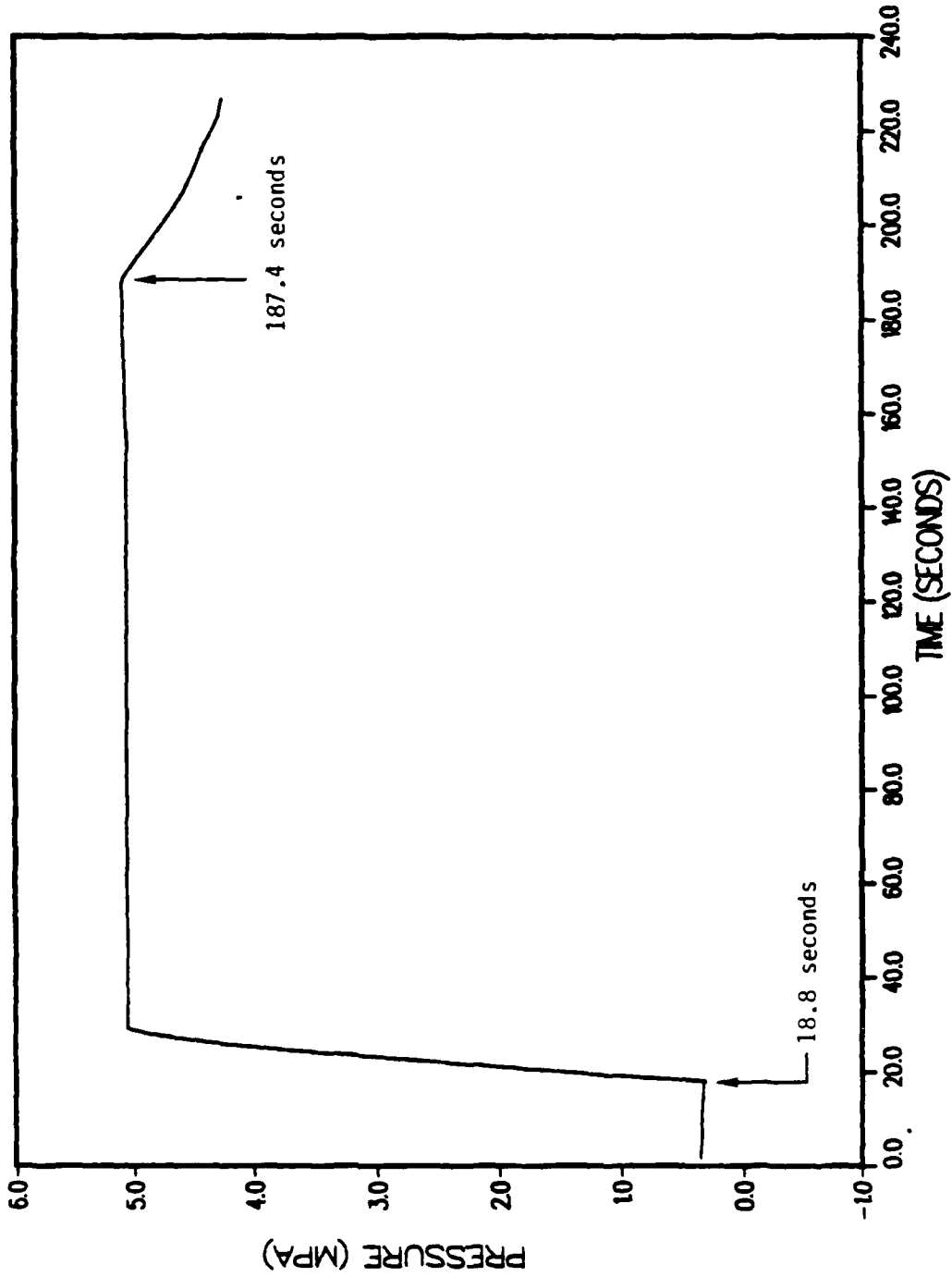


Figure B-5 6-tunnel steam fracture experiment (SFT No. 1) diagnostic hole "3" pressure history.

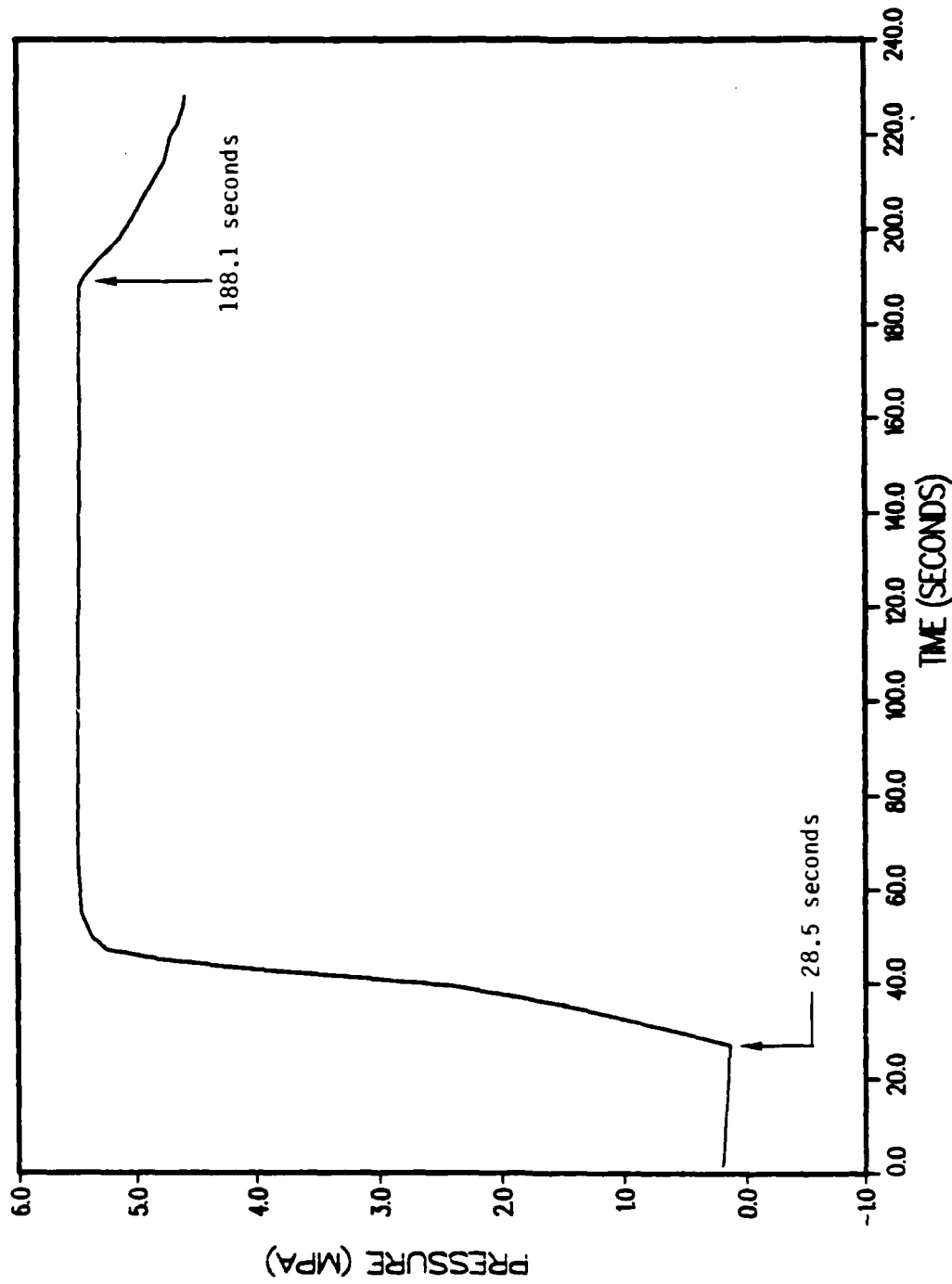


Figure B-6 G-tunnel steam fracture experiment (SFT No. 1) diagnostic hole "4" pressure history.

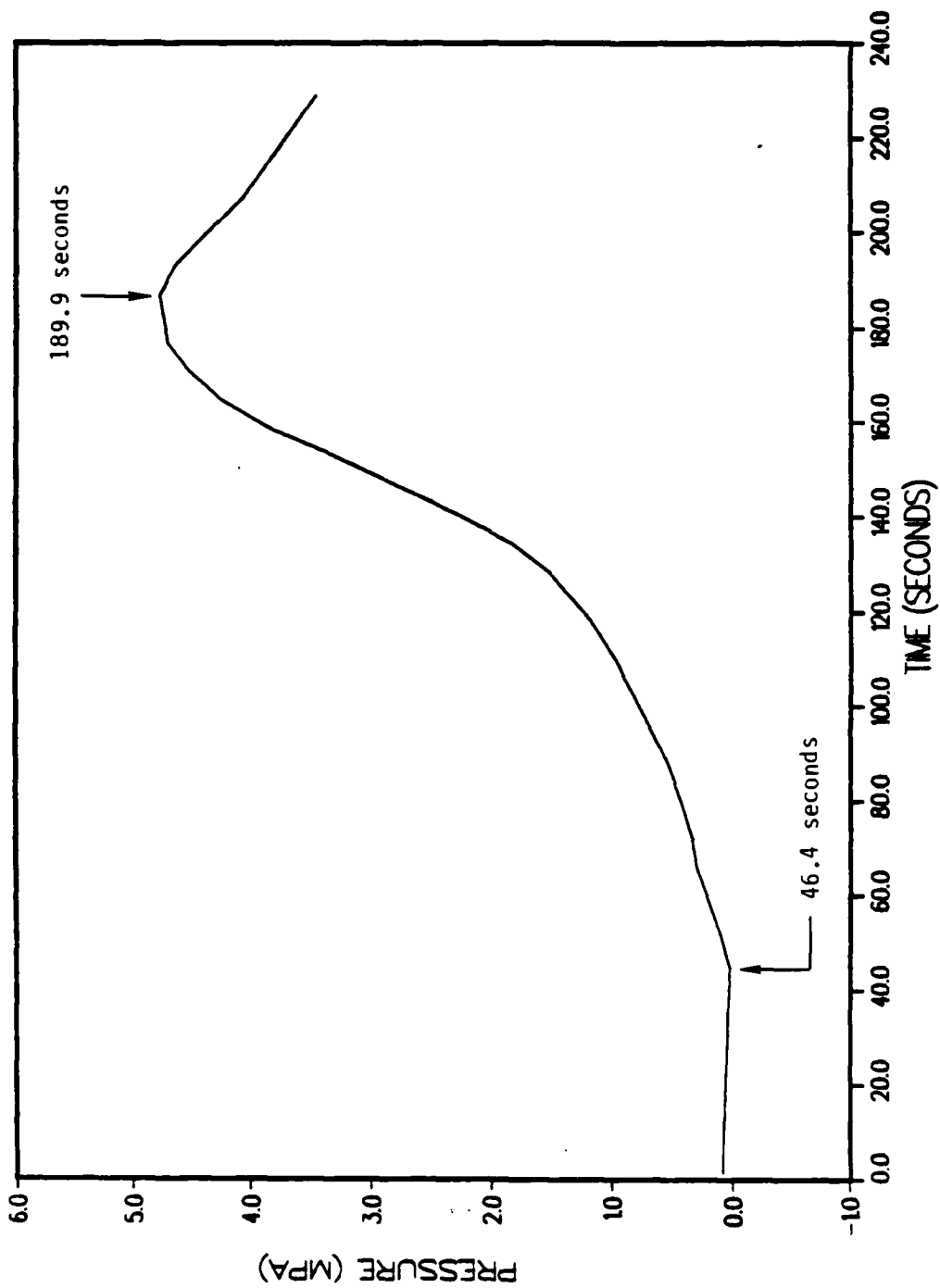


Figure B-7 G-tunnel steam fracture experiment (SFT No. 1) diagnostic hole "C" pressure history.

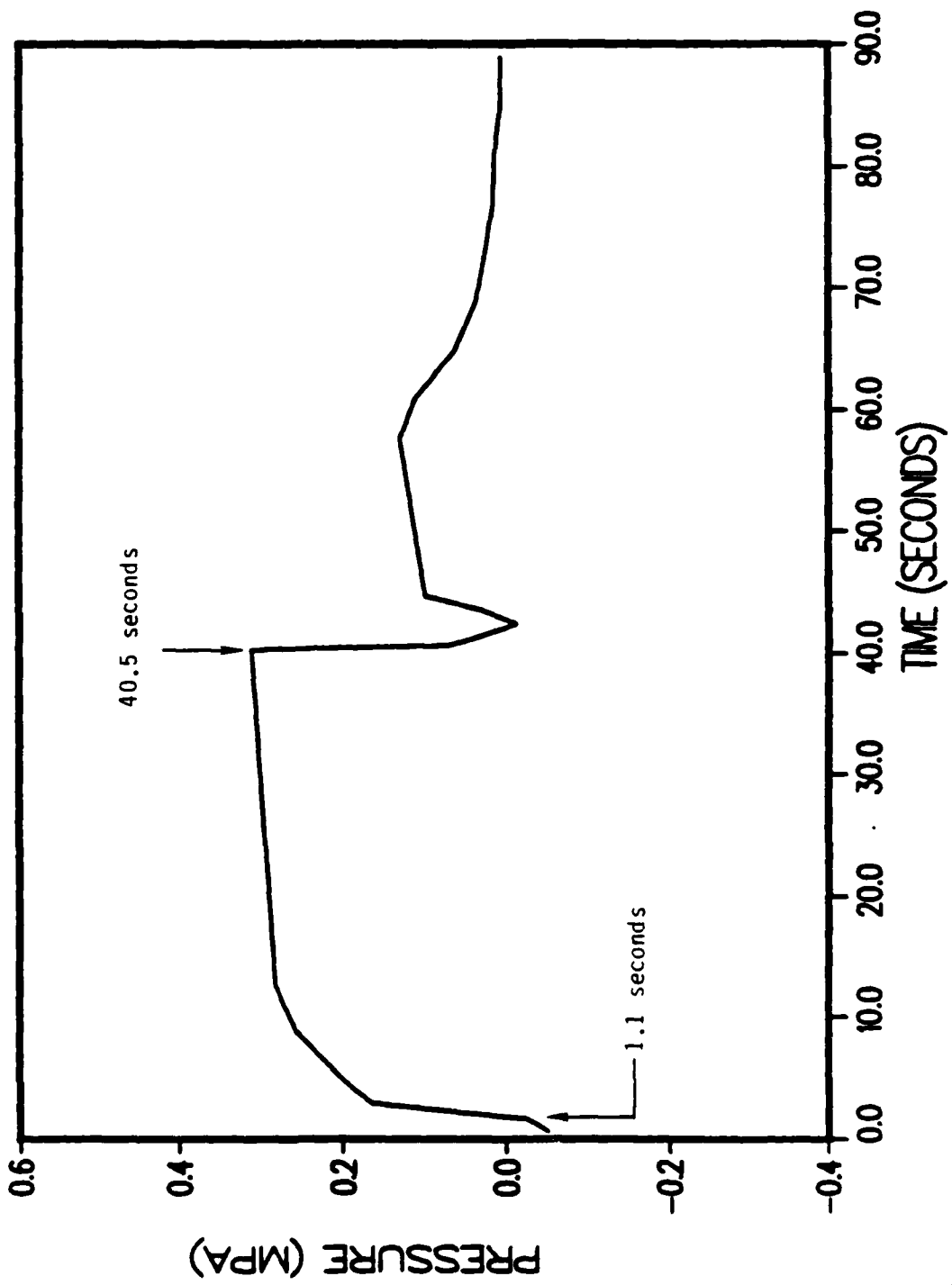


Figure B-8 P-tunnel CS 11+90 steam fracture experiment (SFT No. 2) diagnostic hole "A" pressure history.

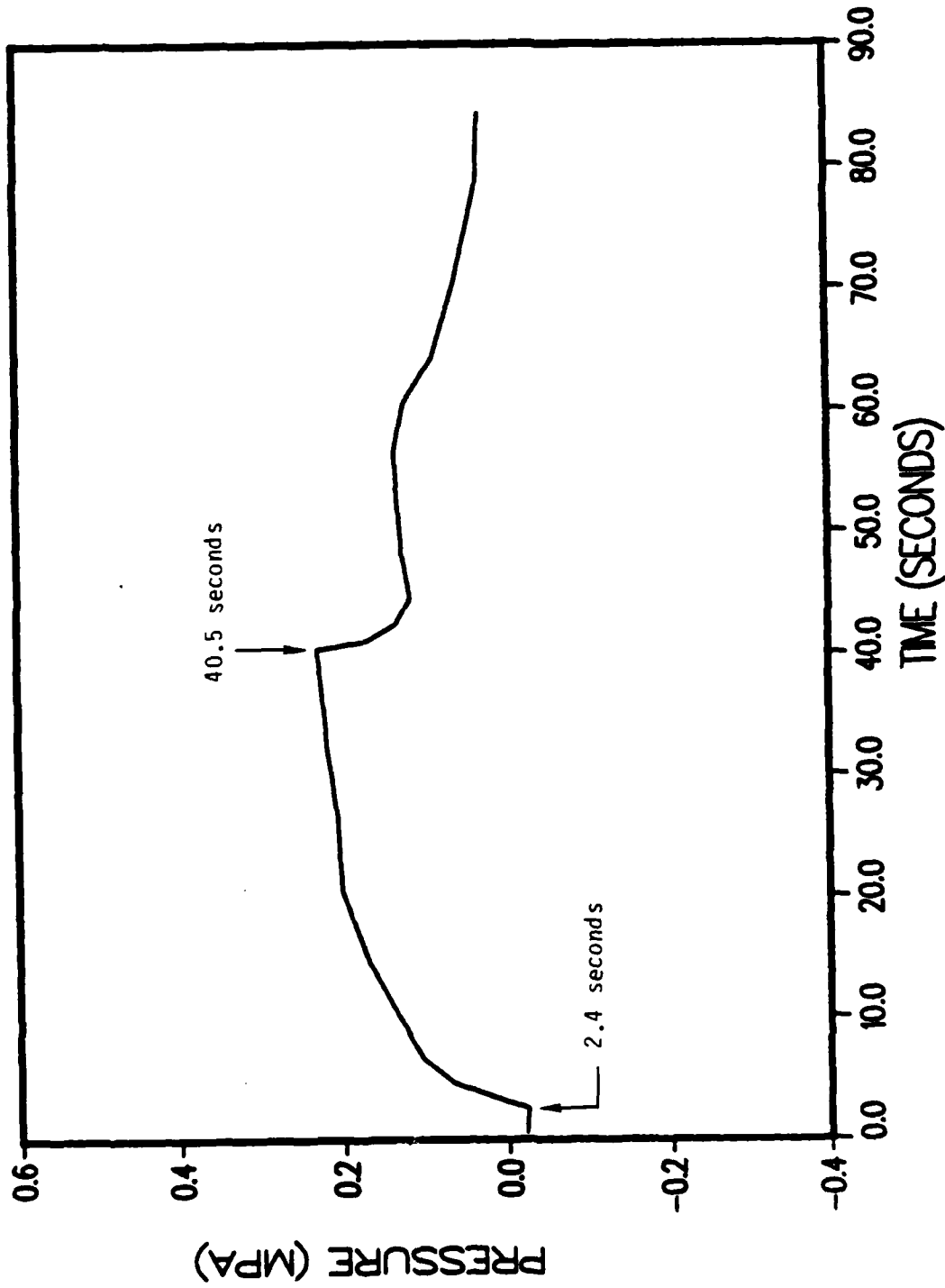


Figure B-9 P-tunnel CS 11+90 steam fracture experiment (SFT No. 2) diagnostic hole "B" pressure history.

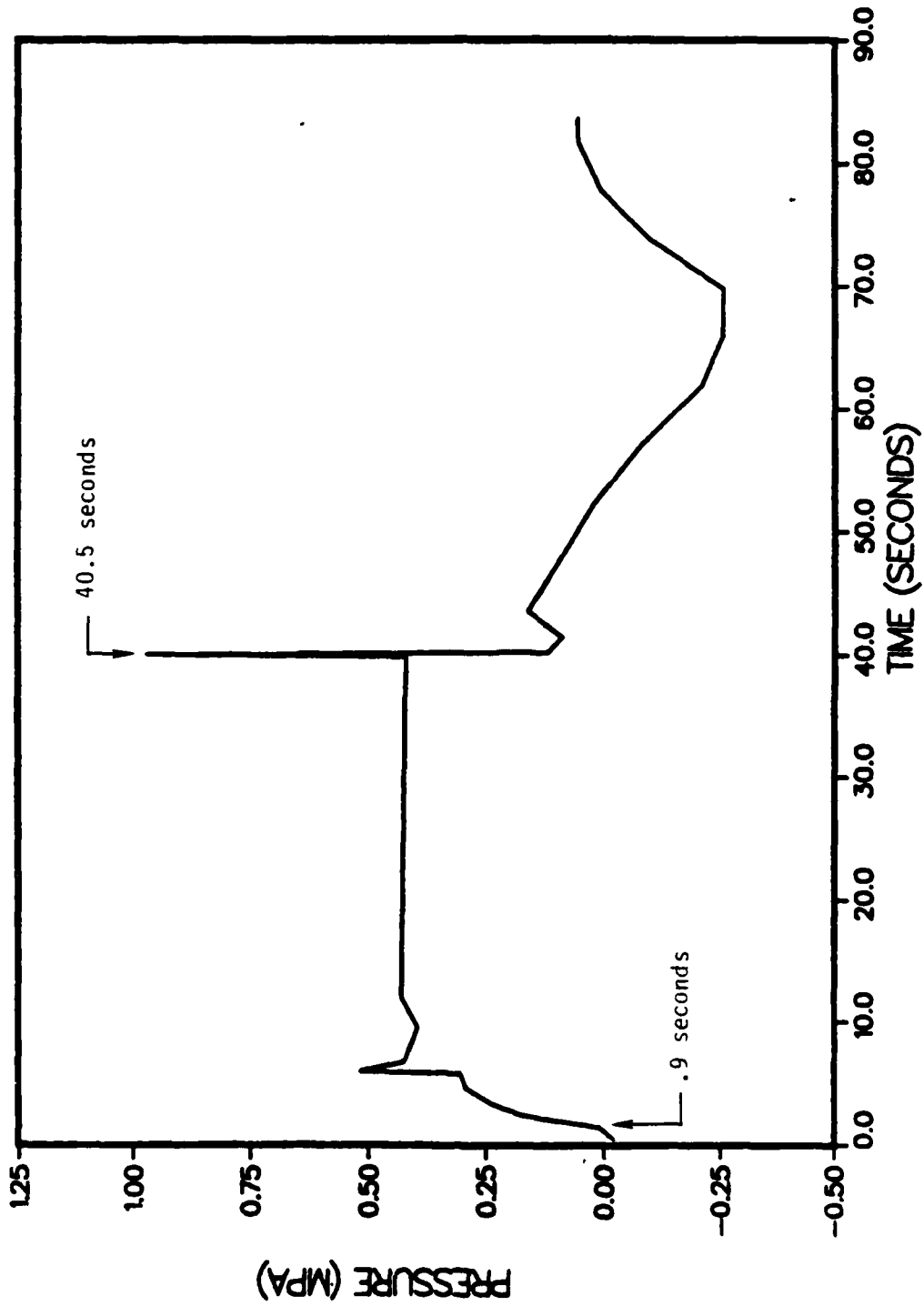


Figure B-10 P-tunnel CS 11+90 steam fracture experiment (SFT No. 2) diagnostic hole "1" pressure history.

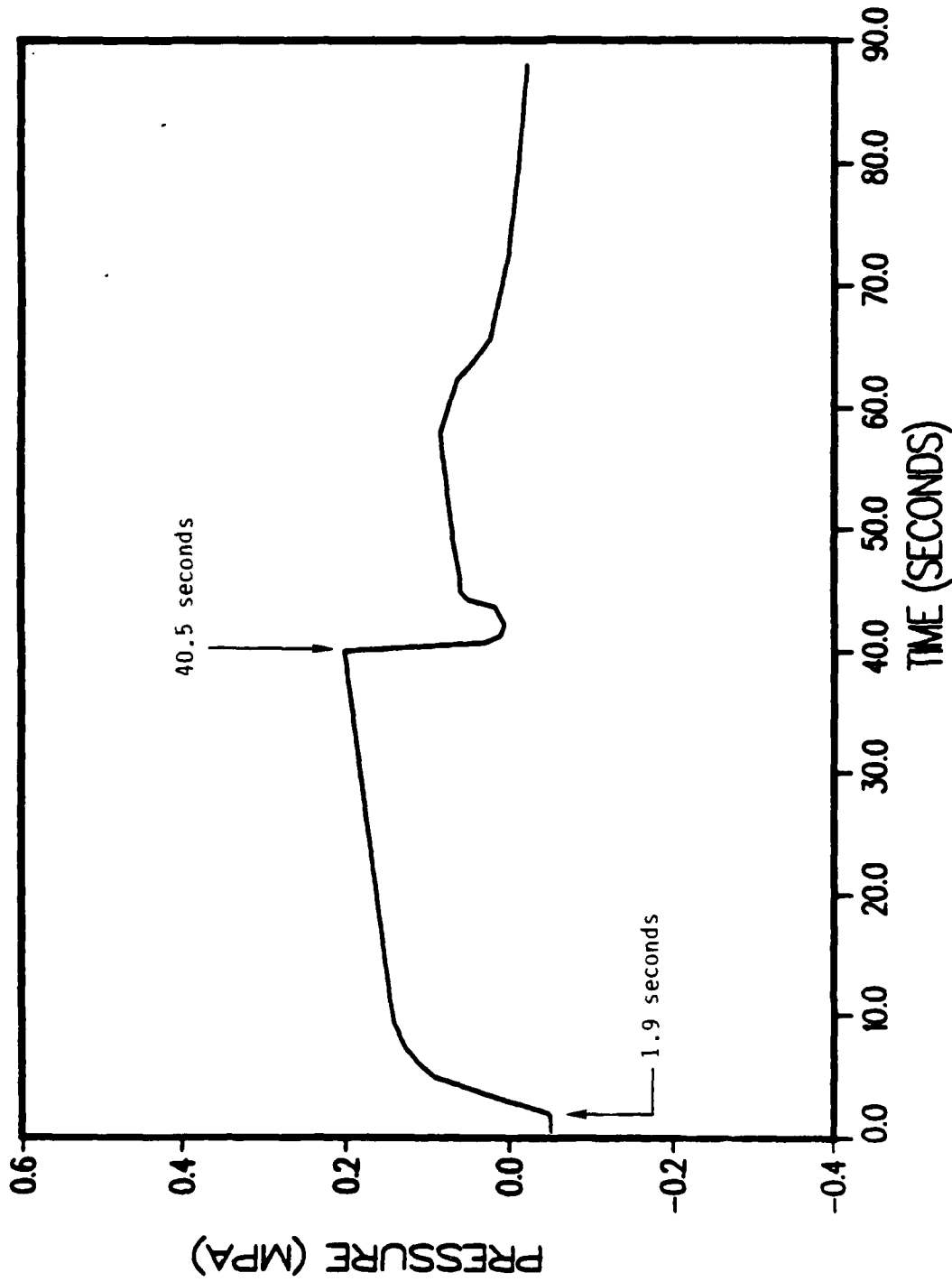


Figure B-11 P-tunnel CS 11+90 steam fracture experiment (SFT No. 2) diagnostic hole "2" pressure history.

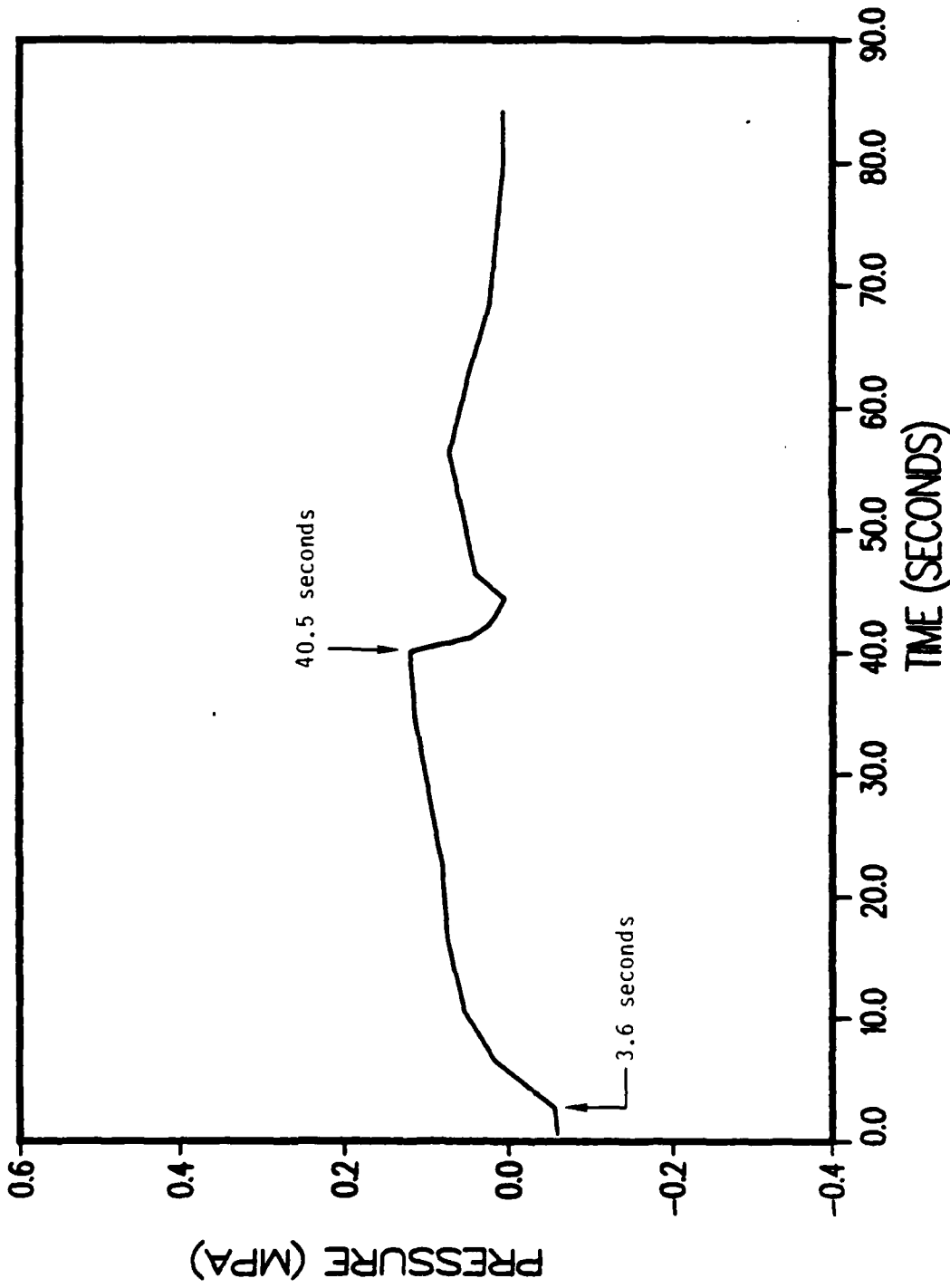


Figure B-12 P-tunnel CS 11+90 steam fracture experiment (SFT No. 2) diagnostic hole "3" pressure history.

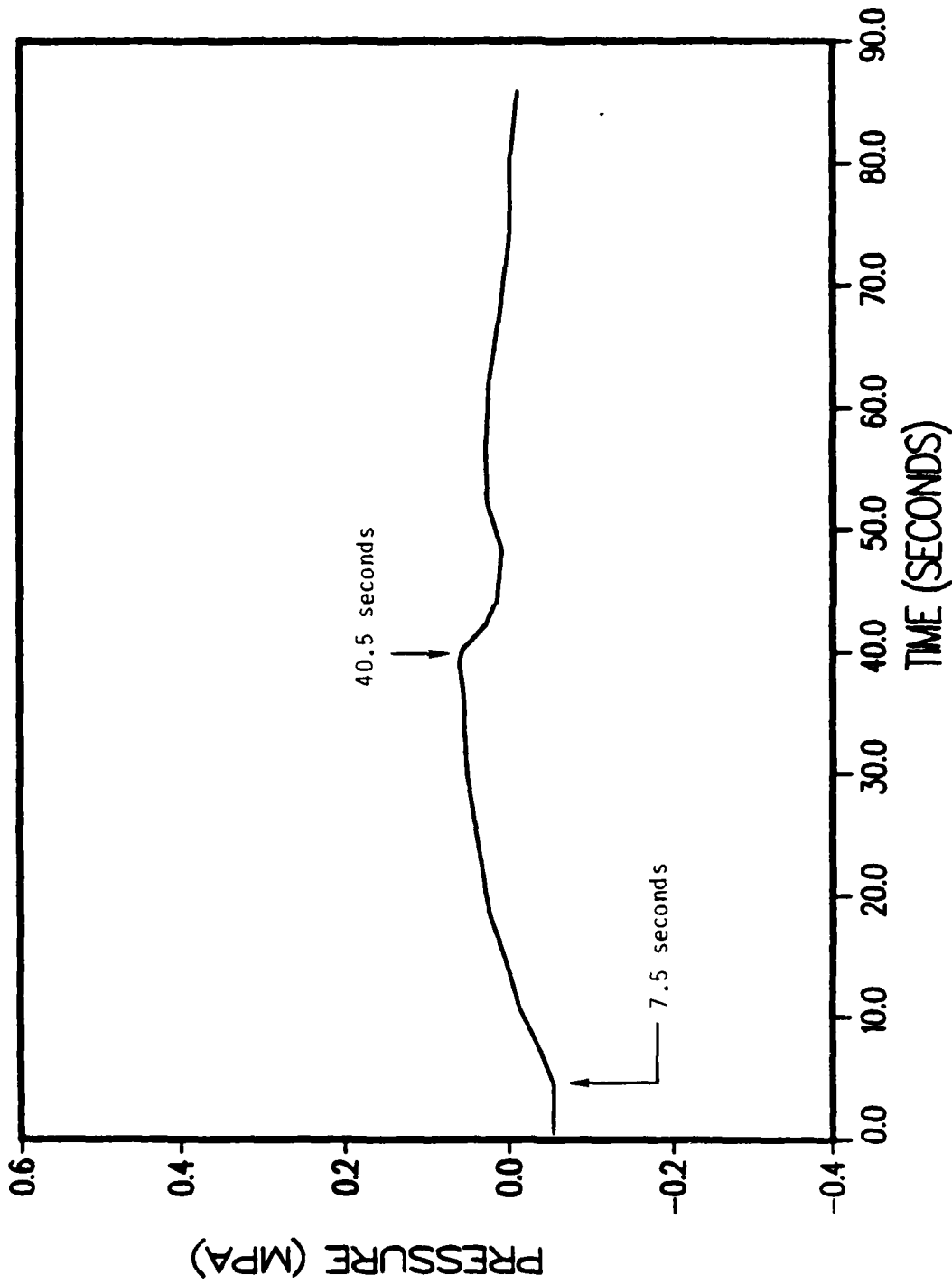


Figure B-13 P-tunnel CS 11+90 steam fracture experiment (SFT No. 2)
diagnostic hole "4" pressure history.

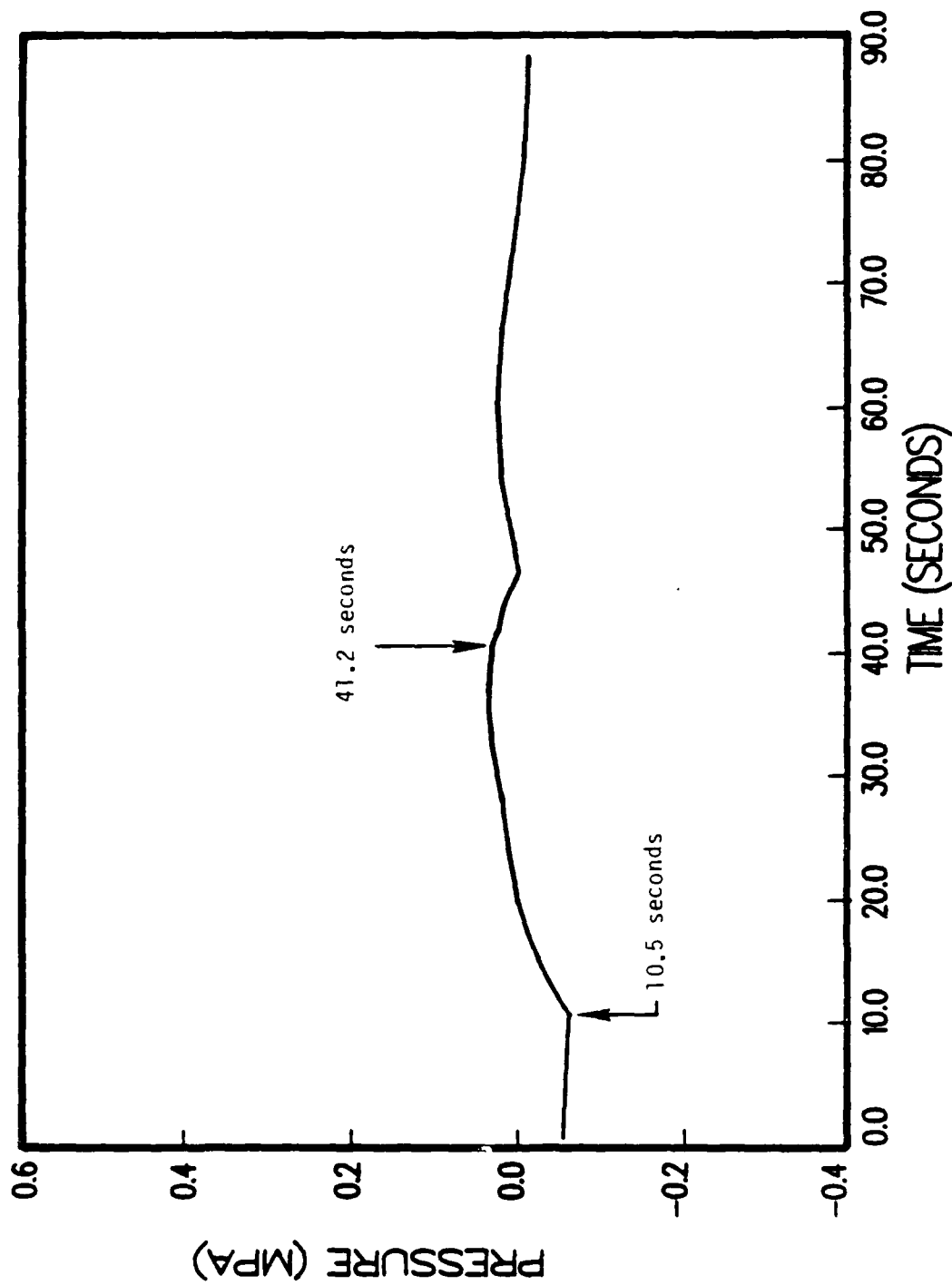


Figure B-14 P-tunnel CS 11+90 steam fracture experiment (SFT No. 2) diagnostic hole "C" pressure history.

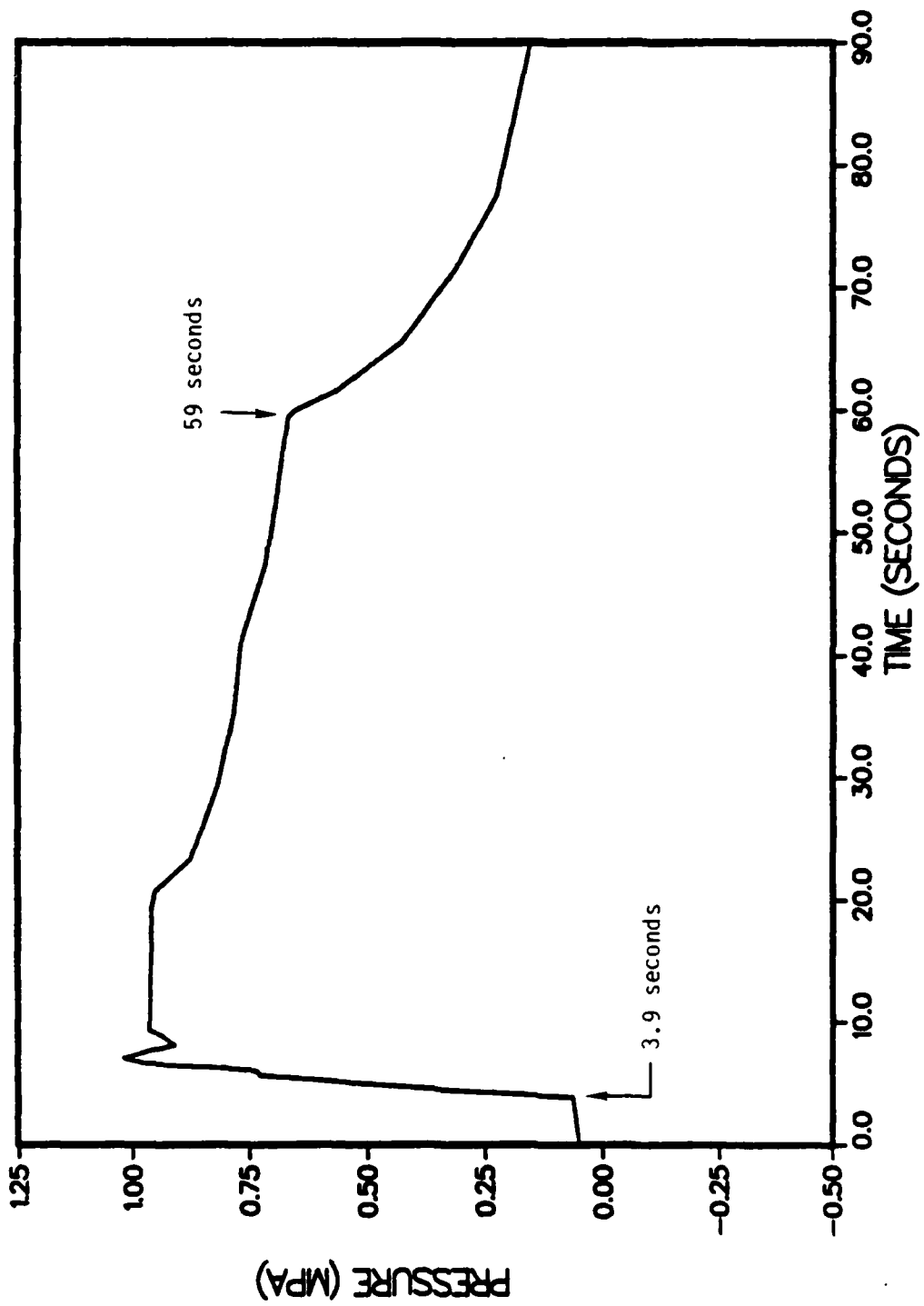


Figure B-15 P-tunnel CS 11+24 steam fracture experiment (SFT No. 3) diagnostic hole "A" pressure history.

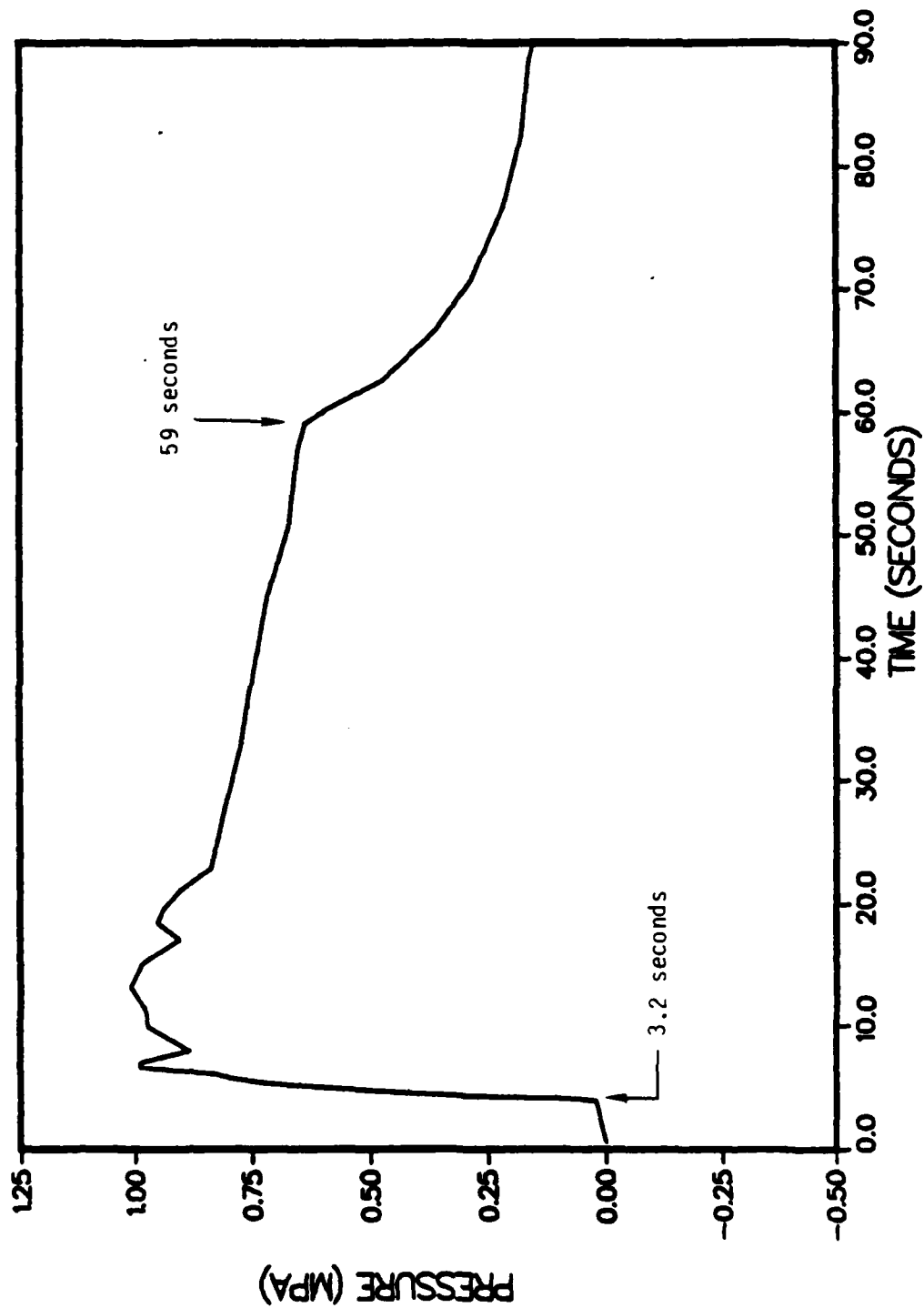


Figure B-16 P-tunnel CS 11+24 steam fracture experiment (SFT No. 3) diagnostic hole "B" pressure history.

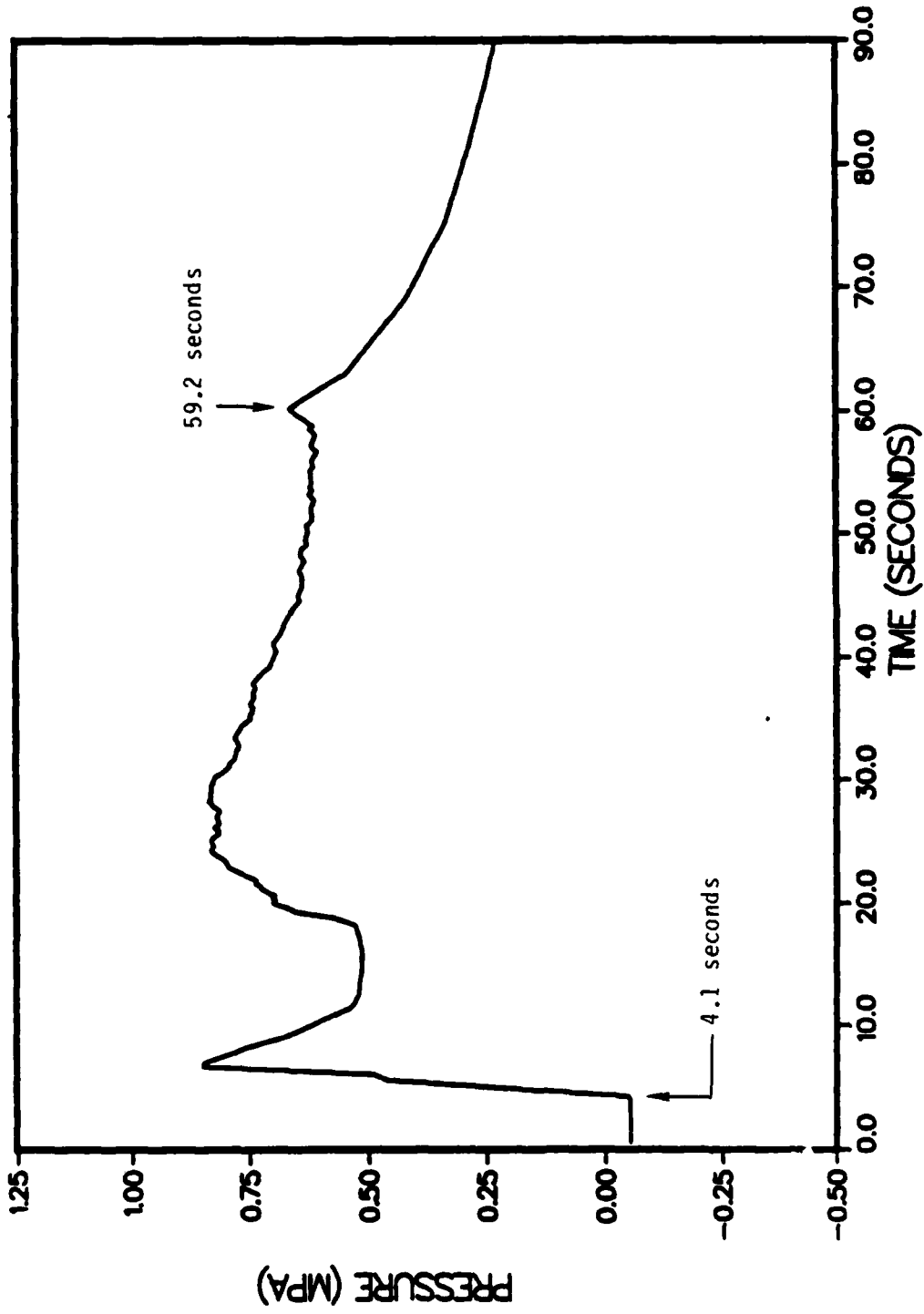


Figure B-17 P-tunnel CS 11+24 steam fracture experiment (SFT No. 3)
diagnostic hole "1" pressure history.

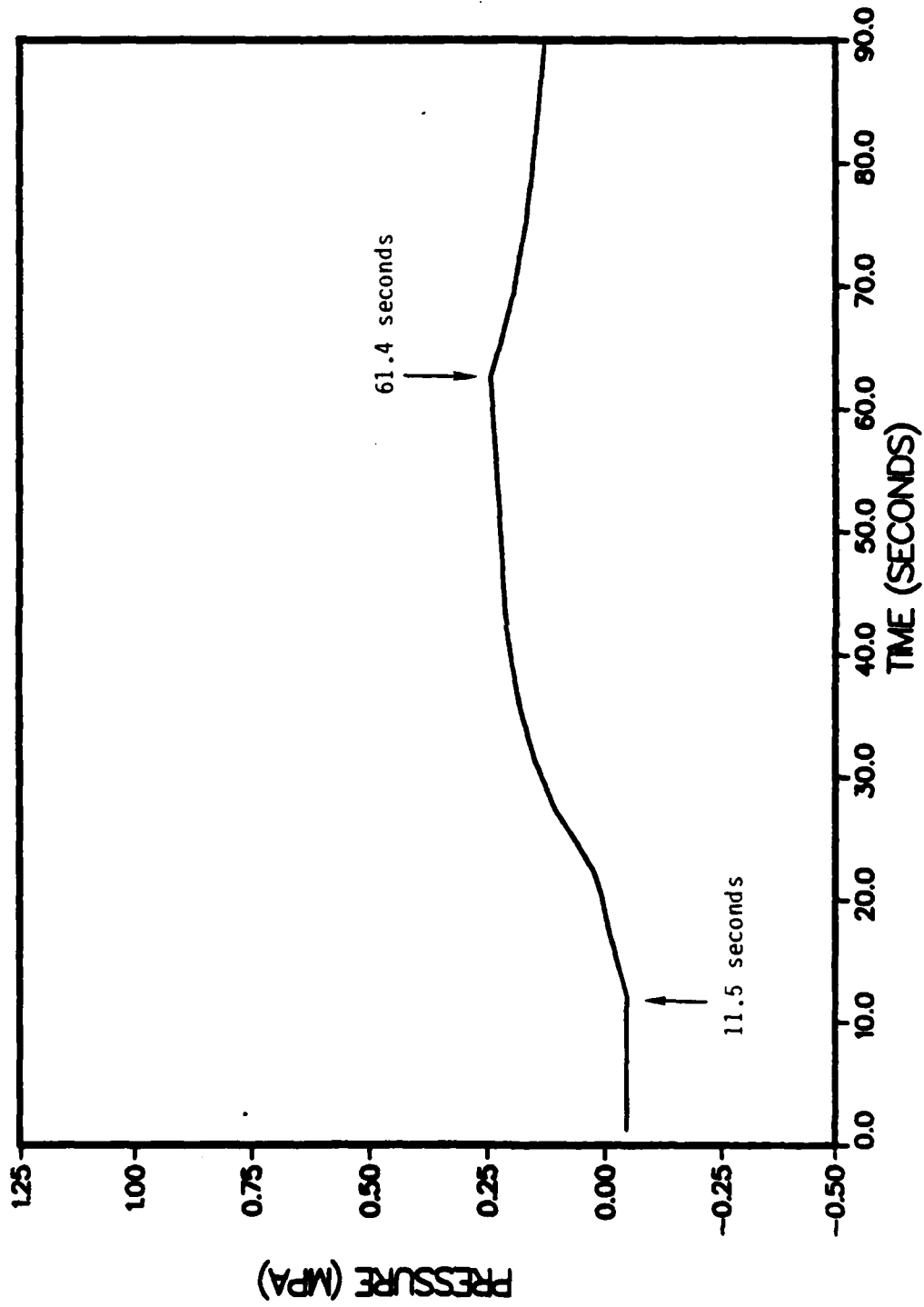


Figure B-18 P-tunnel CS 11+24 steam fracture experiment (SFT No. 3) diagnostic hole "2" pressure history.

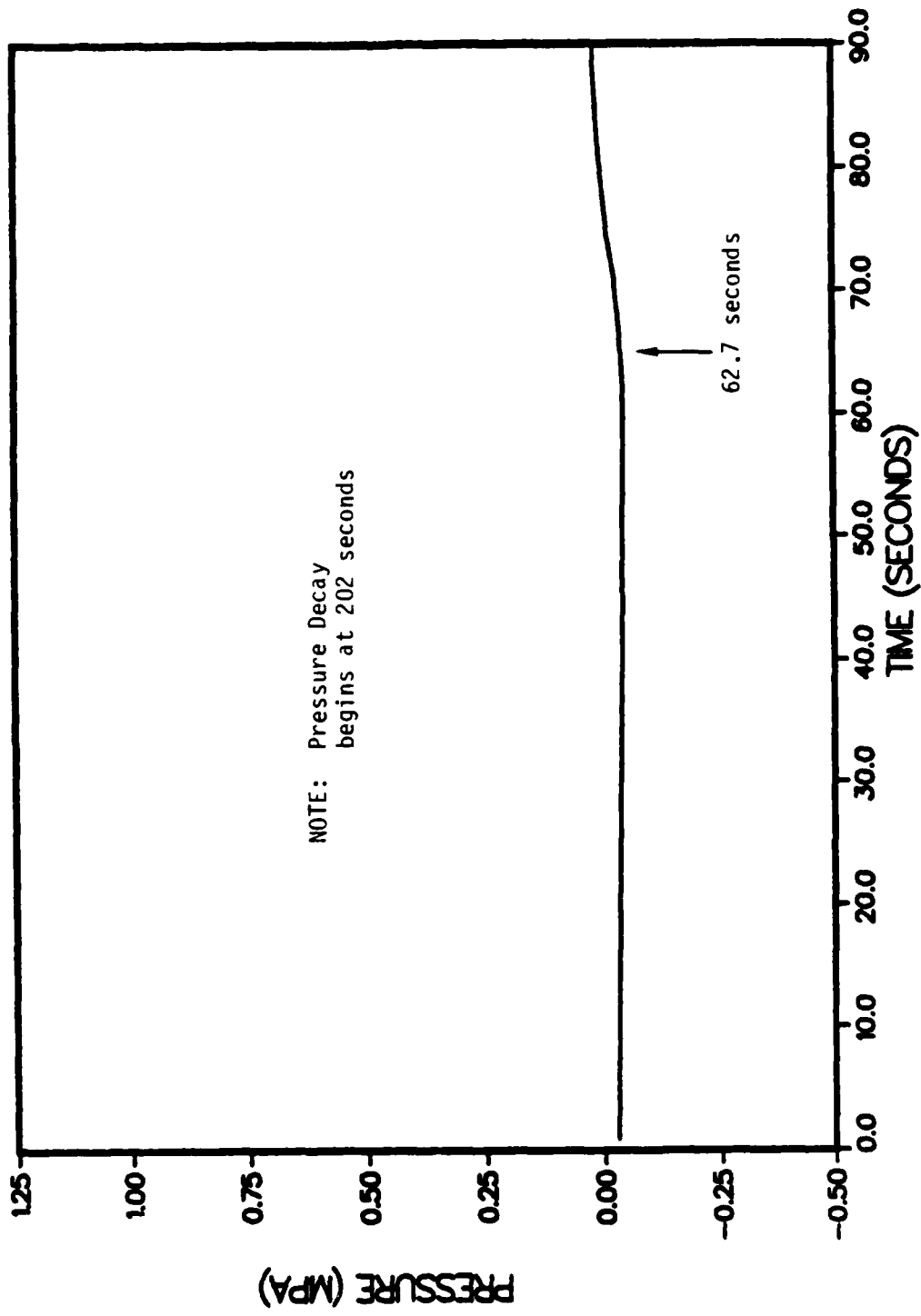


Figure B-19 P-tunnel CS 11+24 steam fracture experiment (SFT No. 3) diagnostic hole "3" pressure history.

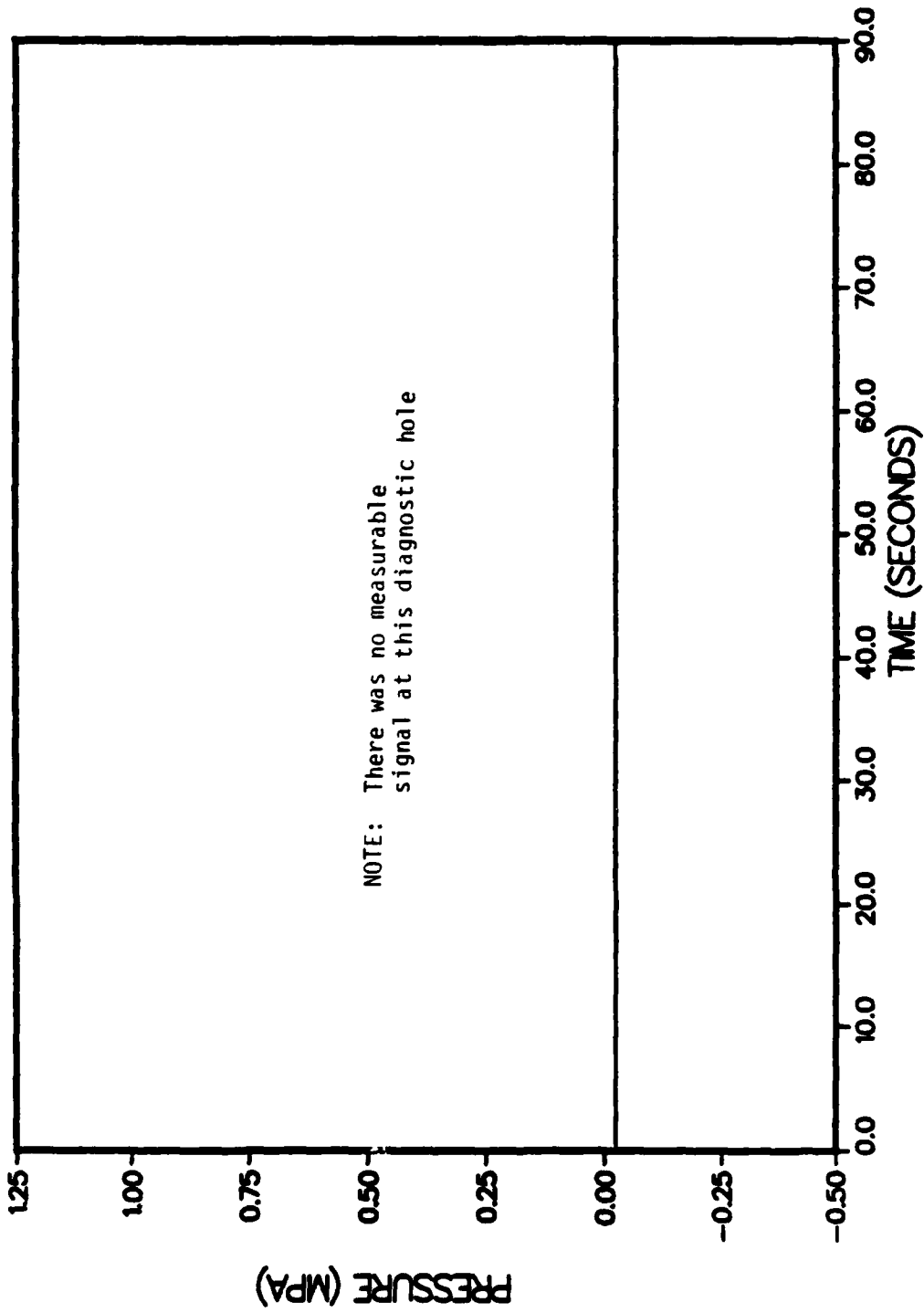


Figure B-20 P-tunnel CS 11+24 steam fracture experiment (SFT No. 3) diagnostic hole "4" pressure history.

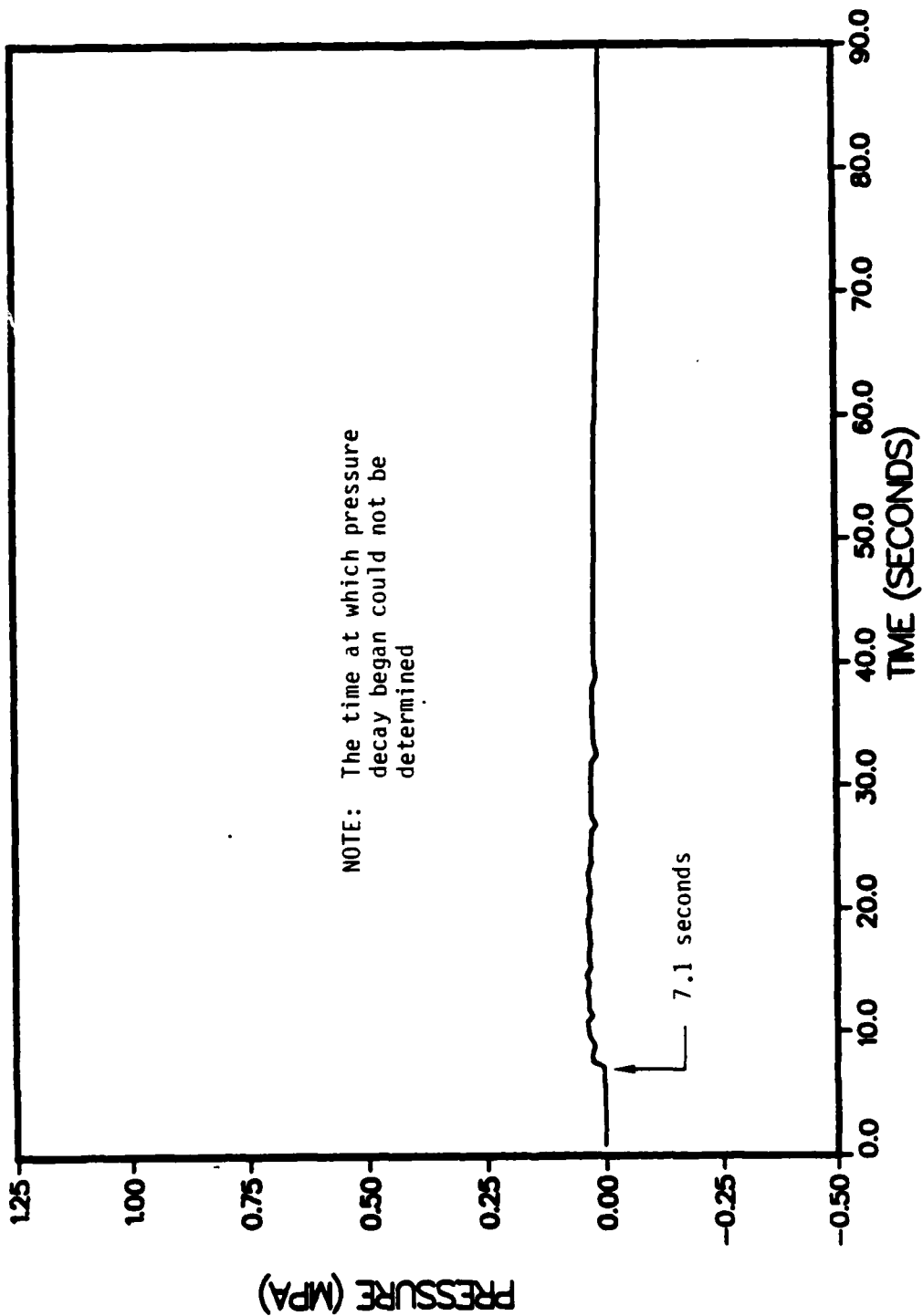


Figure B-21 P-tunnel CS 11+24 steam fracture experiment (SFT No. 3) diagnostic hole "C" pressure history.

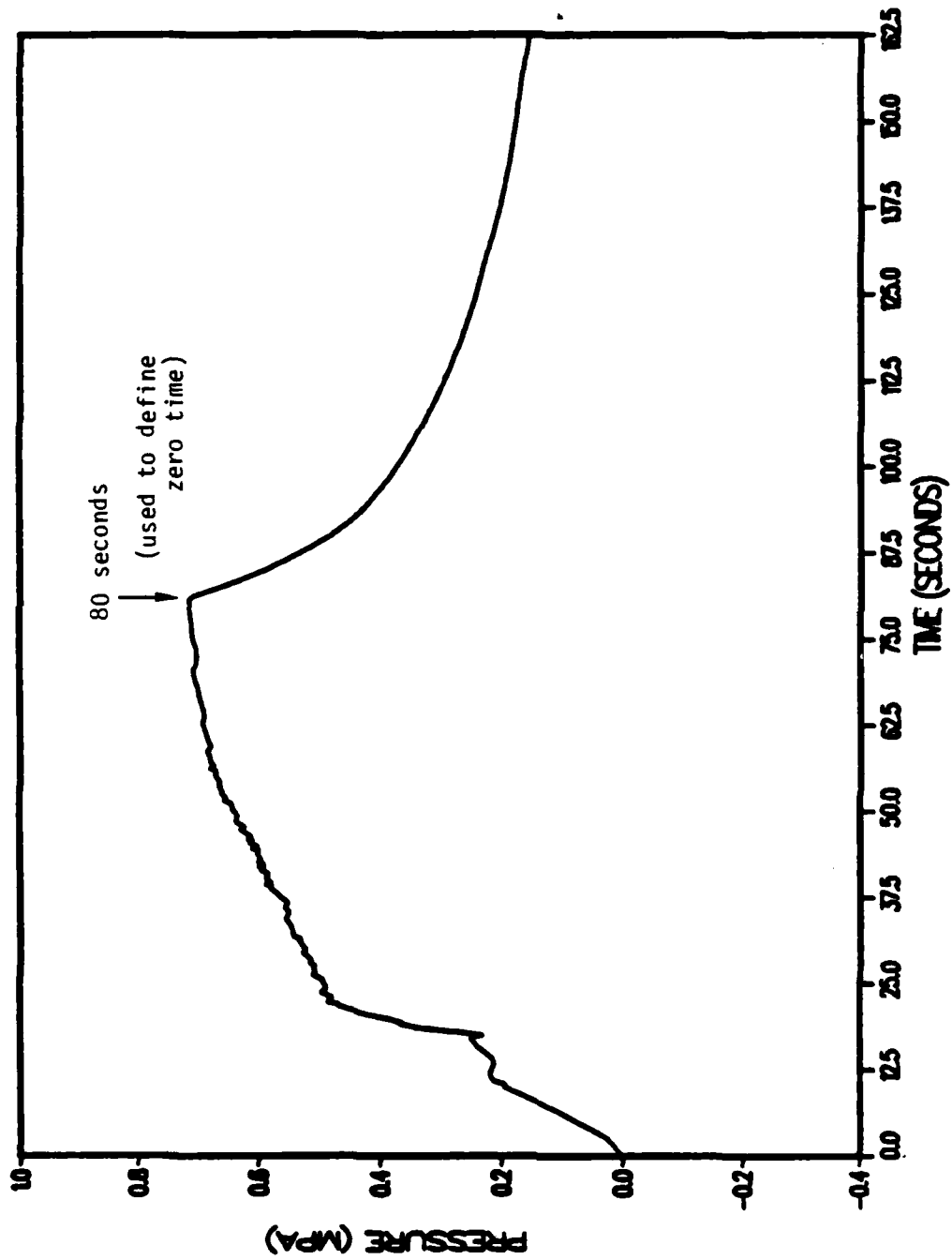


Figure B-22 P-tunnel CS 11+24 steam fracture experiment (SFT No. 4)
diagnostic hole "A" pressure history.

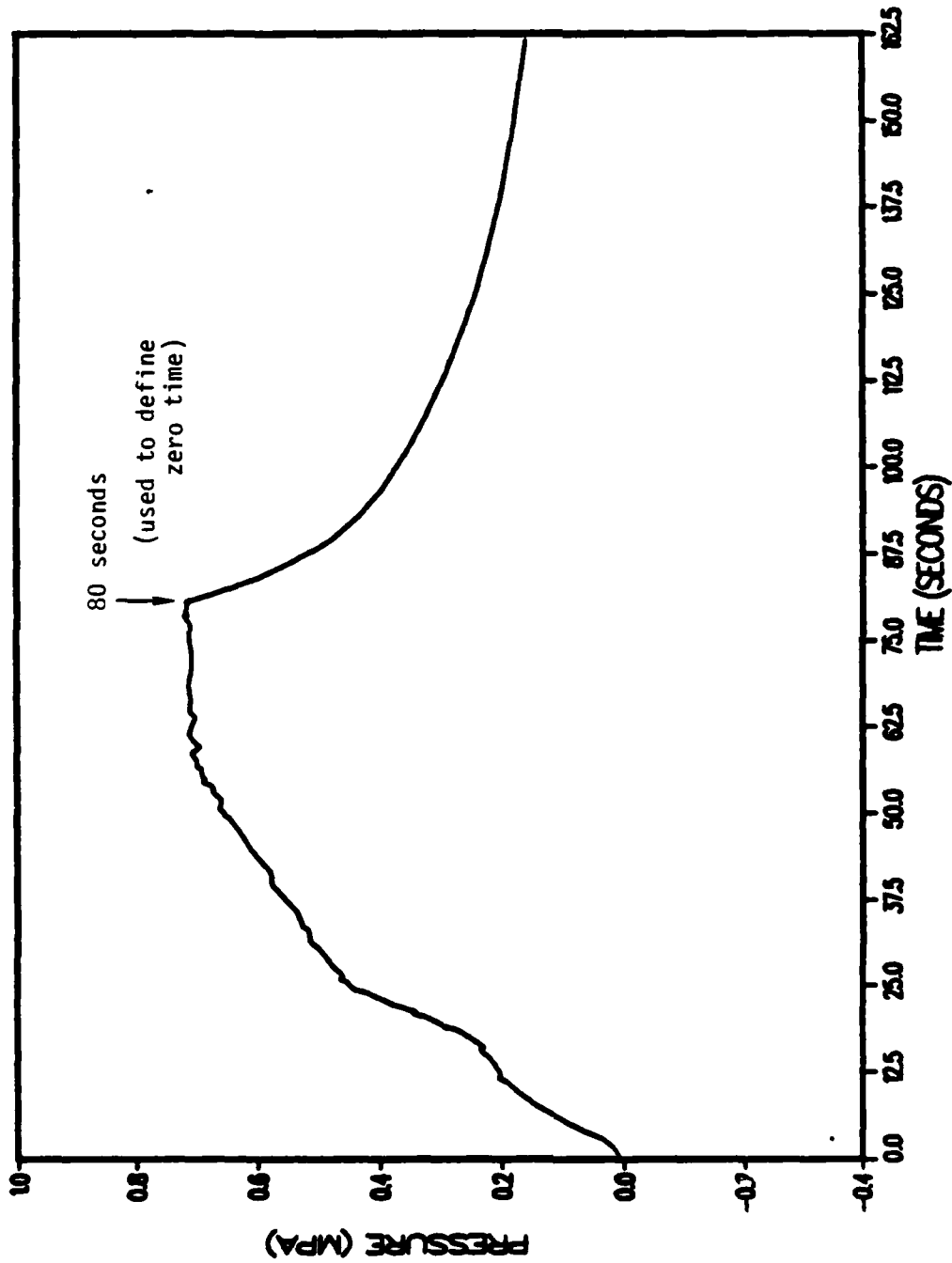


Figure B-23 P-tunnel CS 11+24 steam fracture experiment (SFT No. 4) diagnostic hole "B" pressure history.

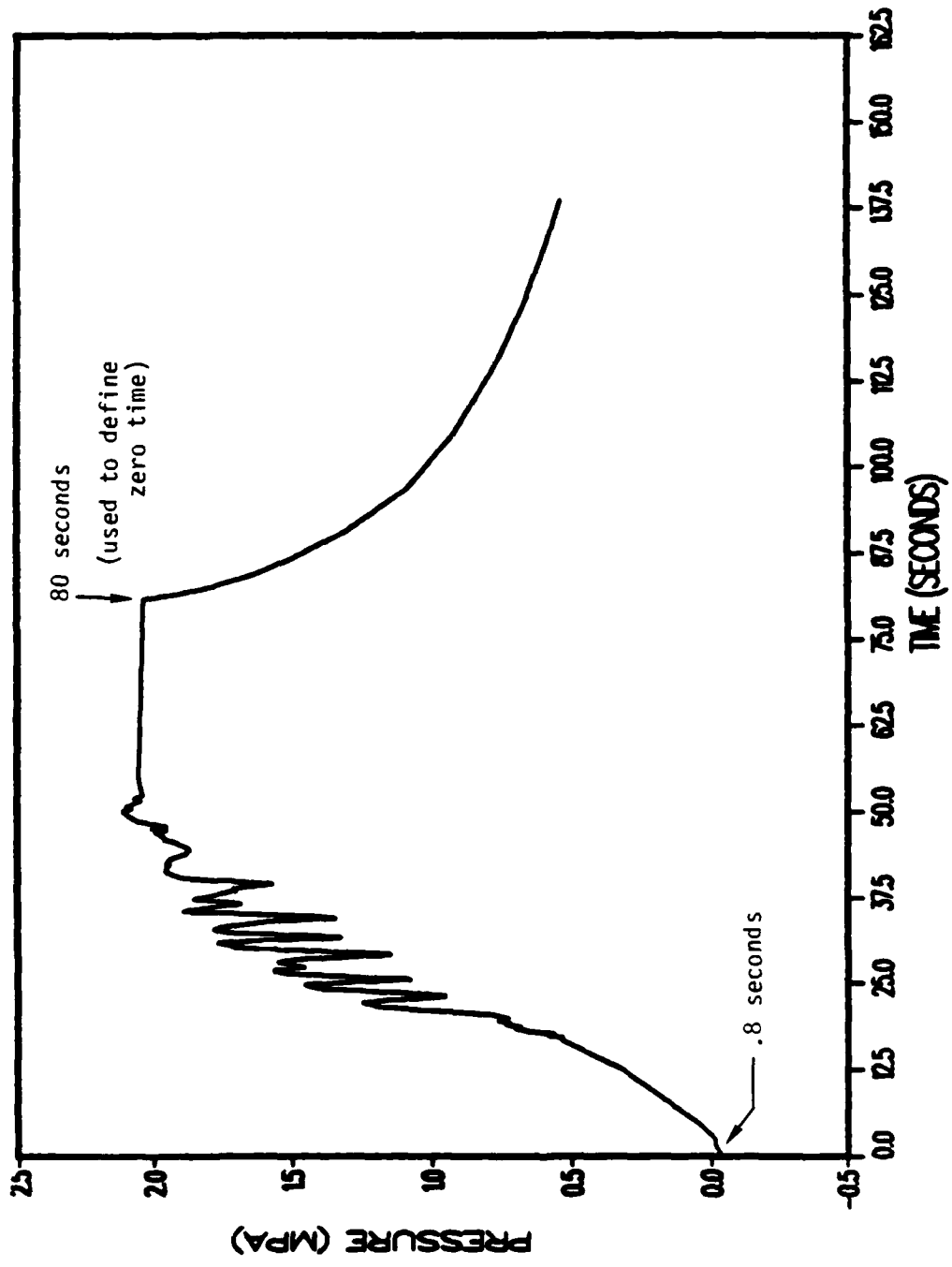


Figure B-24 P-tunnel CS 11+24 steam fracture experiment (SFT No. 4) diagnostic hole "1" pressure history.

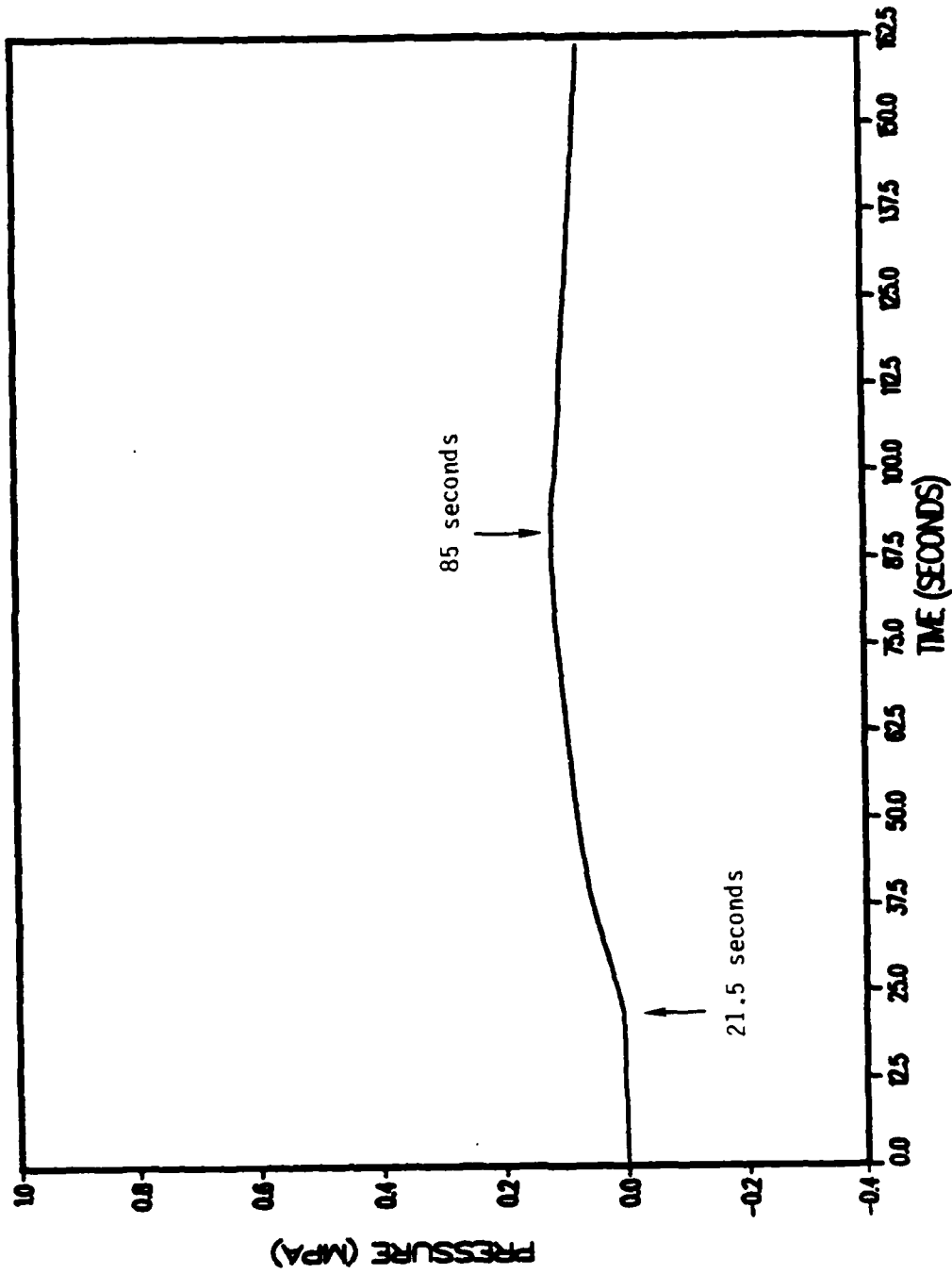


Figure B-25 P-tunnel CS 11+24 steam fracture experiment (SFT No. 4)
diagnostic hole "2" pressure history.

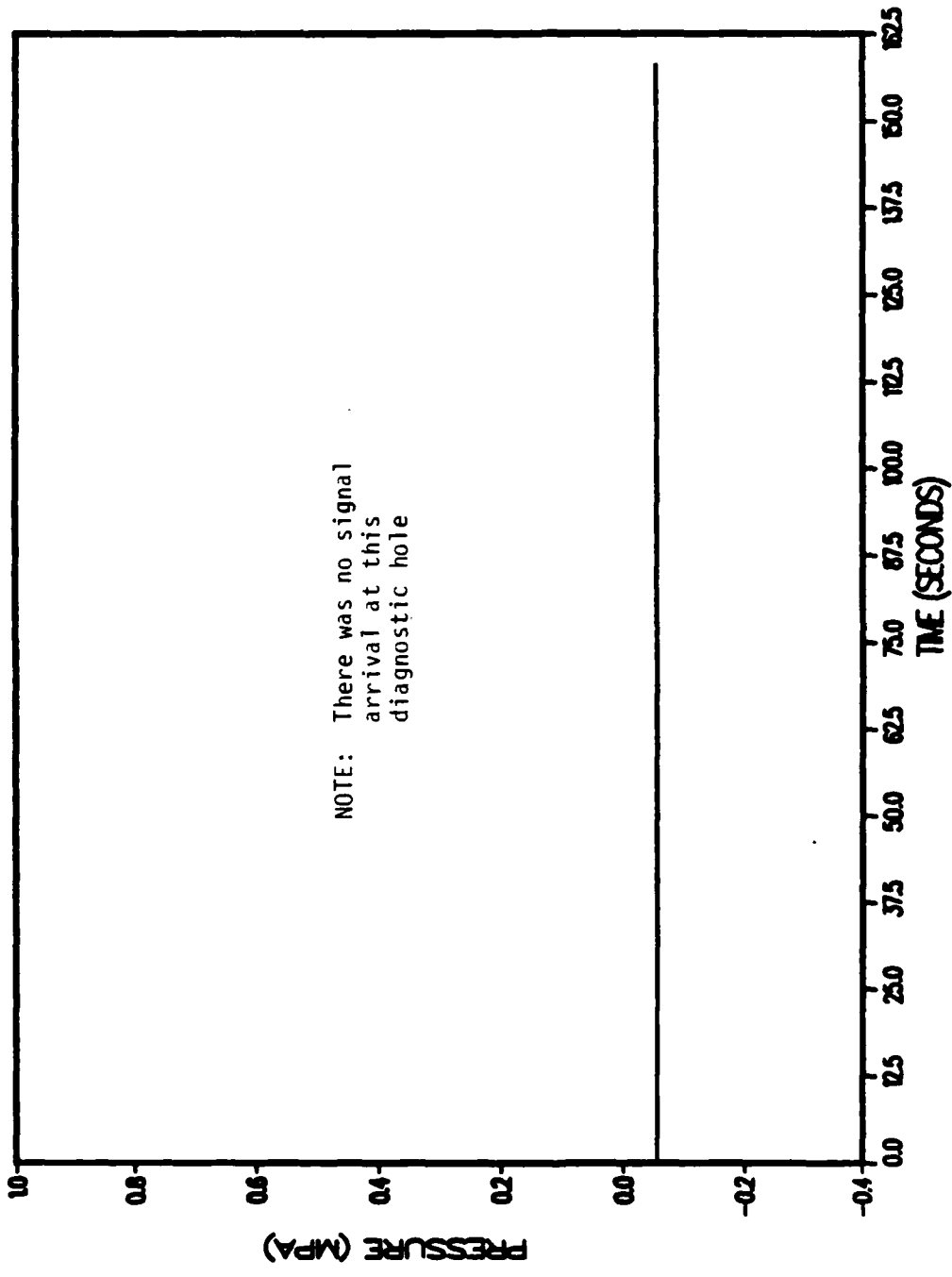


Figure B-26 P-tunnel CS 11+24 steam fracture experiment (SFT No. 4) diagnostic hole "3" pressure history.

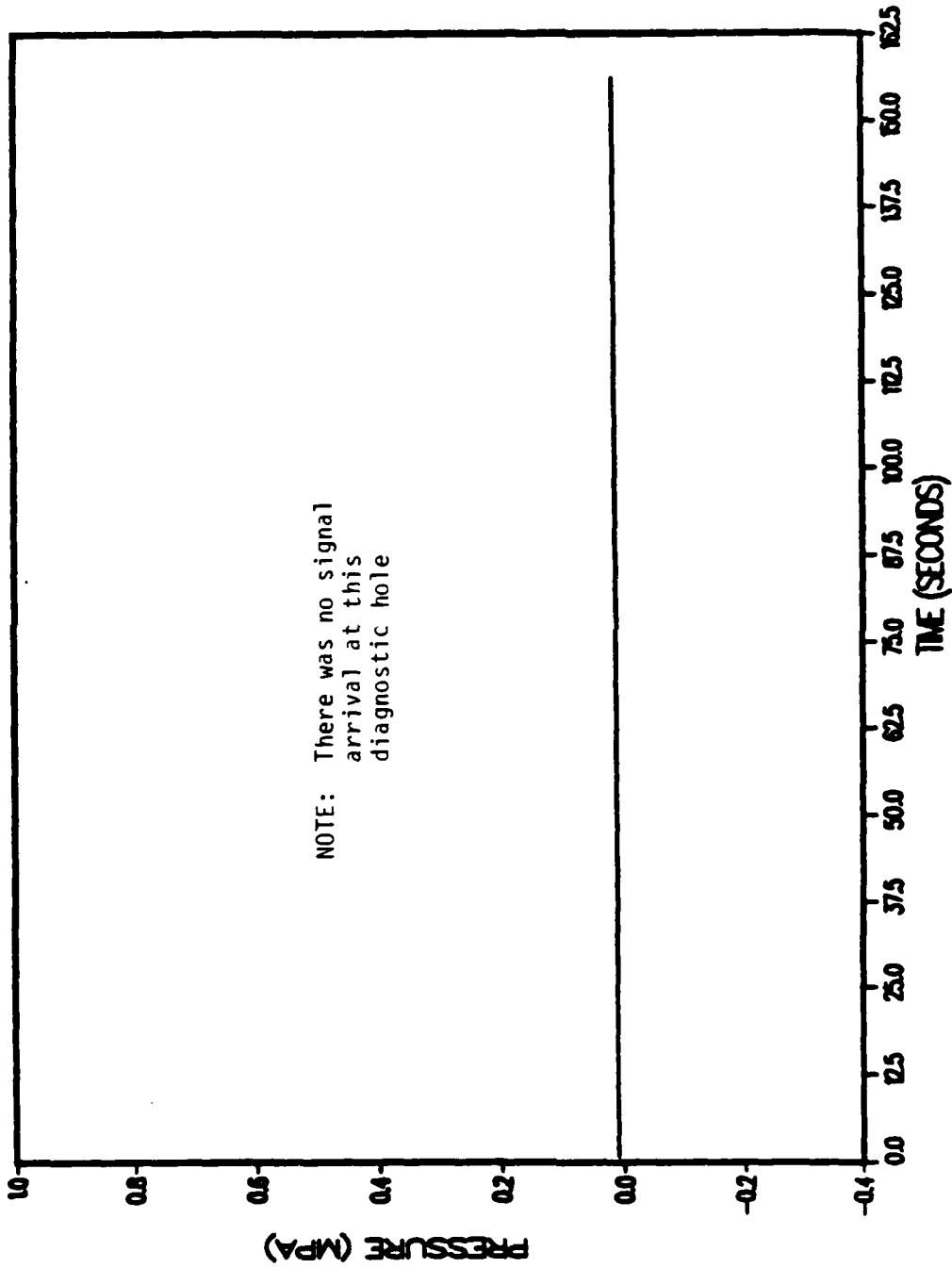


Figure 8-27 P-tunnel CS 11+24 steam fracture experiment (SFT No. 4) diagnostic hole "4" pressure history.

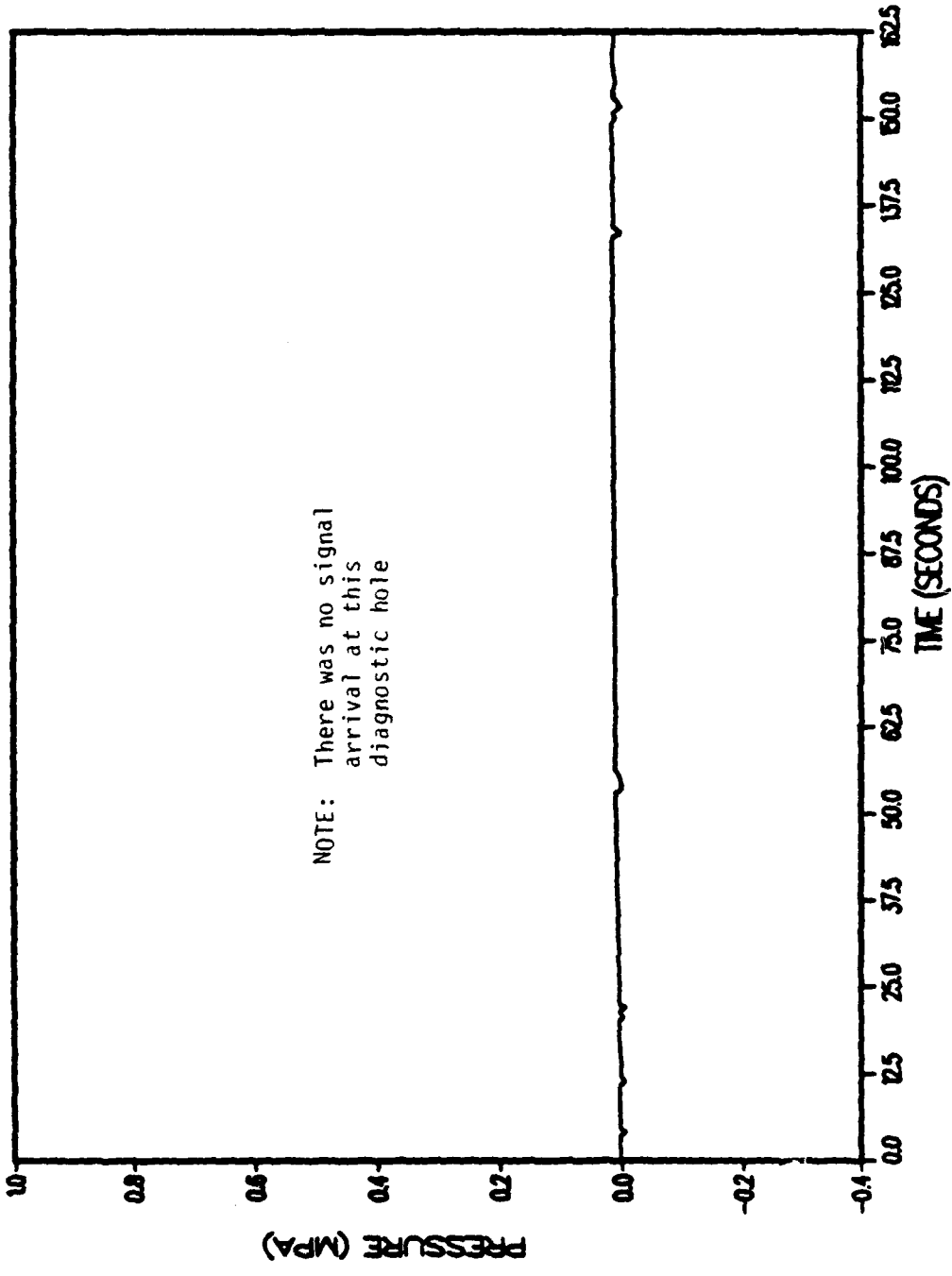


Figure B-28 P-tunnel CS 11+24 steam fracture experiment (SFT No. 4) diagnostic hole "C" pressure history.

APPENDIX C
IN SITU PERMEABILITY TEST ANALYSIS

Prior to performing the P-Tunnel steam fracture tests, low pressure airflow tests were conducted in the source and diagnostic holes. Test results are given in Tables 1 and 2. In addition, air and water flow tests were performed in the CS 11+90 source region following the steam fracture test. These results are presented in Table A-7. Permeability values were determined from the test data, as described below.

The in situ tests were conducted as follows. Air or water was injected at a relatively constant downhole pressure, and the test continued until the flowrate approached a constant value. The reported permeability values were then determined from the measured pressure and flow data using the steady-state air and water flow equations C1 and C2, respectively. No attempt was made to consider the affects of flow in a partially saturated formation. It must be emphasized that these tests were performed to obtain a rough (i.e., within factors of two or three) permeability values.

$$\dot{w} = \pi L \frac{k}{\mu} \frac{\rho_o}{P_o} \frac{P_o^2 - P_\infty^2}{\ln r_o/r_\infty} \quad (C1)$$

$$\dot{w} = 2 \pi L \frac{k}{\mu} \rho \frac{P_o - P_\infty}{\ln r_o/r_\infty} \quad (C2)$$

where, the symbols are

- k Permeability (cm²)
- L Test Region Length (cm)
- P Pressure (dyne/cm²)
- r Radius (cm)
- w Flowrate (gr/sec)
- ρ Density (gr/cm³)
- μ Viscosity (dyne-sec/cm³)

and the subscripts denote

- o Test Region
- ∞ Free Field

DISTRIBUTION LIST

DEPARTMENT OF DEFENSE

Defense Intelligence Agency
ATTN: RTS-2B

Defense Nuclear Agency
ATTN: SPTD, T. Kennedy
4 cy ATTN: STTI-CA

Defense Technical Information Center
12 cy ATTN: DD

Field Command, Defense Nuclear Agency
ATTN: FCT, Col G. Ballantine
ATTN: FCTT, C. Bloemker
ATTN: FCTT, W. Summa
3 cy ATTN: FCTK, C. Keller
3 cy ATTN: FCTK, E. Rinehart

DEPARTMENT OF THE AIR FORCE

Air Force Weapons Laboratory
ATTN: NT
ATTN: SUL

DEPARTMENT OF ENERGY

Department of Energy
Nevada Operations Office
ATTN: P. Murda

OTHER GOVERNMENT AGENCIES

Central Intelligence Agency
ATTN: OSWR/NED

US Geological Survey
ATTN: P. Orkild
ATTN: R. Carroll

DEPARTMENT OF ENERGY CONTRACTORS

Desert Research Institute
ATTN: D. Schulke Sec Off for C. Case
ATTN: D. Schulke Sec Off for P. Fenske

University of California
Lawrence Livermore National Lab
ATTN: B. Hudson
ATTN: C. Olsen
ATTN: R. Terhune

Sandia National Laboratories
ATTN: Library & Sec Class Div

Los Alamos National Laboratory
ATTN: B. Travis
ATTN: C. Keller
ATTN: F. App
ATTN: Reports Library
ATTN: R. Brownlee
ATTN: T. Kunkle

DEPARTMENT OF ENERGY CONTRACTORS (Continued)

Sandia National Laboratories
ATTN: C. Smith
ATTN: Org 7112, C. Mehl
ATTN: Org 7112, J. Plimpton
ATTN: R. Bass

DEPARTMENT OF DEFENSE CONTRACTORS

California Research & Technology, Inc
ATTN: M. Rosenblatt

Kaman Tempo
ATTN: DASIAC

Kaman Tempo
ATTN: DASIAC

Pacific-Sierra Research Corp
ATTN: H. Brode, Chairman SAGE

Pacific Technology
ATTN: D. Patch

Physics International Co
ATTN: H. Wampler
ATTN: J. Shea
ATTN: J. Gordon

R & D Associates
ATTN: P. Haas

Rand Corp
ATTN: B. Bennett

S-CUBED
ATTN: C. Dismukes
ATTN: R. Duff
2 cy ATTN: E. Peterson
2 cy ATTN: H. Wu
2 cy ATTN: P. Lagus

Science & Engrg Associates, Inc
ATTN: C. Keller
ATTN: J. Cramer

Science & Engrg Associates, Inc
ATTN: J. Stockton

SRI International
ATTN: A. Florence

END

FILMED

4-86

DTIC